Development of Guidelines for the use of Intermediate Diaphragms on Precast Concrete Beam Superstructures

MDOT Research Administration Reference Number: OR19-003

FINAL REPORT

August 27, 2021

Authors:

Christopher D. Eamon
Fatmir Menkulasi
Bellikoth V. Bhaktha
Mario Quagliata

TECHNICAL REPORT DOCUMENTATION PAGE

1. Report No. **SPR-1702**	2. Government Accession No. N/A	3. Recipient's Catalog No.	
4. Title and Subtitle Development of Guidelines for the Use of Intermediate Diaphragms on Precast Concrete Beam Superstructures		**5. Report Date** 08/27/2021	
		6. Performing Organization Code N/A	
7. Author(s) Christopher D. Eamon Fatmir Menkulasi Bellikoth V. Bhaktha Mario Quagliata		**8. Performing Organization Report No.** N/A	
9. Performing Organization Name and Address Wayne State University Department of Civil and Environmental Engineering 5050 Anthony Wayne Dr. Detroit, MI 48202		**10. Work Unit No.** N/A	
		11. Contract or Grant No. 2019-0314 Z1	
12. Sponsoring Agency Name and Address Michigan Department of Transportation (MDOT) Research Administration 8885 Ricks Road P.O. Box 33049 Lansing, Michigan 48909		**13. Type of Report and Period Covered** Final Report, 10/1/2019 to 7/31/2021	
		14. Sponsoring Agency Code N/A	
15. Supplementary Notes Conducted in cooperation with the U.S. Department of Transportation, Federal Highway Administration. MDOT research reports are available at www.michigan.gov/mdotresearch.			

16. Abstract
This study examines the need for intermediate diaphragms (IDs) and lateral support on low skew, low curvature prestressed concrete (PC) bridges while in-service and under construction. AASHTO beam, bulb tee, and spread box beam sections across a variety of span lengths and girder spacings were considered. To examine the in-service effect of IDs on vehicular live load distribution, validated finite element analysis (FEA) models were used to determine the change in distribution factor (DF) on a set of hypothetical PC girder bridges. During construction, the need for beam lateral bracing upon girder seating until deck cure was analyzed, considering the failure modes of girder rollover and lateral torsional buckling (LTB). Girder rollover was modeled with an analytical approach calibrated to numerical (FEA) results, while LTB was modeled with a validated, material and geometrically nonlinear FEA procedure. It was found that IDs provide little change in DF for typical structures, while elastomeric bearing pad properties and beam length significantly affected beam stability during bridge construction. Lateral bracing guidelines were developed as a function of section type, span, girder position, overhang length, and bearing pad width to provide stability during construction.

17. Key Words		18. Distribution Statement		
diaphragms; bridges; prestressed concrete; instability; buckling; finite element analysis		No restrictions. This document is also available to the public through the Michigan Department of Transportation.		
19. Security Classif. (of this report) Unclassified	20. Security Classif. (of this page) Unclassified	21. No. of Pages 168	22. Price N/A	

ACKNOWLEDGMENTS

DISCLAIMER

This publication is disseminated in the interest of information exchange. The Michigan Department of Transportation (hereinafter referred to as MDOT) expressly disclaims any liability, of any kind, or for any reason, that might otherwise arise out of any use of this publication or the information or data provided in the publication. MDOT further disclaims any responsibility for typographical errors or accuracy of the information provided or contained within this information. MDOT makes no warranties or representations whatsoever regarding the quality, content, completeness, suitability, adequacy, sequence, accuracy or timeliness of the information and data provided, or that the contents represent standards, specifications, or regulations.

TABLE OF CONTENTS

LIST OF TABLES

LIST OF FIGURES

EXECUTIVE SUMMARY

Intermediate diaphragms (IDs) have been primarily used to prevent girder instabilities during construction and to more evenly distribute vehicle live loads among girders in-service. In some cases, IDs have been used for other reasons as well, such as to aid in horizontal load sharing from over-height vehicle collisions. However, the AASHTO Load and Resistance Factor Design (LRFD) Bridge Design Specifications provides limited guidance for the use of IDs on prestressed concrete (PC) bridges, which are only required on moderately or significantly curved box beam bridges. For other PC structures, no guidance is provided.

Numerous studies have suggested that IDs have a relatively minor influence on in-service structural behavior, though in some cases may be needed for stability during construction. However, the need for IDs on low skew, low curvature PC structures is unclear. If the use of IDs on these structures can be reduced or eliminated, several benefits may be realized, such as a reduction of fitment problems; decreasing the time and cost of construction; as well as a longer-term minimization of maintenance costs associated with ID and connection deterioration. Thus, the objective of this study is to examine the need for IDs on PC bridges and to provide recommendations for placement.

The first tasks of the research were to survey the State DOTs for ID use and to determine typical PC bridge geometries for consideration. It was found that most states surveyed required IDs for low skew, low curvature PC bridges, though placement and specific requirements varied significantly. The large majority of States required IDs for construction stability, whereas few considered them useful for vehicular live load distribution. A study of the MDOT bridge inventory data indicated that most PC girder bridges were built from 1950-1980; have a single span less than 100 ft in length; are two-lane; and low skew and low curvature.

The next tasks were to develop and validate finite element analysis (FEA) models of structural response considering IDs for in-service use as well as stability during construction, which included assessment of lateral torsional buckling (LTB) and rollover. In-service models were validated by comparing results to data found in the literature for two laboratory test bridges and one field test. The final models for assessment of load distribution were linear elastic and used quadratic solid elements for the deck and girders. For LTB, models were validated using test data in the literature for three beam specimens that failed in LTB. Various modeling approaches were studied, and it was found that using the Concrete Damage Plasticity model along with a three-stage loading process, including prestress, beam self weight, then application of construction loads, worked best. These models used solid elements for the girder and bar elements for reinforcement. These fully nonlinear, large-strain, large displacement models were solved explicitly, and best represented the experimental LTB capacity results when concrete was assumed to be in a cracked state. For girder rollover, a modeling approach similar to LTB was used, but in this case the bearings were also directly modeled with solid elements. A single rollover result with sufficient documentation was available for model validation. It was found that rollover capacity was sensitive to bearing properties.

The models were then used in a parametric analysis to study ID performance. For live load distribution, hypothetical two lane bridges of various spans, girder spacing, and beam type were

considered (AASHTO, bulb tee, and box). Special cases of skew, curvature, changes in deck width, number and type of ID, and span continuity was also studied. It was found that IDs have a generally increasing effect on live load distribution as the ratio of girder flexural stiffness to transverse deck flexural stiffness increases, as well as ID stiffness increases. When using 1 ID at midspan, the average decrease in girder distribution factor (DF) across the cases considered is approximately 3%. No significant changes were found for the cases of skew, curvature, or continuity. Among the typical cases, the maximum decrease in DF ranged from 5-9%, depending on beam type. However, special cases (for example, overly-stiff beams with wider girder spacing paired with concrete diaphragms) resulted in significantly greater changes in DF. The DF values found from the FEA models without IDs were generally significantly lower than those specified in AASHTO LRFD.

For rollover and LTB instability analyses, two beam lengths were considered; those suitable for HL93-mod and HS25 loading, depending on girder spacing. It was determined that the FEA approach developed to model rollover was too complex and time consuming to conduct the size of the parametric study desired (approximately 150 cases), where different girder sections, lengths, and bearing characteristics were used. Therefore, the FEA model was used to validate and refine an analytical procedure that was specifically developed for this study to evaluate rollover, based on an existing PCI method. Limit states considered included cracking, bearing lift-off, as well as rollover. Generally, it was found that AASHTO beams, and some of the bulb tees and box beams required bracing, depending on construction loads, bearing pad properties, span, and other parameters.

For LTB, the developed FEA approach was used to evaluate beam performance under service loads and three strength-based load combinations. In some cases, it was found that a longer span girder, carrying the uncured slab, did not have the compressive flexural capacity to support the additional construction loads imposed, and thus could not be evaluated for instability at the appropriate length designed for in-service use. Beams nearly always passed the service limit state, while Strength I was the governing strength limit state. Similar to rollover results, the LTB analyses determined that AASHTO beams and some bulb tee girders require 1 ID for stability, while box beams did not.

Based on all results (in-service live load distribution, rollover, and LTB), two sets of recommendations were made for the use of IDs and lateral bracing in general, as a function of various parameters such as girder length, type and size, bearing width, overhang size, bracing location, and modeling assumptions. In development of the first, minimal set of recommendations, it was found that exterior beams with wider lower flanges (bulb tees and 48 in. wide box beams) may avoid the need for lateral bracing during construction in some circumstances, depending on span, bearing width, section size, and overhang length; while all interior girders except AASHTO types may avoid the need for lateral bracing in some circumstances. Within the alternative conservative set of recommendations, all exterior girders require bracing, although bracing placement, at beam ends or at midspan, may vary in some circumstances. For interior girders, all except box beams in some circumstances require bracing.

CHAPTER 1: INTRODUCTION

1.1 Statement of the Problem

The AASHTO LRFD Bridge Design Specifications require that diaphragms are to be used at abutments, piers, and hinge joints in most structures. However, intermediate diaphragms are only specifically required on moderately or significantly curved (inside radius of 800 ft or smaller) box beam bridges. For other structural types and geometries, including precast concrete girder bridges with low skew and modest curvature, no guidance is provided.

In general, intermediate diaphragms are primarily used to prevent girder instabilities during construction; to enhance gravity load distribution among girders; and to aid in horizontal load sharing from over-height vehicle collisions. However, given that numerous studies have suggested that intermediate diaphragms (IDs) have relatively minor influence on in-service structural behavior (Cai et al. 2008), a question arises whether IDs can be reduced in number, or eliminated entirely, for low skew, low curvature precast concrete (PC) bridges. This is particularly so if sections more resistant to instability such as box beams or bulb-tees are used. If structurally feasible, reducing or eliminating IDs could bring significant benefits, such as a reduction of fitment problems, time, and cost of construction, as well as a longer-term minimization of maintenance problems associated with deterioration.

The importance of diaphragms is somewhat unknown, as a variety of recommendations exist (Dupaquier 2016). Although IDs may perhaps provide limited benefit in-service, in some instances, significant safety concerns exist without diaphragms, particularly during construction or deck removal, when girders are most susceptible to instability. These concerns were realized during the Red Mountain Freeway (AZ) bridge failure in 2007, when nine, 114 ft AASHTO Type V girders collapsed during construction, when no diaphragms were present. Although the precise cause of the collapse is unknown, analysis suggested that a combination of bearing eccentricity, girder sweep, and sloped bearings were the primary factors (Oesterle et al. 2007). Similar instability failures occurred on the I-80 Bridge (PA) in 2005, where 150 ft AASHTO girders collapsed without IDs due to inadequate bracing and unexpected girder sweep (Garlich et al. 2015), as well as during the collapse of the Souvenir Blvd. Bridge in 2000 (Quebec), where AASHTO girders toppled prior to diaphragm placement.

Given the desire to remove diaphragms in-service but to maintain erection safety, several states, such as Alabama, Florida, Kansas, and Texas, specify temporary bracing during construction but have moved to eliminate permanent IDs (Dupaquier 2016). As PC girder failures are rare, however, these events clearly depend on a set of particularly unfavorable combinations of girder type, bridge geometry, and field conditions.

With these uncertainties, as well as the questionable benefit of diaphragms on in-service structures, it is currently unclear whether diaphragms are needed on PC bridges, and if so, under what set of conditions. The purpose of this study is to determine the need for IDs on bridges using standard MDOT PC girders including AASHTO, bulb-tee, and box beam types.

1.2 Objectives of the Study

The specific research objectives of this study, are to (for PC bridges):

1. Determine the current practice of State DOTs with respect to ID use.

2. Develop FEA models to assess the need for IDs.

3. Develop guidelines for the use of IDs.

1.3 Summary of Research Tasks

This research is composed of the following tasks:

Task 1. State-of-the-Art Literature Review

Task 2. Survey State DOTs to Determine ID use on PC Girder Bridges

Task 3. Develop FEA Models and Assess the Performance of IDs

Subtask 3.1. Develop Initial Models

Subtask 3.2. Validate Model and Refine as Necessary

Subtask 3.3. Conduct Parametric Analysis

Task 4. Develop Guidelines

Task 5. Prepare Project Deliverables

CHAPTER 2: LITERATURE REVIEW

2.1 Introduction

The literature review represents a summary of research related to the development of guidelines for the use of intermediate diaphragms (IDs) on prestressed concrete (PC) bridges. The review included a broad search of technical engineering journals, conference proceedings, as well as technical reports relevant to the topic published by state Departments of Transportation (DOTs) and the National Cooperative Highway Research Program (NCHRP). The review focused on research identifying the influence of IDs in various stages of the bridge lifetime, including during construction and in-service; the effect of bridge geometry and other factors on ID effectiveness; finite element analysis (FEA) approaches that have been used to model diaphragm behavior, particularly those which were found to be accurate as well as computationally efficient; and experimental and/or field test results that can be used to validate FEA models.

2.2 AASHTO Standards

The AASHTO Standard Specifications (2002) require that IDs are placed for PC T-beam bridges at positions of maximum moment for spans greater than 40 ft, while for spread box beams, IDs are only needed for spans greater than 80 ft, and for "precast box multi-beam bridges" only if necessary. For cast-in-place box beams, IDs are not required on PC bridges with a radius of curvature 800 ft or greater, while for all other types of PC box bridges, with a radius of curvature less than 800 ft, IDs "may be required", implying the need for a refined analysis. The specifications also state that IDs may be omitted in any case if testing or structural analysis indicates that they are unnecessary.

AASHTO LRFD (2020) reduced the scope of requirements for IDs for PC bridges. Section 5 (concrete structures) addresses pier and continuity diaphragms, as well as those used to anchor post-tensioning strands. It further states that diaphragms are to be provided at abutments, piers, hinge joints, and with regard to cast-in-place RC segments, provided at bottom flange angle points in structures with straight haunches. However, with regard to IDs, AASHTO LRFD only states that IDs are required for spread box beam bridges with a radius of curvature less than 800 ft, and that they may otherwise be used "where necessary", with no specific requirements and minimal guidance given. It should be noted that the AASHTO LRFD girder distribution factor equations were developed assuming no IDs (Zokaie et al. 1991),

2.3 Current DOT Standards

The MDOT Bridge Design Guide provides diaphragm details for concrete and several steel alternatives, and currently specifies that IDs are to be used at the midspan of PC I-beam bridges. Other DOTs have implemented various approaches to ID use on PC bridges, the details of which have evolved over time. Two decades ago, 8 states required no permanent IDs.   Among those that did require them, various rationales influenced ID policy. For example, Iowa required concrete IDs for PC bridges if traffic passes beneath the structure, but steel IDs for structures that do not span over traffic lanes (Garcia 1999). In general, a wide variety of ID usage was found. Cai et al. (2008) and Gull et al. (2014) conducted subsequent surveys and found similarly varying results.

Dupaquier et al. (2016) recently surveyed state DOTs for ID use on PC bridges, where the following questions were asked (summarized for brevity): (1) What type of IDs are specified or allowed as alternates for PC girder bridges? (2) When are IDs required for PC girder bridges? (3) How and why were ID standards developed, and have they recently changed? (4) What standard details for IDs are used? From the survey, it was found that 4 states (AL, FL, KS, TX) do not use permanent IDs on PC bridges, and only require temporary bracing during construction. Moreover, 5 states have no standard; 20 specify only concrete IDs; 13 specify only steel, and 8 allow both. However, all states surveyed agreed that IDs or a similar temporary bracing system is necessary during construction. Similar to past practices, it was found that various reasons drive current ID policy. For example, ALDOT requires no IDs for PC girders, and specifies that the contractor is responsible for bracing during construction. FDOT similarly forgoes permanent IDs, except to minimize spreading damage to other girders in the event of an over-height vehicular collision. In contrast, out of a desire to distribute vehicular collision force, Mississippi DOT specifies that only concrete IDs are to be used. A sample of some other particular findings were:

1. Alabama DOT does not consider IDs to be effective for live-load distribution.
2. Alaska DOT eliminated the use of steel K-brace IDs due to constructability issues, while concrete IDs have been shown to be cost effective.
3. Delaware DOT uses ID details from Maryland DOT.
4. Florida DOT requires temporary bracing during construction and has developed software for evaluation of lateral stability of girders during construction. However, permanent IDs are not used.
5. Hawaii DOT requires cast-in-place concrete IDs to assist live load distribution unless it is demonstrated to be unnecessary.
6. The Idaho Transportation Department allows both steel and concrete IDs but, does not specify details. To accommodate accelerated bridge construction methods, steel IDs are most frequently used.
7. Tennessee DOT uses steel cross bracing to expedite construction.

Dupaquier et al. also surveyed the literature regarding the use of IDs to mitigate damage from over height vehicle impacts, and found no clear consensus to indicate their benefit for this purpose.

2.4 DOT Reports

PennDOT (Lin and Vanhorn 1968) conducted a field test of a spread box beam bridge with and without IDs placed at midspan. It was found that under single lane loading, girder distribution factors were slightly altered due to the presence of diaphragms. However, under two lane loading, no significant benefit was found with regard to load distribution due to the diaphragms.

Iowa DOT (Abendroth et al. 1991; 1995) investigated the performance of reinforced concrete (RC) and steel IDs in PC bridges subject to lateral loads due to over-height truck impacts, as well as to determine the feasibility of using steel in place of RC diaphragms. The study conducted numerical modeling as well as full-scale experimental testing of a PC girder-slab bridge with IDs. ANSYS was used to develop finite element models. Supports were modeled as fixed or pinned ends, while horizontal loads were applied to one girder at mid-span. Reasonable agreement was found between numerical and experimental results, although it was hypothesized that connection

12

slippage, longitudinal deck cracks, and prying were some features that were not be modeled and may have led to discrepancies. Horizontal load distribution was determined to be a function of diaphragm type and location, whereas vertical load distribution was found to be relatively independent of the type and location of IDs.

Later, Iowa DOT (Abendroth et al. 2004) further studied the potential for damage reduction using IDs for bridge girders subjected to impacts from over-height vehicles. In this study, finite element model results were compared with laboratory model bridge results from previous work (i.e. Abendroth et al. 1990). ANSYS was used to model the bridges, where solid elements were used to model the deck and girders, while shells were used to model abutments and end diaphragms. To model RC IDs, shell elements were used, while alternative steel IDs were modeled with truss elements. The lateral impact loads were applied at the bottom flange of exterior girders at and away from diaphragm locations. The impact load considered was applied at five different locations, though multiple simultaneous girder impacts were not considered. Here, a 120 kip load was applied at the location of the ID and a 60 kip load applied elsewhere on the girder. Model and experiment discrepancies were approximately 15-20%. It was found that X-brace and K-braces with horizontal struts provided equivalent levels of rigidity, while RC IDs provided a higher degree of impact protection than the steel diaphragms. It was further noted that the diaphragms provided more impact-damage protection in skewed bridges than non-skewed bridges, and the type of diaphragm had little influence on the dynamic characteristics of the bridge.

Kentucky DOT (Griffin et al. 1998) studied the influence of IDs on load distribution in PC-girder bridges. They specifically considered 2 bridges with a 50 degree skew angle. One of the bridges had concrete IDs, while the other had no IDs. It was observed that the bridge with IDs experienced increased deterioration of the girders, and the cause of this was further investigated. Field tests and static and dynamic experimental studies were conducted. Testing was done using two fully-loaded, tandem coal hauling trucks, and girder and diaphragm strains were recorded. Calibrated finite element models of the bridges were constructed in SAP90 using frame, shell and solid elements, where frame elements were used to model pier diaphragms and rigid links were developed to connect the end diaphragms with girders at the abutments. Shell elements were used to simulate deck, and diaphragms, barriers, and girders were modeled with solids. Model calibration was done by a trial and adjustment process until model results matched experimental data by altering spring stiffnesses connecting the end abutments and the elastic modulus of structural components. The modeling revealed that the concrete spalling on the ID bridge resulted from excessive girder compressive stresses and stress concentrations at the diaphragm and girder interface. It was further found that the IDs did not significantly reduce girder moments nor aid with load distribution, and the bridge without ID experienced stresses and displacements within AASHTO limit. Use of IDs were recommended only during construction or deck replacements.

LADOT (Cai et al 2008) also examined the need for IDs on PC girder bridges with bulb-T sections and common types of AASHTO girders. The study was conducted using simple and more complex finite element models to explore the effect of various bridge geometries and parameters. The models were developed using GT-STRUDL and ANSYS, where a typical two-lane bridge was considered. Girder type, girder spacing, span length, ID type, skew angle, the compressive strength of concrete, and the number of spans were the primary parameters of consideration. A standard HS-20 truck was used for live load. The study concluded that span length, skew, diaphragm

stiffness and diaphragm location influenced the performance of IDs on load distribution, but continuity, girder spacing, and number of spans were found to be insignificant. It was found that IDs reduced deflection and live load distribution of interior girders and increased the deflection and load carried by exterior girders. From a 5-15% change in load distribution effect was found due to IDs, depending on the assumed connection stiffness between the IDs and girders. The study also led to the development of formulas to determine the effect of diaphragms on load distribution for interior and exterior girders. The study further found little differences in concrete and steel IDs when used during construction. LADOT further funded several studies from 2004-2011, though these concentrated on the effectiveness of pier diaphragms on live load continuous PC structures rather than IDs (Saber et al. 2004; Saber 2009; Okeil 2011). Through this work, it was concluded that these elements had little impact on load distribution.

TxDOT (Stith et al. 2010) developed recommendations for IDs during construction for horizontally curved girders. Although this study did not concern PC girders, many of the stability concepts explored are relevant to current MDOT research. The study focused on early stages of construction and deck replacement when there is little or no additional bracing. ABAQUS was used for modeling where truss elements were used to model the cross frames and bottom braces and plate elements were used to represent the webs and beam elements to represent flanges. Field and laboratory test data were used to verify finite element models. A parametric study was conducted considering radius of curvature, flange width to depth ratio, length to depth ratio, and lift point locations. Eigenvalue buckling and geometrically nonlinear buckling analyses were carried out. It was found that during erection, torsion-induced warping in horizontally curved girders may exceed bending stresses. Although lateral-torsional buckling (LTB) was the often dominant mode of failure during construction, girder curvature also contributes to geometric instability resulting in a propensity to tip over. Recommendations for cross sectional proportioning, and girder lifting, erection, and construction were provided.

Florida DOT (Gull and Azizinamini 2014) developed a set of recommendations for the use of IDs for steel I-girders in design and construction. Straight I-girder bridges, I-girder bridges with skewed supports, and curved I-girder bridges were investigated. For these bridges, three specific load conditions are were considered: no-load, erected-fit with dead load only, and final fit with total dead loads. A simplified FEA model was introduced to simulate lack-of-fit conditions and calculate final cross-frame forces, flange lateral bending stress, vertical reactions, vertical deflections, and cross-frame forces. Different cross-frame configurations, detailing methods, framing layouts and design methods for sizing cross-frame members were described. It was found that diaphragm fitment forces can be significant and may influence girder displacement and stability. They can be simulated in the analysis by imposing prestrains or activating element birth and death options commonly available in commercial FEA codes. While erected fit and final fit detailing methods were recommended for straight and skewed bridges, no-load fit detailing was recommended for horizontally curved bridges.

KDOT sponsored several research projects in the last several decades concerning diaphragms and girder behavior during construction. One of these projects produced a program that could be used to evaluate the torsional response of edge girders during construction, although stability nor other types of failure modes were not evaluated (Roddis et al. 2002). A later study (Roddis et al. 2008) examined diaphragm requirements for steel plate girders to prevent lateral torsional buckling,

while a more recent research effort investigated the placement of diaphragm orientation and placement on lateral flange bending stresses when considering skewed steel bridges (Zhou et al. 2016).

2.5 National Cooperative Highway Research Program (NCHRP) Reports

NCHRP 725 *Guidelines for Analysis Methods and Construction Engineering of Curved and Skewed Steel Girder Bridges* (White et al. 2012) presents results from the analysis of about 70 bridges to determine the effectiveness of different FEA approaches when examining girder stability. For this, the results of various methods were compared with detailed 3D FEA results for accuracy, depending on the parameter investigated. Various codes were considered for the analyses, including STLBRIDGE, VANCK, MDX, LARSA-4D, and ABAQUS. It was found that models that represent girders and diaphragms with beam elements, which typically neglect warping torsional stiffness, often misrepresent diaphragm stiffness. It was further found that diaphragm fitment forces can be significant and may influence girder displacement and stability. It was found that these forces become important when structures with curvature and/or skew are considered, though generally may be neglected for straight, non-skew structures. Recommendations were made for improving modeling efforts. Some of these included representing cross-frames with a shear-deformable beam element; an effective torsional constant which significantly improved the accuracy of 2D analyses; and a simplified method to calculate flange lateral bending stresses. The authors further developed guidelines for the erection of curved and skewed steel bridges. Recommendations were made with regard to erection sequence, crane type, temporary bracing, bearing blocking, tie-downs and jacking devices. It was found that twisting of structures and torsional displacement in horizontally curved and skewed bridges are unavoidable, but curved and skewed I-girder and tub girder bridges have performed well in the majority of cases considered.

NCHRP 298 *Performance of Elastomeric Bearings* (Roeder et al. 1987), and NCHRP 596 *Rotation Limits for Elastomeric Bearings* (Stanton et al. 2008) documents typical bearing pad properties, expected tilt, and rotational performance limits. Such factors are important when girder stability is considered.

NCHRP has sponsored various other research projects that partially or fully concerned diaphragms in the last several decades: NCHRP 322 *Design of simple-span Precast Prestressed Bridge Girders Made Continuous* (Oesterle 1988); NCHRP 519 *Connection of Simple-Span PC Girders for Continuity* (Miller et al. 2004); NCHRP 620 *Development of Design Specifications and Commentary for Horizontally Curved Concrete Box-Girder Bridges*; NCHRP 776 *Bridge System Safety and Redundancy* (Ghosn and Yang 2014), and IDEA 172 *Bidirectional-Ductile End Diaphragms for Seismic Performance and Substructure Protection* (Wei and Bruneau 2015), although none of these concerned IDs for low-curvature, low-skew PC bridges. The two NCHRP studies that did primarily address diaphragms for PC girders (NCHRP 322 and 519) involved pier diaphragms used to develop a live load continuous connection rather than IDs.

Most recently, NCHRP 962, *Proposed Modification to AASHTO Cross-Frame Analysis and Design* (Reichenbach et al. 2021) suggested revisions to AASTHO LRFD diaphragm provisions for steel girder bridges based on field tests as well as extensive numerical modeling. It was found that diaphragms produce most forces on the girder due to live loads when bridges are highly

skewed or greatly curved, whereas straight, non-skew bridges generally produce small diaphragm forces. It was also found that simplified modeling approaches for IDs, such as representing cross-bracing as a single beam element between girders, or using truss elements, can lead to significant discrepancies between the ID model and its actual stiffness.

2.6 Federal Highway Administration (FHWA) Reports

FHWA Report NHI-15-044 *Engineering for Structural Stability in Bridge Construction (*Garlich et al. 2015) confirmed from earlier work that when girders are placed without lateral support of the deck, the two primary failure modes of concern are rollover, or girder tipping, and lateral torsional buckling (LTB). The propensity to tipping as well as LTB is dependent on several factors such as loads, bridge geometry and bearing configuration, and imperfections in the girders such as sweep and twist. Although idealized simple and continuous supports are often assumed for design, it was found that girder instability during construction, particularly with regard to rollover, is significantly influenced, if not a primary function of, the bearing properties. Influential bearing factors include slope, tilt angle, skew, and stiffness. PC girder rollover is often caused by an initial girder rotation, compounded by a deviation in flatness of the bottom flange and bearing roll flexibility. A particular load case of interest for stability as well as girder strength is when the outer wheel of the screed machine rests on the deck overhanging the fascia girder. This, including the dead load of the uncured deck, imparts a significant torsional force to the exterior girder through the deck formwork overhang bracket. This may result in a critical stability issue to be considered. A further issue is ensuring the use of sufficient model detail such that important geometric parameters known to significantly affect diaphragm-influenced stability response can be accurately represented. Some of these include girder sweep, camber, twist, flange flatness, and bearing alignment, expected limits for which can be obtained from PCI quality control standards for precasters (MNL 116-99) and elsewhere.   Each of these effects can be well-modeled with the shell or shell-solid model types.

2.7 Technical Literature

2.7.1 FEA Modeling Approaches for Diaphragms on PC Girder Bridges

Cai et al (2002) analyzed prestressed concrete bridges by conducting field load tests and developing FEA models to determine the effects of diaphragms. It was found that the live load strains obtained from field testing were much lower than those predicted by the AASHTO specifications. It was determined that various factors such as higher concrete strengths, unintended composite action, diaphragms, and barriers may significantly affect bridge performance. The field tests involved six bridges with various span lengths, skew angles, number of lanes, and type of AASHTO PC girder. Testing was conducted with two test vehicles placed side-by-side and strain gauges placed at the bottom of the girders. Strain and deflection measurements were compared with theoretical predictions. The FEA models were constructed using GT STRUDL, where the deck was represented with shell elements and the girder, diaphragms, and parapet were modeled with beams. To account for the correct distance between the deck and girder centroids, the girders were attached to the deck using rigid links. Models were developed with partial IDs, full IDs, and no IDs. Models with no or partial IDs better matched the results of field tests than those using full IDs. The effect of concrete cracking was simulated by reducing diaphragm stiffness. The study also showed that increasing diaphragm stiffness reduces the load distribution factor and maximum

strains in girders. The AASHTO LRFD specifications overestimated distribution factors from 14% to 40%. It was also found that the maximum stresses estimated in the FEA models was much higher than the tensile strength of concrete, suggesting concrete diaphragm cracking and a weak connection between the girder and ID.

A few years later, Cai et al (2007) summarized the current practice regarding ID modeling in PC bridges. The study discussed the importance of quantifying the actual stiffness contribution of the diaphragm and noted that the presence of a weak connection between IDs and girders will significantly influence diaphragm performance. In particular, it was noted that most cast-in-place concrete diaphragms are connected to the girder with a cold joint and firmly joined at spot locations with reinforcing bars. Because the joint may crack, the connection stiffness is a function of the load level applied. To analyze the contribution of IDs, FEA was used with ANSYS, were detailed models utilizing solid elements for the deck, girders, and diaphragms. Simplified models were also constructed where the girders and diaphragms were modeled with beam elements. Several alternative modeling approaches were compared, such as modeling the diaphragm as truss members. The simplified models were found to be relatively accurate and efficient by Cai et al. 2007 as well as in earlier work (Cai and Shahawy 2002; Eamon and Nowak, 2002). The PC bridge models studied used AASHTO Type IV and BT-72 girders and various cases of diaphragms. A significant difference in deflection, strain and load distribution resulted, depending how the diaphragm and its connection was modeled. Based on a literature review, the study also found that the influence of diaphragms on mitigating damage from over-height truck impacts was unclear.

Cai et al (2009) expanded their earlier work to develop empirical formulas to quantify the influence of IDs on load distribution. This parametric study analyzed various bridge configurations using FEA with or without IDs, where girder spacing, slab thickness, span length, skew angle, girder type, and compressive strength of concrete were included in study. Girder spacing, continuity, and compressive strength showed no impact on load distribution due to IDs. GT STRUDL was used to develop linear elastic FE models to analyze the bridge configurations. Plate elements were used to model the deck while line elements were used to model beams and diaphragms. Diaphragms and beams were offset from the centroidal axis of the deck using rigid links. This simplified model was compared to an all-solid element model developed in ANSYS, where load distribution factors and girder strains were found to be within 2%- 4%. The presence of IDs decreased the distribution factor (DF) for interior girders and increased DF for exterior girders. It was also found that increasing the distance between IDs decreased their effectiveness. Skew angle correction factors, representing the ratio of change in DF that IDs have on a straight bridge to that of a skew bridge, were found to be from 0.55 to 0.40 for 30-50 degree skews. Overall, IDs were found to effect DF up to about 10%.

Eamon and Nowak (2002; 2004; 2005) studied the effects of diaphragms along with barriers and sidewalks, on bridge load distribution and ultimate capacity, where both elastic and inelastic analyses were considered. FEA models of various girder bridge geometries, girder, and diaphragm stiffness were modeled and loaded with two HS-20 truck configurations. Simplified FEA models were constructed where the deck was modeled with solids and the girders and diaphragms with beam elements using ANSYS. The models were validated by comparing results to available experimental load distribution data. The studies found that diaphragms in general have little effect on load distribution, bridge ultimate capacity, as well as and reliability in the study. IDs reduced

maximum girder moments up to 13% with an average reduction of 4% across the bridge geometries considered. As a result of this work, a girder distribution factor (GDF) modification expression was proposed (α_d) to approximate the effects of midspan IDs, taken as a multiplier to the existing AASHTO DF:

$$\alpha_d = 1 + (L-10)(S-2)\left(\frac{K_d - 690}{490,000}\right)$$

(2.1)

where L is girder span (m), S is girder spacing (m), and K_d is the girder-to-diaphragm stiffness ratio ($K_d = EI_g / EI_d$). A summary of results is given in Figure 2.1
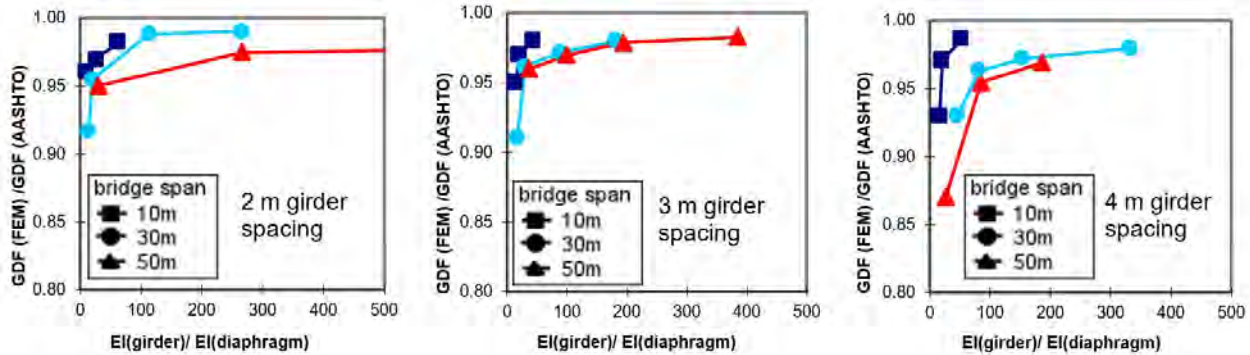
Figure 2.1. GDF for Different Diaphragm Stiffness Ratio, Bridge Span, and Girder Spacing.

Green et al (2002) considered bridge performance with and without IDs, considering different skew angles and temperature changes. FEA models were evaluated with ANSYS using solid elements, while concrete was modeled linear-elastically. A parametric study was conducted to compare deflections and stresses under HL93 loads. The presence of IDs was found to be beneficial for PC girder bridges, reducing maximum deflections by 17% for straight bridges and by about 4%-6% for 60 degree skew bridges. The presence of IDs were also found to significantly decrease deflections due to thermal changes. Later, Green et al (2004) expanded the models to consider bulb-tree girders. Girder performance was analyzed with and without IDs when subjected to HL93 loads as well as the effect of thermal changes. ANSYS was again used to model the bridge using solid elements. Concrete diaphragms were taken to have with a thickness of 0.2 m and were placed at third points along the girder lengths. The girder-diaphragm interface was assumed rigid due to monolithically placed concrete. The study concluded that the presence of IDs reduces girder deflection and effectively increases girder stiffness, where deflection was found to be from 6-19% less than the non-ID bridge, depending on skew.

Li and Ma (2010) presented analysis results for the influence of IDs on a decked bulb-tee girder bridge. FEA models were developed using ABAQUS, where the bridge geometry was represented with shell elements and steel diaphragms were modeled using truss and beam elements. The models were calibrated to available field test data. Different types and numbers of IDs were considered. An example bridge was used to conduct a parametric study, where the influence of IDs on deflection and strain were studied at midspan. The use of IDs reduced maximum girder deflections up to 21% on short span bridges, while it was fund that maximum girder bending moments were most reduced in longer span structures.

18

2.7.2 Other Related Research

Abdel-samad et al. (1968) analyzed multi-cell box girders with diaphragms using thin-wall beam theory. It was found that cross-sectional deformation significantly affects warping, transverse flexural, and well as shearing stresses, and that IDs can reduce this deformation and the resulting stresses.

Sakai and Okumura (1972) analyzed theoretically and experimentally the distortional behavior of box girders with diaphragms. Vlasov's folded plate theory was modified and applied to straight and curved box girders with rectangular and trapezoidal cross sections and curved box-girders. A numerical (finite strip) approach was compared to plate theory results, where no significant differences in response were found.

Sisodiya et al. (1972) investigated the effect of diaphragms to stiffen single and double-cell PC box beam bridges with different skew angles using a FEA approach. It was found that IDs had little effect.

Sithichaikasem and Gamble (1972) studied the effects of diaphragms in bridges with PC girders using plate theory, considering different girder geometries, spacing, torsional stiffness, and location of loads. It was found that when truck wheels are placed on the exterior girders, diaphragms can increase the controlling girder moment. They found IDs to be helpful in all other cases, however.

Dilger and Ghoneim (1988) examined the effect of diaphragms on the performance of skew box beam bridges. It was concluded that using no IDs was a viable alternative to placing skew or orthogonal diaphragms.

Seniwongse, M. (2006) analyzed five different high performance concrete beam bridges in Thailand based on a grillage model, subjected to HS20 trucks. The results indicated that the IDs had negligible effects on girder deflections and stresses. The paper concludes that the IDs can be completely omitted without affecting the serviceability and safety of the structure, in turn saving construction cost and time.

Helwig and Yura (2008a, b) investigated the bracing effect that shear diaphragms, connected to the beam top flanges, have on the stability of cast-in-place beams. Diaphragm stiffness and type of load and load position were investigated. A parametric analysis was conducted using FEA modeling, then design recommendations were provided.

Yang et al. (2008) studied the performance of PC bridge girders with IDs subjected to over-height truck impacts. ABAQUS was utilized to dynamically simulate the impact and bridge response, assuming that the load is applied at the bottom flange of the girder in consideration. The model was used to study the effect of girder spacing, girder type, load, and location and size of IDs. Comparison was made to FE models developed by Abendroth et al. (2004). Design recommendations were developed to implementing the use of IDs in PC girder bridges. Such recommendations included spacing ID within 20-40 ft for 100 ft spans and one ID at the center of 50 ft spans.

Egilmez et al (2012) studied the bracing behavior of Permanent Metal Deck Form (PMDF) systems. Computational and experimental studies were conducted on a twin girder PMDF system in shear. Results from lateral displacement tests were used to measure the lateral stiffness of the assembly, with deformations consistent with the shapes of buckled girders. The results were used to develop a FEA model, so that parametric studies could be conducted. ANSYS was utilized to develop the models, where the PMDF bracing was modeled with truss elements connected to the girders. Laboratory and FEA analyses demonstrated that the PMDF systems can provide significant bracing to steel bridge girders, resulting in a viable bracing alternative that reduces the need for diaphragms in steel girders bridges during construction.

Mohseni et al. (2014) studied the effects of IDs on load distribution factors for moment and shear for concrete multicell box-girder bridges using the FEA program CsiBridge. Here, models were constructed for structures with different skew, span length, IDs, and number of boxes. The models were then loaded with HL93 live load. Validation of the linear elastic models was by comparison to field test results obtained from Ashebo et al (2007), where a three-span continuous bridge was considered. The experimental findings and the finite element model produced similar results. A parametric study was conducted to determine the effects of IDs with regard to span length, skew angle, and ID arrangement. Correction factors were proposed to adjust live load distribution factors when considering IDs.

Vu et al. (2018) studied the effects of IDs on the load carrying capacity of Steel-Concrete Composite Box (SCCB) girder bridges with open steel box sections. ABAQUS was used to develop FEA models of the bridges, where nonlinear inelastic analysis were conducted to capture girder overload behavior. Concrete and steel material models were developed based on material stress-strain curves, while plastic damage models were used to consider changes in strength under compression and tension. Solid elements were used to model the concrete deck and plate elements were used to model flanges, webs, diaphragms, and stiffeners, while concrete slab reinforcement was modeled with quadrilateral surface elements. The validation of the model was conducted by comparing results to tests of a simply supported SCCB girder. A parametric study was conducted that included consideration of wind load and dead and live loads. Bridge dimensions, mesh size, loading conditions, and the effect of ID were examined. Based on the results, IDs were recommended to be placed at the bridge mid-span.

Krahl et al. (2020) used an analytical approach, a variational Rayleigh-Ritz method, to investigate the rollover behavior of PC beams. In this study, nonlinear solutions to rollover are developed, while considering initial imperfections and beam camber. It was found that stability is highly sensitive to initial imperfections, while the initial rotation was found to be most critical.

2.7.3 Potential Model Validation Data

Abendroth et al. (1991). Constructed three-girder experimental PC bridge models with reduced deck thickness and less reinforcement for testing. The specimens had diaphragms at mid-span and at third-span locations. The models were instrumented with strain gauges on the girders, diaphragms, and bridge deck. Deflections and strains were recorded for horizontal and vertical loads exerted on the bridge.

Newmark et al. (1964) constructed and tested a series of quarter-scale models, one of which represented a 60 ft long composite steel bridge with five girders spaced at 6 ft and no barriers or sidewalks, but including diaphragms. The model was loaded with two concentrated loads at midspan, and bridge deflections were recorded.

Beal (1982) tested two 1:5.9 reduced scale concrete bridge deck models based on 5-girder, 72 ft long bridge. The decks were subjected to a series of wheel load tests. The first concrete deck satisfied AASHTO reinforced requirements, whereas second concrete deck had varying amounts of reinforcement. Four concentrated loads were applied near mid-span. Deck strain data were recorded, and deck stresses computed based on measured strains and material properties. Service load bending moments were found to be from 40-65% of those predicted by flexural theory.

Wipf et al (1990) conducted experimental tests on full-scale laboratory deck bridges made of glue-laminated timber of 24 ft width and spanning 26 ft. The bridge included stiffener beams transverse to the span direction. Deck deflections and strains were recorded. SAP was used to develop a finite element model with plate elements while stiffener beams were modeled with beam elements. Differences between numerical and experimental results ranged from about 7-8%, depending on bridge configuration.

Fang et al (1990) conducted an experimental and numerical investigation of a full scale bridge deck representative of that on 49 ft span composite steel girder bridge with 7 ft girder spacing. The deck was loaded with four concentrated loads and stresses on the deck underside were calculated. SAP was used to construct detail FEA models of the deck, where plates were used to model the deck and girders. Overload behavior was also considered, where a smeared cracking model was used to model deck cracking. Numerical and experimental results were found to be in reasonable agreement. The deck slab was found to behave linearly even under overload conditions.

Zureick et al (2009) experimentally examined the LTB stability of 11 nonprestressed reinforced concrete sections from 12-40 ft long, as well as 6 PC beams, accounting for initial sweep, and developed expressions to predict LTB capacity. It was found that the maximum girder length below which LTB occurred varies from 127-193 ft for AASHTO girders of Type I-VI, and maximum AASHTO girder length governed by rollover varies from 75 – 140 ft, using a safety factor of 1.5, depending on girder type.

Hurff and Kahn (2012a) Tested six 32 ft long slender PC beams for lateral torsional buckling (LTB), where load-lateral displacement curves were recorded. It was found that the PC beams behaved similarly to RC sections subjected to LTB, and the response could be well predicted by traditional analytical approaches. Further, beam stability was sensitive to initial imperfections such as sweep and rotation.

Hurff and Kahn (2012b) tested a 100 ft PCI BT-54 PC beam placed on elastomeric bearings for rollover. Vertical and lateral displacements, as well as torsional deformations and strains, were recorded at midspan and the supports. The effect of initial imperfections such as sweep, rotation, bottom flange flatness, and bearing pad stiffness were considered. Load-lateral displacement and

rotation data were recorded. It was found that sweep and rotation imperfections significantly impacted results. The experimental data could be reasonably predicted by numerical analysis.

Eamon et al. (2016) conducted field tests on two live load continuous PC girder bridges. Girders were instrumented with strain gauges at midspan and near the central pier. Strain data were recorded for 15 different loading patterns using 11-axle trucks. Girder distribution factors (GDFs) were calculated and compared with AASHTO values. FEA models of the bridges were constructed using solid elements for the deck and plate elements to represent the girders and diaphragms. Good agreement was found between the experimental and numerical results.

2.8 Summary

In general, IDs are primarily used to prevent girder instabilities during construction; to enhance gravity load distribution among girders; and to aid in horizontal load sharing from over-height vehicle collisions. As summarized above, a literature review revealed that some studies have found IDs to be useful during construction and potentially during deck replacement to aid in girder stability and prevent lateral torsional buckling and rollover. However, most studies have found that IDs minimally influence live load distribution, generally within the range of 10% and often less. A few studies have examined the ability of IDs to mitigate over-height vehicle collision damage, but a variety of results and recommendations were obtained. Various FEA modeling techniques have been used to model bridge and diaphragm behavior, from complex all-solid models, using plates for the deck and/or girders, to using plates or solids for the deck and beam elements to model beams and diaphragms. Most techniques can be used to accurately represent experimental data for load distribution if models are carefully constructed, though usually only more refined models are reliable for examining girder instabilities during construction. Correspondingly, there appears to be a consensus that diaphragms are needed to ensure stability during construction/deconstruction when girders are not otherwise laterally braced. There is no consensus on the need for diaphragms on an in-service bridge.

CHAPTER 3: ANALYSIS OF MDOT BRIDGE DATABASE

3.1 Introduction

To determine typical bridge geometries for analysis, records from the MDOT bridge inventory were analyzed to determine the frequency of occurrence of various characteristics of PC beam bridges. The analysis was limited to beam-type PC bridges only; including all types of PC bridge structures will produce a larger data pool with different results. Because the bridge inventory does not indicate girder spacing, an additional set of PC beam bridge plans obtained from MDOT was also evaluated. These plans were further used to verify the reasonableness of girder spacing, span, and girder size used in the later parametric analysis.

3.2 Results of Bridge Inventory Analysis

Considering all years of construction, overall, 5468 MDOT bridges appear in the inventory, where 24% (1332) are PC beam bridges. Of these, only 3 are recorded as continuous structures, though clearly many more are designed as live-load continuous and not specifically indicated as such in the database. Tables 3.1-3.9 describe the characteristics of PC beam bridges. Note that a complete set of data does not appear for all entries, thus the total number of bridges in each table may not sum to the total of 1332. In summary, 21% of PC bridges are box beam and an additional 15% are spread box beam structures. The remaining 64%, recorded as "composite" or "non-composite" are assumed to be girder structures (Table 3.1). The majority (57%) of structures were built between 1950-1979, where 16% were build prior to 1950 and 27% built from 1980-present (Tables 3.2 and 3.2a). Most PC bridges (32%) have a single span in the main bridge unit, although 2-4 spans are fairly common as well, accounting for 20, 25, and 17% of structures, respectively. In total, 94% of structures have from 1-4 main unit spans (Table 3.3). The large majority (97%) have no approach spans (Table 3.4). Ignoring structures less than 20 ft in length, most (76%) have a maximum span length less than 100 ft, while 91% have a maximum span less than 120 ft and 96% less than 150 ft (Table 3.5). The total bridge length is highly variable, with a significant number of structures spread throughout a wide range of lengths (Table 3.6). Most (58%) have deck widths less than 60 ft, while 75% have widths less than 80 ft (Table 3.7). Approximately 42% have zero skew; 64% have skew no greater than 15 deg; 81% have skew within 30 deg; and 93% have skew no greater than 45 deg (Table 3.8). Finally, the most common design load used (42%) was greater than HS-25, whereas the least common (3%) was HL-93 (Table 3.9).

Only considering bridges built from 2000-2019, 217 PC beam bridge records exist. None of these are reported as continuous. Comparing this set of structures to the set built across all years, little difference can be seen in terms of frequency of structure types (Table 3.1), number of approach spans (Table 3.4), total bridge length (Table 3.6), and skew (Table 3.8). However, a larger proportion of modern structures have a single main unit span (58% vs 32% for all years), and a smaller proportion of modern structures are built with maximum spans from 40 – 80 ft, deck widths from 30-40 ft, and considering a HS-20 design load.

Table 3.1. Structure Type.

All Years		2000-2019		
No.	Frequency	No.	Frequency	Beam Type
709	0.53	113	0.52	Composite
150	0.11	19	0.09	Non-composite
279	0.21	51	0.24	Box
194	0.15	33	0.15	Spread box

Table 3.2. Year Built.

No.	Frequency	Year Built
14	0.01	1900-1909
1	0.00	1910-1919
48	0.04	1920-1929
86	0.06	1930-1939
57	0.04	1940-1949
170	0.13	1950-1959
377	0.28	1960-1969
217	0.16	1970-1979
89	0.07	1980-1989
56	0.04	1990-1999
126	0.09	2000-2009
91	0.07	2010-2019

Table 3.2a. Year Built From 2000-2019.

No.	Frequency	Year Built
31	0.17	2000-2004
60	0.33	2005-2009
51	0.28	2010-2014
39	0.22	2015-2019

Table 3.3. Number of Spans in Main Unit.

All Years		2000-2019		
No.	Frequency	No.	Frequency	Spans
430	0.32	125	0.58	1
261	0.20	45	0.21	2
331	0.25	31	0.14	3
232	0.17	9	0.04	4
31	0.02	1	0.00	5
21	0.02	4	0.02	6
22	0.02	2	0.01	> 6

Table 3.4. Number of Approach Spans.

All Years		2000-2019		
No.	Frequency	No.	Frequency	App. Spans
1291	0.97	212	0.91	0
2	0.00	1	0.00	1
14	0.01	2	0.01	2
3	0.00	0	0.00	3
6	0.00	0	0.00	4
17	0.01	19	0.08	> 4

Table 3.5. Maximum Span Length.

All Years			2000-2019			
No.	Frequency	Freq. 20' +	No.	Frequency	Freq. 20' +	Max Length
189	0.14	--	35	0.16	--	< 20'
63	0.05	0.06	20	0.09	0.09	20 - 30
72	0.05	0.06	12	0.06	0.06	30 - 40
114	0.09	0.10	10	0.05	0.05	40 - 50
149	0.11	0.13	10	0.05	0.05	50 - 60
136	0.10	0.12	12	0.06	0.06	60 - 70
152	0.11	0.13	11	0.05	0.05	70 - 80
94	0.07	0.08	18	0.08	0.08	80 - 90
93	0.07	0.08	15	0.07	0.07	90 - 100
70	0.05	0.06	18	0.08	0.08	100-110
58	0.04	0.05	14	0.06	0.06	110 -120
41	0.03	0.04	10	0.05	0.05	120 -130
30	0.02	0.03	8	0.04	0.04	130 -140
27	0.02	0.02	7	0.03	0.03	140 -150
11	0.01	0.01	3	0.01	0.01	150 -160
9	0.01	0.01	5	0.02	0.02	160 -170
8	0.01	0.01	5	0.02	0.02	170 -180
4	0.00	0.00	1	0.00	0.00	180 -190
11	0.01	0.01	3	0.01	0.01	> 190

Table 3.6. Total Bridge Length.

	All Years			2000-2019		
No.	Frequency	Freq, 20'+	No.	Frequency	Freq, 20'+	Length
160	0.12	--	31	0.14	--	< 20'
91	0.07	0.08	20	0.09	0.09	20 - 30
59	0.04	0.05	11	0.05	0.05	30 - 40
33	0.02	0.03	7	0.03	0.03	40 - 50
27	0.02	0.02	7	0.03	0.03	50 - 60
18	0.01	0.02	6	0.03	0.03	60 - 70
19	0.01	0.02	5	0.02	0.02	70 - 80
19	0.01	0.02	7	0.03	0.03	80 - 90
27	0.02	0.02	5	0.02	0.02	90 - 100
36	0.03	0.03	5	0.02	0.02	100-110
45	0.03	0.04	5	0.02	0.02	110 -120
49	0.04	0.04	5	0.02	0.02	120 -130
43	0.03	0.04	7	0.03	0.03	130 -140
52	0.04	0.04	6	0.03	0.03	140 -150
41	0.03	0.03	6	0.03	0.03	150 -160
55	0.04	0.05	6	0.03	0.03	160 -170
73	0.05	0.06	10	0.05	0.05	170 -180
32	0.02	0.03	4	0.02	0.02	180 -190
29	0.02	0.02	4	0.02	0.02	190 -200
180	0.13	0.15	19	0.09	0.09	200 -250
108	0.08	0.09	12	0.06	0.06	250 -300
41	0.03	0.03	8	0.04	0.04	300 -350
39	0.03	0.03	10	0.05	0.05	350 -400
15	0.01	0.01	3	0.01	0.01	400 -450
8	0.01	0.01	2	0.01	0.01	450 -500
43	0.03	0.04	5	0.02	0.02	> 500

Table 3.7. Deck Width.

All Years		2000-2019		
No.	Frequency	No.	Frequency	Deck Width
78	0.06	16	0.07	< 20'
48	0.04	2	0.01	20 - 30
227	0.17	8	0.04	30 - 40
417	0.31	63	0.29	40 - 50
132	0.10	31	0.14	50 - 60
140	0.11	30	0.14	60 - 70
84	0.06	22	0.10	70 - 80
38	0.03	5	0.02	80 - 90
24	0.02	7	0.03	90 - 100
49	0.04	8	0.04	100 - 120
27	0.02	2	0.01	120 -140
24	0.02	7	0.03	140 - 160
16	0.01	4	0.02	160 - 200
11	0.01	3	0.01	200 - 250
8	0.01	4	0.02	250 - 300
7	0.01	2	0.01	> 300

Table 3.8. Skew.

All Years		2000-2019		
No.	Frequency	No.	Frequency	Skew
553	0.42	80	0.40	0˚
119	0.09	30	0.15	1 - 5
76	0.06	11	0.05	6 -10
86	0.07	13	0.06	11 - 15
88	0.07	15	0.07	16 - 20
67	0.05	10	0.05	21 - 25
72	0.05	12	0.06	26 - 30
156	0.12	19	0.09	31 - 45
63	0.05	6	0.03	46 - 60
30	0.02	6	0.03	60 +

Table 3.9. Design Load.

All Years		2000-2019		
No.	Frequency	No.	Frequency	Design Load
138	0.10	20	0.11	< HS-20
271	0.20	11	0.06	HS-20
174	0.13	23	0.12	HS-20-Mod
557	0.42	83	0.45	HS-25+
39	0.03	9	0.05	HL-93
160	0.12	40	0.22	> HL-93

3.3 Results of Bridge Plan Set Analysis

The plans of fifteen recently constructed or reconstructed PC bridges, many on I-75, were reviewed to extract geometric information. Of these, (single) spans ranged from 31 to 156 ft, with an average single span of 106 ft. About half of the structures were single span, a single structure was three span, and the remaining structures were two span. Girder spacing ranged from approximately 6 to 9 ft, with an average of 7.6 ft. Most girder types were bulb tee (with a single MI-1800 girder bridge), with two box beam bridges, and one AASHTO beam bridge. A detailed summary of this information is given in Appendix A.

CHAPTER 4: SURVEY OF STATE DOTS

4.1 Summary

A survey was submitted in January, 2020 in Word document form to the State DOT research offices to document the current practice for intermediate diaphragm use on PC bridges. Twenty-two responses were received. Participating States are given in Table 4.1 below.

Table 4.1. Participating States.

Alaska	Maine
Arkansas	Minnesota
Colorado	Missouri
Delaware	Mississippi
Florida	North Carolina
Idaho	New Hampshire
Illinois	New York
Indiana	Ohio
Iowa	Rhode Island
Kansas	South Carolina
Louisiana	Utah

Detailed survey responses from all participating states are given in Appendix B. A brief summary of the questions and the responses are given below. Note that all questions were answered by all respondents except FDOT, where no response was given for questions 2, 3, 5, and 7. However, FDOT indicated in question 1 that IDs were not required for these structures; thus, the missing responses were recorded as "NA or "not required".

Q1. Does your State require intermediate diaphragms (IDs) for low skew, low curvature PC bridges?

Yes:	15
No:	3
Depends:	4

Q2. If required, where and under what conditions must they be placed (e.g. based on bridge geometry, beam size, end bearing details, deck overhang, sequence of deck placement, etc.?) If a reference exists that summarizes these requirements, can you please provide a link to, or name of, the reference?

A single IDs is required at midspan:	3
IDs are a function of span (from 0-4 IDs, depending on DOT):	8
IDs are a function of beam type (either 1 ID at midspan or no IDs):	1
IDs are a function of span and beam type (from 1-3 IDs, depending on DOT):	5
A stability analysis is required to assess the need for IDs:	2
NA/none required:	3

Q3. If required, what is the purpose(s) of IDs on these structures?

       Resist lateral loads (wind, seismic, vehicle impact, and/or ship collision):   8
       Vertical live load distribution: 2
       Construction stability: 16
       Other ("utilities"; redundancy):   2
       NA/none required   3

       Note that all reasons provided by a single DOT were marked above, so the total results above exceed the number of DOTs responding to the survey.

Q4. If you do not use IDs to mitigate the effects of over-height vehicle impacts, is there another mechanism that you use for this purpose?

       None: 10
       Provide adequate clearance: 5
       Use to resist vehicle impact: 7

Q5. What type of IDs (cast-in place concrete, steel cross-bracing, or another configuration) are allowed on these structures? Does the allowed type change in different scenarios?

       Concrete only: 3
       Concrete or steel: 8
       Steel only: 8
       NA/none required: 3

Q6. In cases when there is an end diaphragm/dependent backwall, do you require the installation of the end diaphragm prior to the placement of the deck?

       Yes: 6
       No: 14
       NA/not clear answer: 2

       Note that for the above, a respondent was counted as 'yes' only if the backwall or end diaphragm was used to serve as bracing during the deck pour. For those in the 'no' category, many indicated that the backwall was cast monolithically with the deck.

Q7. Does the placement of end diaphragms prior to the placement of the deck affect the policy for requiring IDs?

       No or Not applicable: All respondents (22)

Q8. Does your State have a clear policy that distinguishes between the responsibilities of the contractor and the engineer of record to provide stability during construction? If so, can you please briefly describe?

No clear policy: 5
Contractor's responsibility: 13
Engineer's responsibility: 4

Q9. Has your State recently changed its policy on ID placement for low skew, low curvature PC bridges? If so, why?

No: 19
Yes: 3

The three DOTs answering 'yes' were: LADOT, where policy was revised based on a 2008 research project; MSDOT, who discontinued ID use in 2014; and UDOT, where rules for ID use were recently revised but yet to be implemented.

Q10. Has your State recently sponsored any research on this topic? If so, can you please provide a link to, or name of, the reference?

No: 20
Yes: 2

The 'yes' respondents were FDOT, who sponsored a 2014 study focused on steel girders, and LADOT, which sponsored research in 2008 on this topic.

In summary, most of the states surveyed require IDs in some or all cases; allow the use of steel IDs more often than concrete; vary the number of IDs required as a function of span and/or beam type, and use IDs for construction stability or non-vehicular load distribution. About half of the respondents place the responsibility of stability during construction on the contractor.

CHAPTER 5: MODEL VALIDATION

5.1 Introduction

5.1.1 Modeling Needs

In the bridge life cycle, three primary modeling configurations of concern are: 1) girders are placed, but without the deck, both before and after lateral support is provided, such as from backwalls, diaphragms, or temporary bracing; 2) girders supporting an uncured deck and construction loads (during construction/deck replacement), and; 3) girders act compositely with the deck (in service, under various load levels). The FEA models developed must have the ability to address each of these scenarios.

In configurations 1 and 2, where the girders are placed without lateral support of the deck, various studies have indicated that the two primary failure modes of concern are rollover, or girder tipping, and lateral torsional buckling (LTB) (Garlich et al. 2015; White et al. 2012). Note, however, that although possible, LTB is rarely an issue with PC or bulb-tee beams (Hurff and Kahn 2012), and especially not for box girders. In configuration 3, when the bridge is a complete structural system used in service, various field and numerical studies have demonstrated that instability is not a concern, even up to a complete overload failure of the entire bridge where multiple girders reach ultimate capacity in parallel (Eamon and Nowak 2004). In this case, the primary effect of the ID is to alter live load distribution to the girders. Therefore, the purpose of analyzing configuration 3 is to quantify this effect, and to determine when, or if, IDs are needed to assist in load distribution.

Thus, three types of model configurations are required to address the concerns above: 1) to assess the in-service bridge, where the effect of IDs on live load distribution is the primary concern; 2) to assess girder LTB instability during initial construction and deck replacement; and 3) to assess girder rollover instability during initial construction and deck replacement.

5.1.2 General Considerations

For a feasible parametric analysis, a balance must be maintained between accuracy and computational efficiency. To this end, various types of elements have been used to model bridges in the last several decades. Five common model types, in order of decreasing complexity, are:

- All solids, in which the complete structural geometry is explicitly modeled;
- A shell/solid combination, where the deck is modeled with one element type and the girders with the other;
- All shells, where the deck, girder flanges and webs are modeled with shells;
- Beam combination, where girders are represented with beam elements and the deck with shells or solids; and,
- All beams (grillage), where the entire bridge is modeled as a grid of beams.

Each of these model types has been used to successfully capture live load distribution to the girders. However, more difficult to model accurately is transverse load distribution within the deck and the corresponding interaction of the diaphragms (Bakht and Jaeger 1989). This is particularly

true with models that represent girders and diaphragms with beam elements (i.e. beam combination and all beam), which typically neglect warping torsional stiffness and often misrepresent diaphragm stiffness (White et al. 2012). Another concern with using beam elements is that the girder centroids are not properly offset from the deck. Although methods have been proposed by the Principal Investigator and others to address these issues (Eamon 2000; White et al. 2012; Cai et al. 2007), such as using rigid links as offset elements and artificially increasing element torsional or flexural stiffness, these introduce additional approximations which have uncertain accuracy in previously unverified modeling situations. Garlich et al. (2015) concluded that such models are generally not sufficiently accurate for bridge stability analyses. In contrast, the shell and solid model types have been found by numerous researchers to have the ability to well-represent bridge behavior and the influence of IDs when construction instabilities as well as in-service behavior is considered (Gull et al. 2014; White et al. 2012; Stith et al. 2010, etc.). Here, caution must be used to model the deck with shell elements, which requires the use of rigid links to properly offset the deck centroid. Using the rigid link approach has the potential to introduce unintended inaccuracies with diaphragms under certain load and bridge geometry scenarios.

In this study, the global response of the structure is of primary interest rather than localized stress analysis, and as such, highly detailed geometric modeling of cross-sectional shapes and IDs represents needless complexity. As discussed above, however, accurately representing torsional stiffness as well as positioning the centroids of major cross-section elements is warranted. A further issue is ensuring the use of sufficient model detail such that important geometric parameters known to significantly affect diaphragm-influenced stability response can be accurately represented. Some of these include girder sweep, camber, twist, flange flatness, and bearing alignment (Garlich et al. 2015), expected limits for which can be obtained from PCI quality control standards for precasters (PCI MNL-116-99) and elsewhere. Each of these effects can be well-modeled with the all solid or shell-solid model types expected to be used in this research (Garlich et al. 2015).

Therefore, for all model types, either an all solids, shell/solid, or all shells idealization will be used, which have the potential to provide the greatest accuracy and avoid many of the modeling difficulties with simpler representations discussed above.

5.2 Model Validation: In-Service Bridge System

5.2.1 Modeling Considerations

For the in-service case, a linear, static analysis is suggested, as geometric non-linearities are insignificant and the onset of material nonlinearity in a PC girder in service (assuming cracking is unacceptable) may be taken as a failure. Note some minimal acceptable cracking may occur in reinforced concrete components (e.g. concrete ID, deck). This can be accounted for in the linear analysis as needed by utilizing equivalent cracked-elastic properties for the deck, diaphragms and connections, and/or girders. However, cracking is generally not expected for well-maintained structures designed to AASHTO LRFD that are subjected to service loads.

Very few suitable model validation data exist for entire bridge systems. A survey of the literature recovered only two laboratory-based bridge structural systems sufficiently documented to allow model assessment of vertical load distribution: a quarter-scale bridge using steel girders and a

reinforced concrete deck studied by Newmark et al. (1946), and a small but full-scale PC bridge studied by Abendroth et al. (1991). Although PC girder bridges are the focus of this study, as discussed above, of critical importance is the ability of the FEA approach to model the response of a girder bridge in the linear range. As such, using the linear elastic material properties of steel, concrete, or any other material, has no significance when assessing the ability of the model to represent the behavior of the structure in the linear range. Thus, the steel girder bridge model can also provide valuable data to assess the validity of the approach used. A much larger number of bridge field test data exist. This data, unfortunately, is often of limited use for general model validation due to the many unknowns that exist for the field structure which are well controlled in the laboratory. Chief among these unknowns are the boundary conditions, where the end walls, approach slap, and even bearings, provide various and generally unknown degrees of longitudinal and rotational constraint, constraints that are well-known to have significant effect on system behavior. Thus, using this data is not the focus of this task. However, two field test results are included for comparison. Specific validation models and results are discussed below.

5.2.2 Validation Model 1: Newmark Test Data

5.2.2.1 Test Specimen

Newmark et al. (1946) constructed a series of quarter-scale steel girder bridges in the laboratory to assess the effect of several parameters on vertical load distribution. These models are based on a full-scale simple span, 5-girder bridge of 60 ft length and 24 ft width. The model considered for this validation study is specimen C15 from Test Series III. The scaled bridge properties relevant to this study are: span 15 ft; girder spacing 1.5 ft; steel girders M8 x 6.5; slab depth 1.75 in; L3x2x3/16 diaphragms (single angle) placed at midspan; C4x5.4 diaphragms (single channel) placed at ends; Young's Modulus E of deck 3750 - 4000 ksi (unclear; given as 3750 ksi and 4000 ksi in alternative locations in the report). A diagram of the bridge specimen is shown in Figure 5.1.
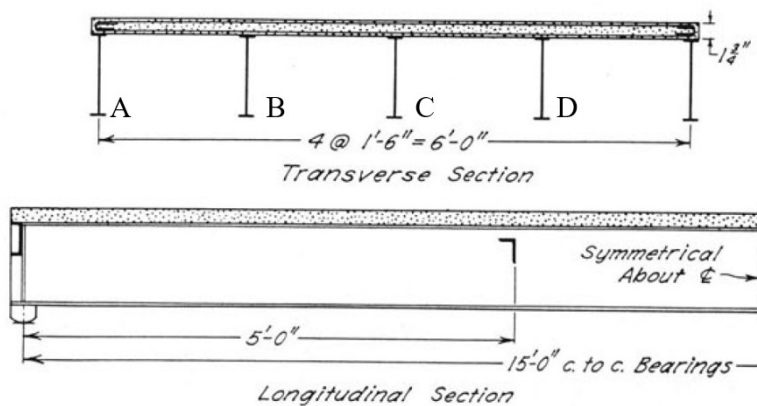
Figure 5.1. Bridge Model C15 (from Newmark et al. 1946).

The bridges were tested by moving a 700 lb. point load transversely across the deck, where girder strains were recorded.

5.2.2.2 FEA Model

The model is composed of approximately 22,700 elements, where quadratic (20-node) solids are used for the deck and quadratic (8-node) shells for the girders and diaphragms. The latter are tied to the girder webs. Vertical supports were placed at the center of the lower flanges at the ends of the girders while lateral constraints were placed at the same positions at the center girder only, as well as a single longitudinal constraint on one end of the center girder for stability. Girder steel was modeled with $E = 30,000$ ksi and Poisson ratio $\nu = 0.29$, while given the uncertainty in the deck stiffness, an average modulus of $E = 3900$ ksi was used for the deck, with $\nu = 0.19$. Images of the model are shown in Figure 5.2.
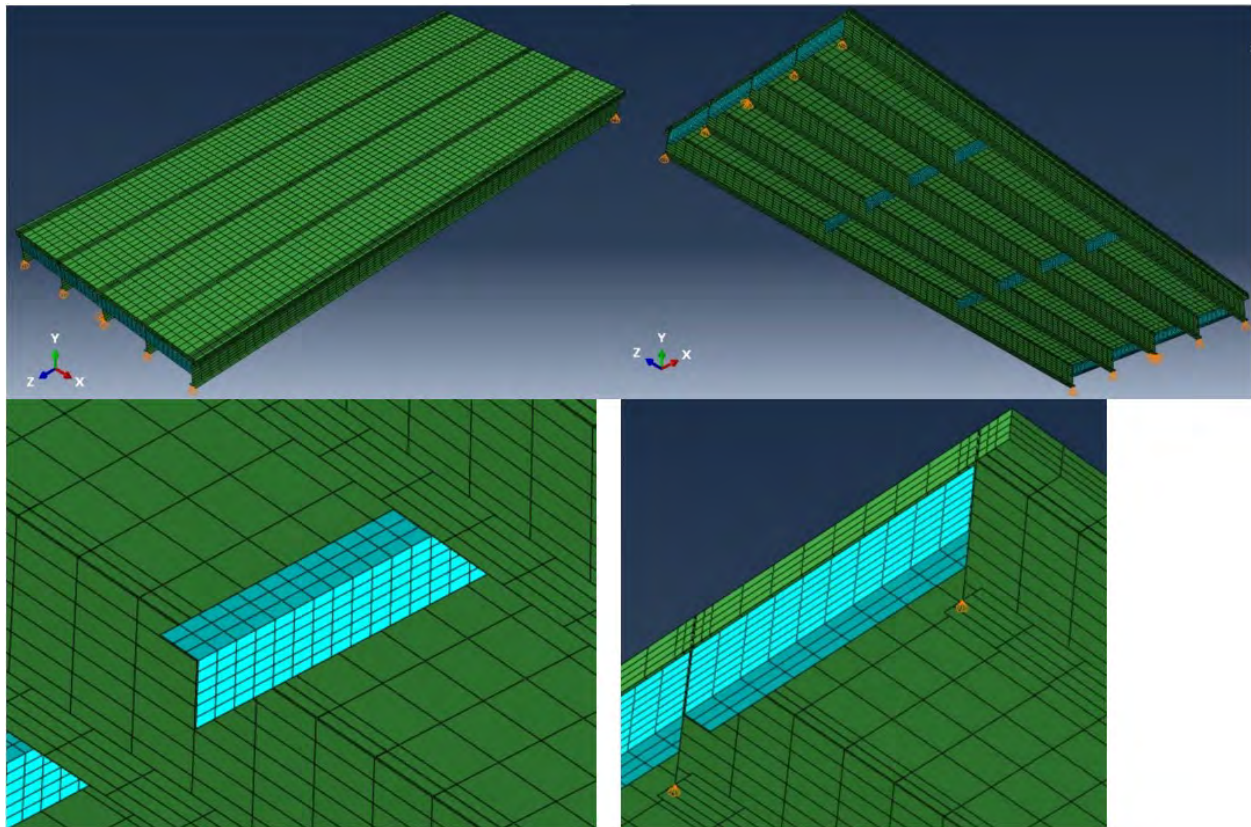
Figure 5.2. FEA Model of Newmark Bridge.

5.2.2.3 Results

Results are provided in Figures 5.3-5.5, which show midspan strains on the center (C), intermediate (B and D), and exterior (A and E) girders, respectively, as a function of load position transversely on the bridge. Girder labels are given in Figure 1 above. Since a nearly identical symmetric response was found experimentally, only one graph is provided to represent both intermediate girders and one to represent both edge girders. On the graphs, a dual position label (i.e. "AB") refers to a load placement on the deck, midway between the adjacent girders.
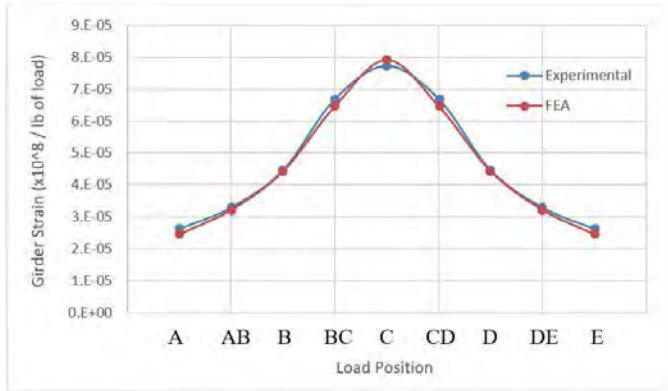
Figure 5.3. Center Girder (C) Strains.
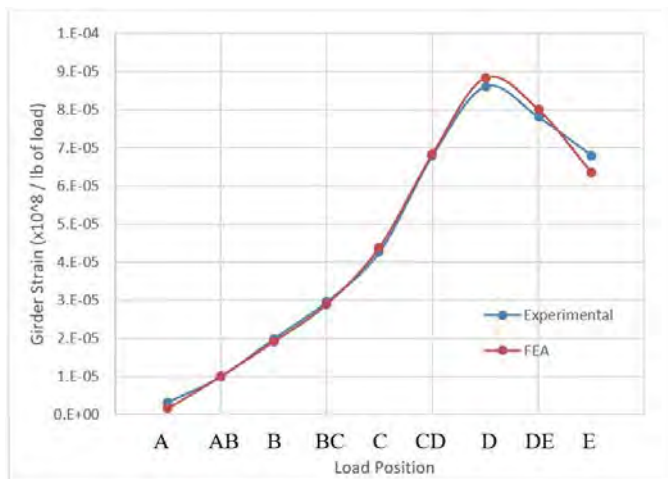
Figure 5.4. Intermediate Girder (D) Strains.
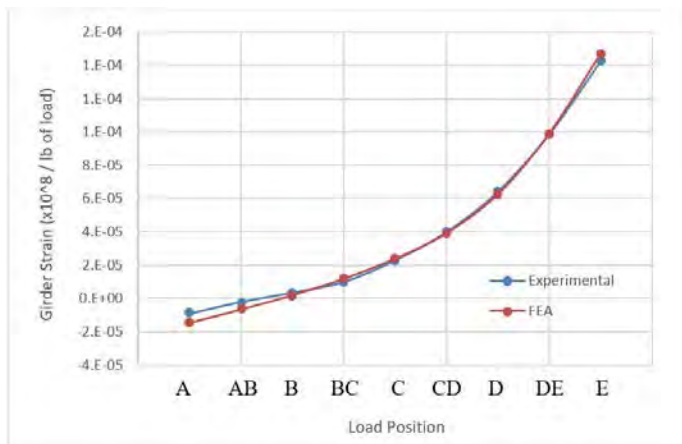
Figure 5.5. Edge Girder (E) Strains.

As shown, excellent agreement exists between experimental and model results. A typical deformed shape of the model is given in Figure 5.6, due to a load applied on the central girder.
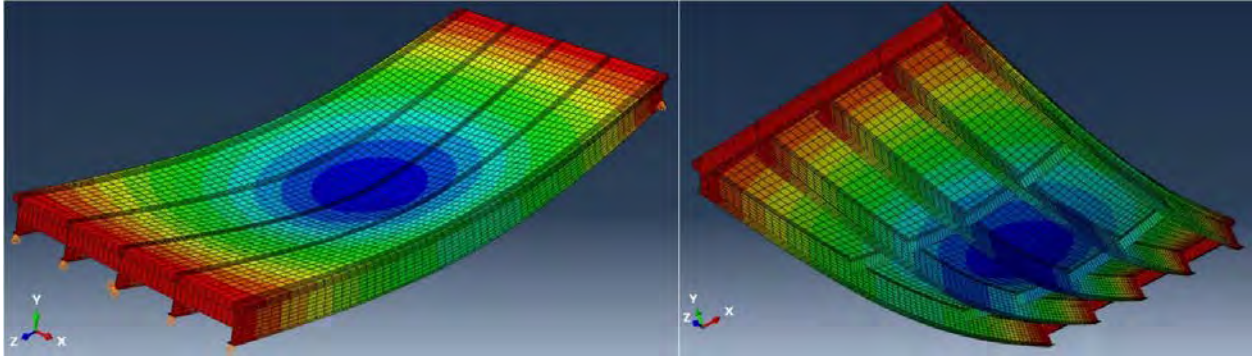
Figure 5.6. Deformed Shape of Newmark Bridge Model Under Load on Center Girder.

Out of interest, this model was used to predict midspan deflection under two 1 kip point loads placed at locations BC and CD with and without the model diaphragms. Results are given in Figure 5.7. The presence of diaphragms results in a maximum deflection difference (and can be expected to produce a similar change in girder distribution factor) on an interior girder of about 6%, which is within the range of typical results found by other studies described in the literature review.
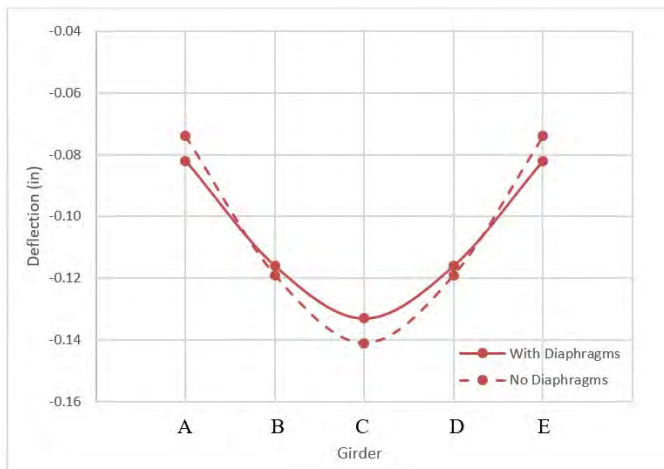
Figure 5.7. Model Deflection Prediction With and Without Diaphragms.

5.2.3 Validation Model 2: Abendroth Test Data

5.2.3.1 Test Specimen

Abendroth et al. (1991) tested a full-scale PC bridge model in the laboratory to assess the effect of diaphragms on horizontal and vertical load distribution. The model is approximately 40 ft long, 18 ft wide, and has three Iowa A38 PC (32 in) girders supporting a 4 in. reinforced concrete deck with 1.5 in. haunches, as shown in Figure 5.8. The boundary conditions are somewhat complicated, as the beams rest upon elastomeric pads with unknown properties, then the girder ends were joined into a continuous 14 in. thick end wall similarly poured into and supported by an 18 in. wide, 42 in. tall abutment that the girder ends (via bearing pads) rest upon, where the

abutment rests on the laboratory floor. Girder concrete has a reported compressive strength of f'_c = 7270 psi, while the deck concrete varied from 4360–6870 psi, depending on location, though 75% of the deck was reported to contain 4360 psi material. No modulus of elasticity data is given. The specimen was loaded vertically (loads pressed upwards from below on the lower girder flanges) as well as laterally in various stages that caused severe deck cracking, in configurations without IDs as well as those that included IDs, where girder strains and deflections were recorded.

A large number of load sequences were tested at different load levels and for the different diaphragm configurations, where 9 points were loaded vertically on the deck surface, and the midspans of the three girders were loaded horizontally. Unfortunately, high levels of load were applied for each individual load test (at each point, up to 25 kips vertically and 75 kips horizontally), which caused progressively worse and significant deck cracking. This cracking has clear implications on the stiffness of the deck, which would be expected to decrease further with each subsequent load test. Thus, significant unknowns exist in the effective stiffness of the deck.
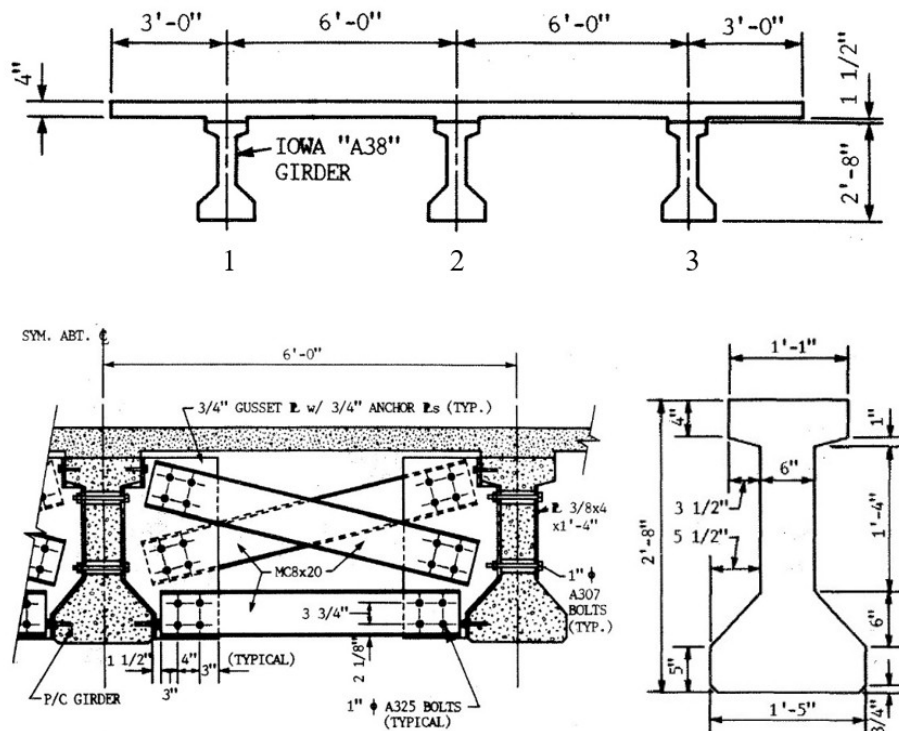
Figure 5.8. Abendroth Test Bridge and Chosen Diaphragm Type (from Abendroth et al. 1991).

5.2.3.2 FEA Model

The model is composed of approximately 11,200 elements, where quadratic solids are used for both deck and girders. Vertical and lateral supports were modeled similarly to those of the Newmark model. Because the construction of the end supports contain numerous unknown stiffness parameters (bearing properties, abutment-endwall-girder connection stiffness; longitudinal and horizontal frictional constraints of the wall on the laboratory floor), a simpler modeling approach was taken that reduces these various unknowns into a single unknown

parameter. Here, the lateral and rotational constraint offered by the actual end conditions was modeled using a translational spring couple placed on the upper and lower flange of each girder. Thus, the equivalent longitudinal and rotational constraints associated the girders could be represented by a single stiffness parameter; this parameter is unknown, but is straightforward to adjust best represent the test results. Although no experimental stiffness data are given, based on recommendations of Abendroth et al. (1991), E for the girders was taken as 4903 ksi, while E for the deck was taken as 3908 ksi, values reported to best correspond to the expected material properties. However, because significant longitudinal cracks were reported in the underside as well as top of the deck, some reduction in E in the transverse direction is appropriate. The actual degree of cracking, and thus the transverse stiffness reduction, is unknown. However, typically reinforced concrete specimens experience a reduction in flexural stiffness on the order of 50% due to cracking. To roughly account for this loss, using an orthotropic material model, E in the transverse deck direction was taken as 2000 ksi. Poisson ratio is taken as 0.19. The diaphragms shown in Figure 8 were coarsely modeled with truss elements representing the cross members and vertical gusset plate members, while shells were used to tie the corners of the diaphragm to the girder flanges. The purpose of the corner shell elements was to provide some mechanism to account for possible diaphragm connection flexibility. In particular, potential bolt slippage within the connections, since the bridge was heavily loaded in the tests. Diaphragm components were modeled as steel (E = 30,000 ksi, ν = 0.29), with areas taken as those of the specified members. Because numerous high concentrated load levels were applied on the bridge deck, it is likely that some slippage in the diaphragm member connections occurred, effectively lowering the stiffness of the diaphragms. To account for this, the connector shell elements were given a reduced thickness that was found to best represented the girder deflection data. Images of the model are shown in Figure 5.9.
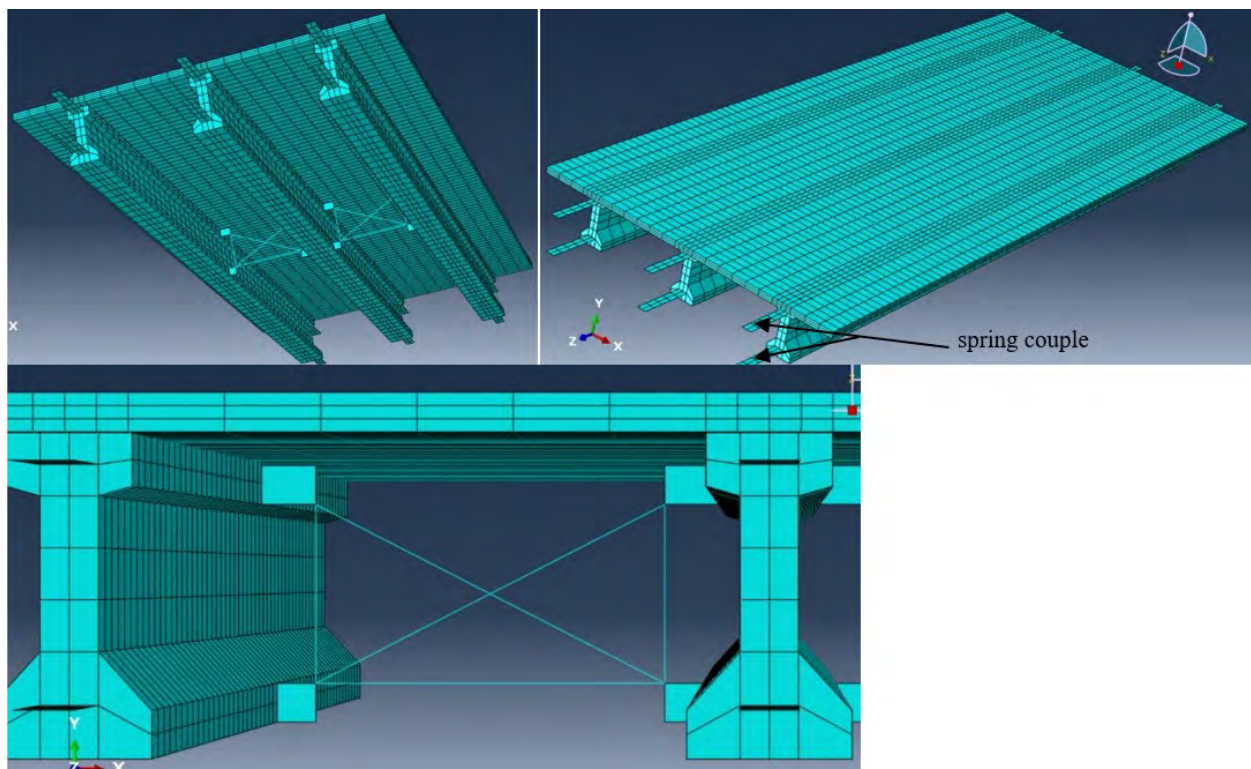
Figure 5.9. FEA Model of Abendroth Bridge.

Deflection results for no diaphragms are given in Figures 5.10 and 5.11, when a 20 kip point load is applied at the midspan of the center and exterior girder, respectively. Notice that for the experimental results, a range of values is shown at some locations. This is because significant asymmetry was reported in the tests, most likely due to different levels of deck cracking, although girder boundary condition restraints, and/or initial discrepancies in material properties or specimen construction may have also contributed. As insufficient information exists to model this asymmetry, two results are provided for an ideally symmetric response, as developed in the FEA model. When diaphragms were installed, deflections were measured at midspan of the center girder as well as at third-span points of the exterior girders. These results are shown in Figures 5.12 and 5.13. In these figures, one set of results assumes that the diaphragm connection flexibility remained constant throughout the series of tests ("constant slip"), while an alternative set of results assumes that the diaphragm connection slippage increases for subsequent tests ("progressive slip"); the later appears to best match the experimental data. Figure 14 provides an image of the deformed shape of the bridge with and without diaphragms. The model shows relatively good agreement with the experimental results.
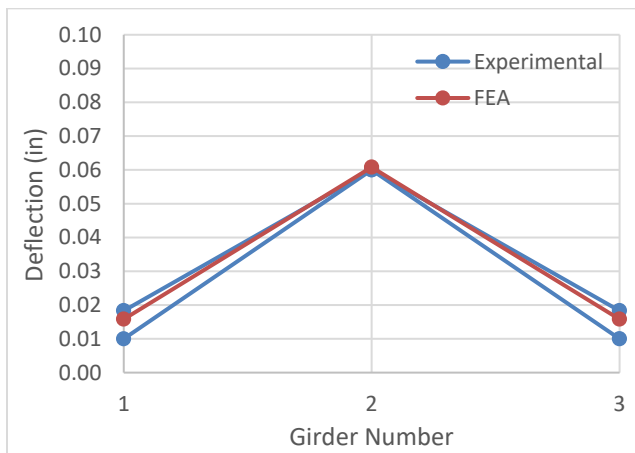
Figure 5.10. Girder Deflections, No Diaphragms, Load at Center Girder (2).
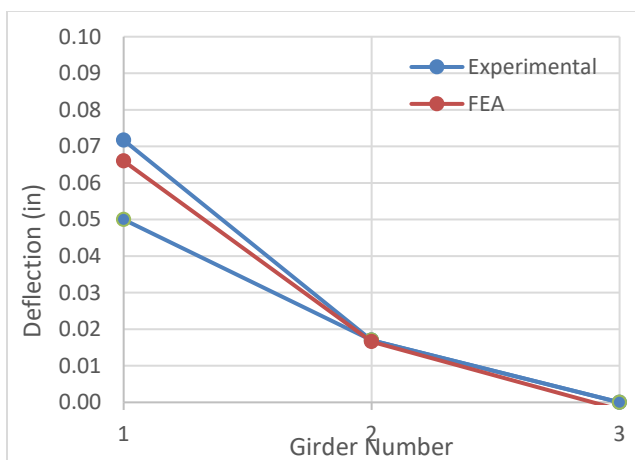
Figure 5.11. Girder Deflections, No Diaphragms, Load at Exterior Girder (1).

40
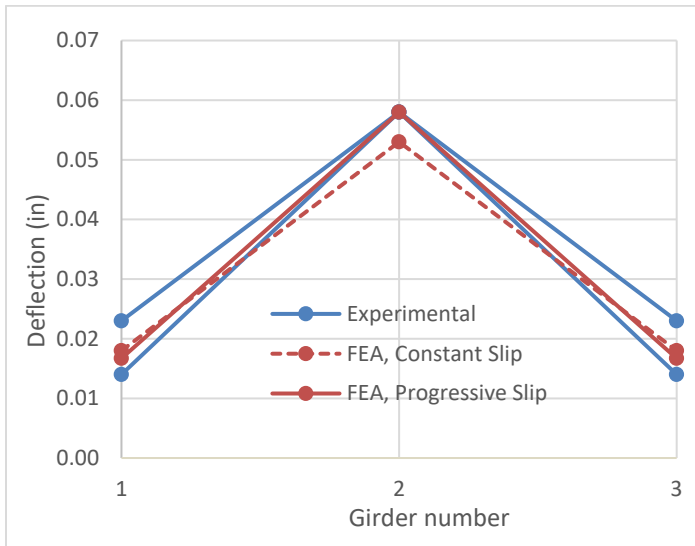
Figure 5.12. Girder Deflections With Diaphragms, Load at Center Girder (2).
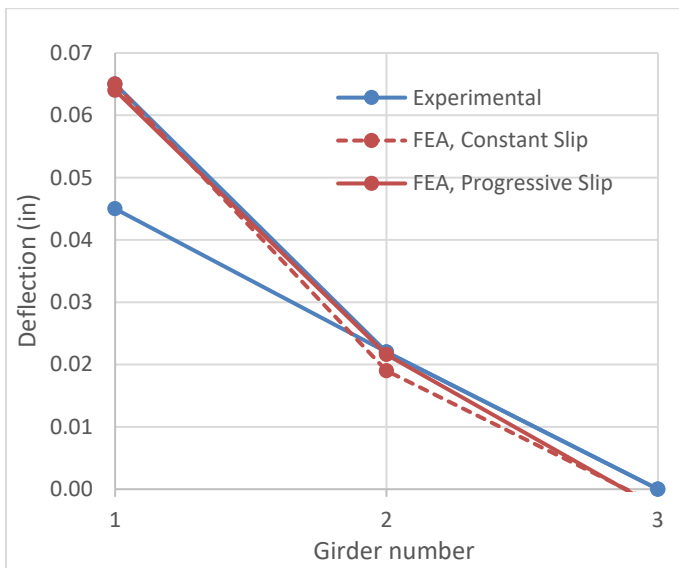
Figure 5.13. Girder Deflections With Diaphragms, Load at Exterior Girder (1).
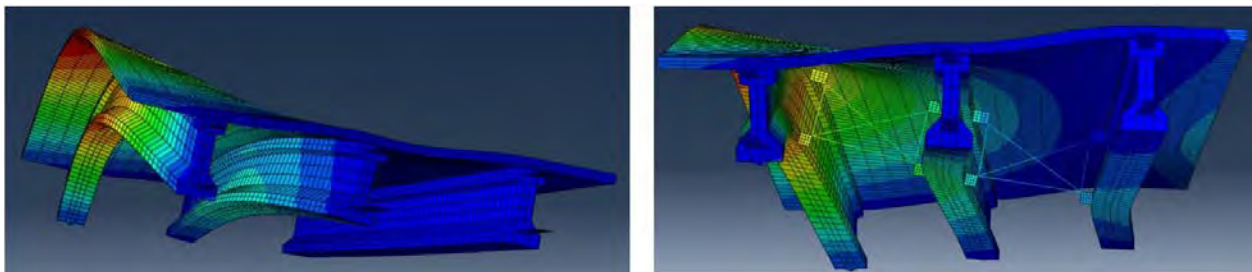
Figure 5.14. Deformed Shape of Bridge Under Load on Edge Girder, Without and With IDs.

5.2.4 Validation Model 3: Eamon Field Test Data

The use of field test data for model validation are generally not as reliable as laboratory data, due to the significant number of additional unknowns unavoidably present in both the structure as well as the test conditions. Thus, although many more studies have documented the response of actual bridges rather than laboratory models of such structures, these studies were avoided for validation purposes. However, to represent this large pool of available results, the field test results of two structures were further considered. The considered field tests are fully described in Eamon et al. (2014; 2016) and represent a dataset uniquely relevant to this study: two nominally identical MDOT PC girder bridges. These structures represent the same design and year of build, and were subjected to the same test conditions. As such, these structures provide an opportunity to illustrate the variance in behavior between two identical structures, and the ability of the model to capture a representative response of a set of actual bridges.

5.2.4.1 Test Bridges

Each bridge is two lane, no skew, with 2 live-load continuous middle spans of 106 ft, girder spacing of 6.4 ft with Type IV prestressed girders, and built in 1993. The structures are on Taft Road and Centerline Road over US-127. A cross-section of the bridges is shown in Figure 5.15.
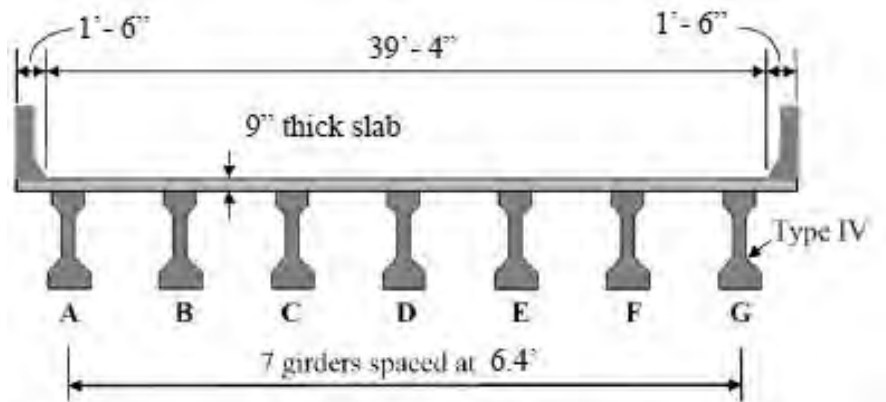
Figure 5.15. Field Test Bridges (Eamon et al. 2016).

The lower girder flanges were instrumented with strain gauges, and the bridges were subjected to a series of loads from two 11-axle trucks, each approximately 150 kips gross vehicle weight. In each test case, the load vehicles were slowly driven across the bridge (walking speed),

5.2.4.2 FEA Model

Approximately 10,000 4-node shell elements were used to idealize all bridge components, including the deck, girders, diaphragms, and barriers (a single model was used for both, since they are geometrically identical). For each case, shell thickness was taken to develop the equivalent component flexural stiffness about the primary bending axis. Support conditions were modeled by constraining nodes at the underside of the girders in the vertical direction at the end spans and in the vertical and horizontal direction at the continuous center support; the two end bearings at the continuous joint, which are relatively close together (center-to-center spacing 15"), were modeled as a single central support. Additionally, spring elements were used to simulate the

42

longitudinal and rotational constraint at the abutment supports, similar to the method used in the Abendroth model. Based on the available data, Young's modulus for concrete was taken as 4,500 ksi. Since no observable cracking was reported on the deck or the girders on either bridge at the time of testing, no reduction was applied to nominal material properties. However, the longitudinal Young's modulus of the elements joining the girders over the center continuous support was reduced to 130 ksi to best represent the actual degree of center joint continuity, which was found to be partially constrained but closer to a pin rather than a continuous joint (Eamon et al. 2016). The underside of the model is shown in Figure 5.16.
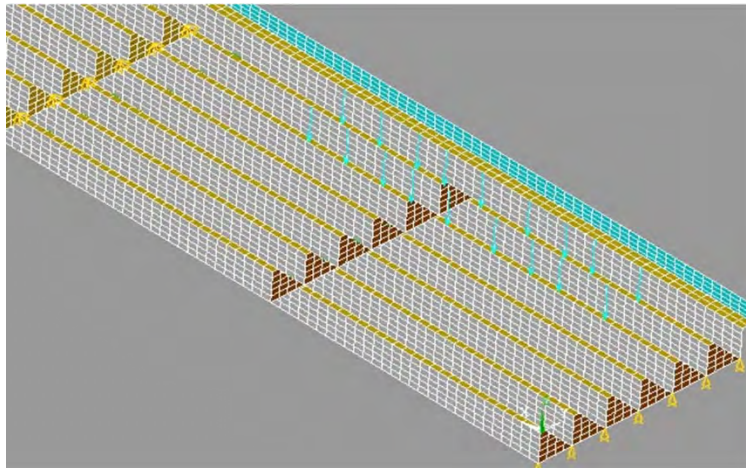
Figure 5.16. FEA Model of Field Test Bridges (half-span shown).

5.2.4.3 Results

Although numerous results are available, three representative cases are provided in Figures 5.17-5.19. Figure 5.17 presents positive moment strain results for two side-by-side trucks; Figure 5.18 for positive moment strains corresponding to one truck placed as close as possible to the barrier; and Figure 5.19 for negative moments for two side-by-side trucks driven as close as possible to the barrier. Presented girder strains correspond to the vehicle position longitudinally that maximized strain in the most heavily-loaded girder. As shown, significant differences in response exist between the two structures. Although some differences may be attributed to slight differences in test vehicle configuration, weight, and placement on the bridge, model simulations have shown that such differences cannot account for the large discrepancies seen between the two structures. Such differences are most likely due to differences in boundary conditions; in particular, the unknown degree of longitudinal and rotational constraint provided at the supports (approach slab, back walls, bearing pads, etc.), A deformed image of the model is given in Figure 5.20. In all cases, the model result falls within, or relatively close to, the strain bounds of the two structures.
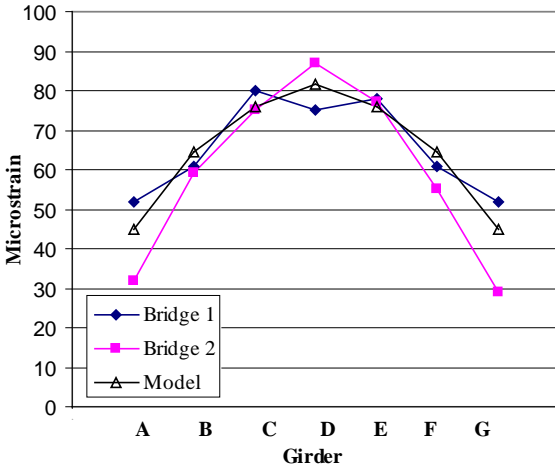
Figure 5.17. Positive Moment Strains, Two Trucks Centered in Lanes.
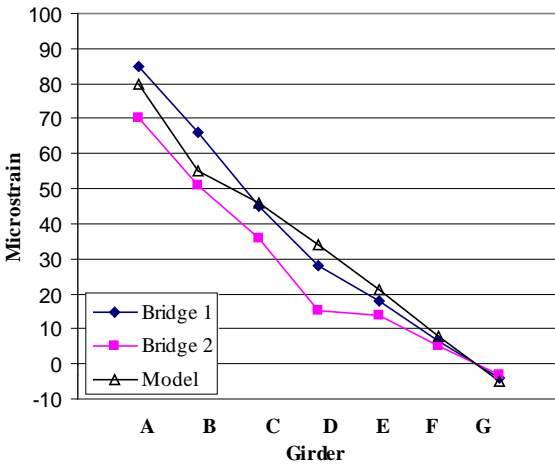
Figure 5.18. Positive Moment, One Truck Near Edge.
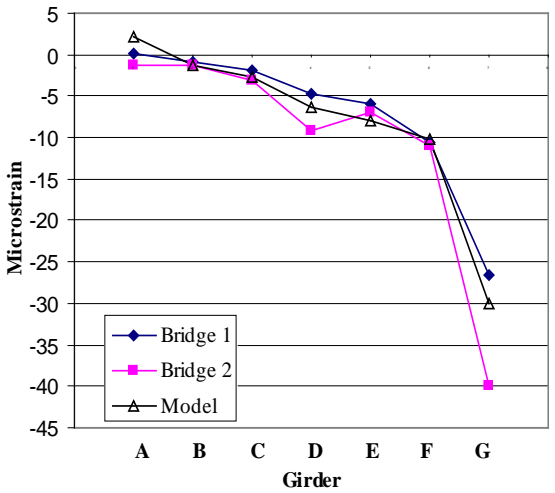
Figure 5.19. Negative Moment, Two Side by Side Trucks Near Edge.
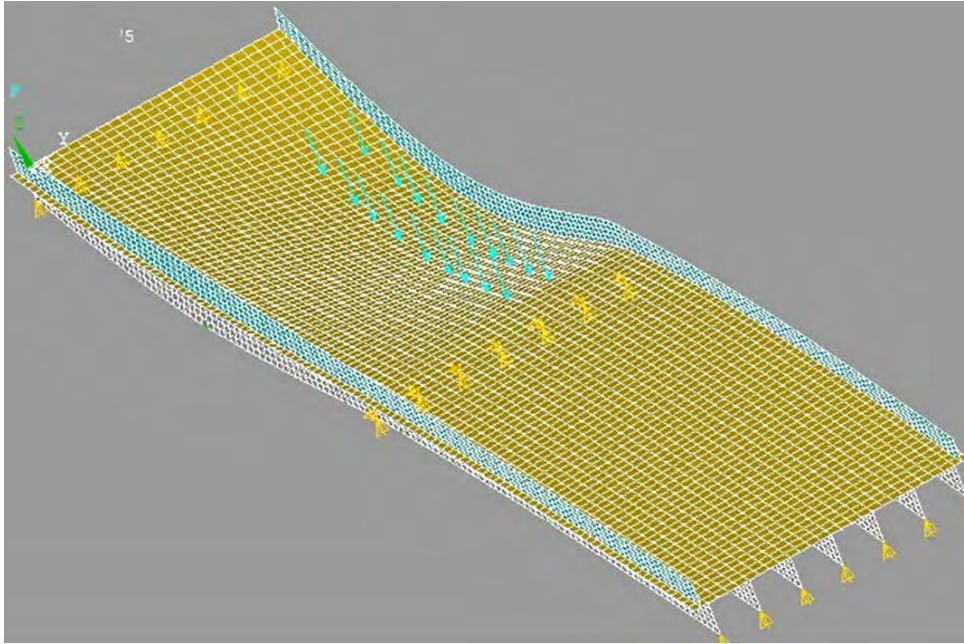
Figure 5.20. Deformed Shape of Bridge (Figure 5.18 Load Case).

5.3 Model Validation: Girder LTB

5.3.1 Modeling Considerations

Although a significant number of experimental studies exist regarding the LTB behavior of steel or even steel-concrete hybrid specimens, much fewer exist for reinforced, and especially prestressed concrete members. When elastic LTB of steel specimens is considered, where no material nonlinearity is expected, results have been found to match closely to the theoretical solutions. As such, there is little to be gained in terms of validation by modeling such member types for this study, as results would mirror those of classic solutions. For the existing LTB studies of RC and PC members, several studies have determined critical lateral buckling loads experimentally (Siev 1960; Sant and Bletzacker 1961; Massey and Walter 1969; Konig and Pauli 1990; Revathi and Mennon 2006; Kalkan 2009; Zureick et al. 2009). Of these, Konig and Pauli (1990), Kalkan (2009), and Zureick et al. (2009) provided initial imperfection measurements of their specimens, where only Konig and Pauli (1990) and Zureick et al. (2009) studied PC specimens. Data regarding imperfections, which pertains to the camber, sweep, and rotation of the specimens, of which rotation (i.e. twist) is most important, influences the critical buckling load when inelastic behavior such as cracking occurs; as expected, a perfectly straight beam generally has a higher critical buckling load than an imperfect beam. This limits the usefulness of the studies for model validation primarily to those which have recorded such information.

There are two general approaches for modeling instability: an Euler buckling analysis and a nonlinear buckling analysis. The Euler analysis determines the critical buckling load by conducting an eigenvalue analysis of the structure, where the lowest (positive) eigenvalue reported corresponds to the load factor that must be applied to the load(s) specified on the structure in the analysis to cause buckling. The Euler analysis is a linear bifurcation analysis, where no material

nor geometric nonlinearities are considered, and the post-peak response cannot be obtained, only the buckling loads and the corresponding proportional mode shapes (i.e. the eigenvectors). Practically, the Euler analysis represents the upper bound of critical load, since imperfections as well as nonlinearities which may reduce capacity are neglected. Note that changing the load position or structural geometry to represent an imperfection may influence the Euler result in some cases, but these effects are generally very small, since geometric nonlinearities are not considered in such an analysis. Because the Euler analysis is nearly always unconservative, this type of analysis is not recommended to determine critical buckling loads. It is a useful part of a more realistic type of analysis, however, as discussed below.

In contrast to the Euler approach, the nonlinear LTB analysis does consider nonlinearities; either geometric, or both geometric and material. In this type of analysis, the critical buckling load is not found from an eigenvalue analysis, but rather from a pushover analysis. That is, the load(s) applied on the structure are slowly incremented upwards until the structure's maximum capacity is reached. Note that a perfectly straight beam subjected to such an analysis will experience no instability, but will fail due to reaching an ultimate limit state such as flexure or shear. To consider LTB, an imperfection must be introduced into the beam geometry. Because geometric nonlinearities are included, the effect of the increasingly eccentric load is accounted for in the geometrically nonlinear analysis. An imperfect beam that is given an initial sweep and/or rotation thus begins to twist and deflect laterally, where stiffness is lowest, as the gravity load is increased. The beam will eventually experience a deformed configuration where further increases in load are not possible; the peak load found in this procedure is taken as the critical buckling load.

A common way to introduce an imperfection onto the beam geometry is via the results of a Euler buckling analysis. That is, first an Euler analysis is conducted, and the buckling mode shape(s) are recorded. A factor is then applied to the mode to scale the deformation to the extent desired. This deformation is then superimposed onto the original geometry (i.e. nodal coordinates) of the initially perfect beam, prior to the nonlinear analysis. Although any geometric imperfection could be imposed, the advantage of imposing an Euler buckling mode is that it may closely represent the worst case imperfection; that is, the imperfect geometry that is most prone to buckle. The first, most critical eigenmode also appears to a reasonable representation of an idealized construction imperfection such as from formwork bowing or eccentric prestressing.

A potentially important consideration is the degree of imperfection imposed. If only geometric nonlinearities are included in the analysis, the extent of the initial imperfection (i.e. the factor applied to the eigenmode) has little to no influence on the critical buckling load, only on the shape of the load-deflection curve. Greater imperfections create smoother curves while lowering the imperfection creates a curve the more closely resembles the idealized Euler bifurcation response, where a sharp distinction is apparent between the stable and instable (i.e. zero stiffness) states. When material nonlinearities are also included, however, the importance of the imperfection may increase, where, as expected, greater imperfections tend to decrease critical buckling load. As such, because only Konig and Pauli (1990) and Zureick et al. (2009) recorded initial beam imperfections, the experimental validation data will be drawn from those studies.

5.3.2 Validation Model Set 1: Benchmark Theoretical Cases

Prior to studying experimental data, a series of simple, benchmark instability test cases were considered using the element types to be used in this study (shells and solids), to verify that the modeling approach could recover known theoretical solutions. Although seemingly trivial, such cases, which provide no unknowns and no possibility for model calibration parameter adjustment, are important to study in order to establish that the fundamental procedure used is valid.

The geometry of the test member, used in all cases, is a rectangular section with depth = 10 in, width = 1 in, length = 200 in, E = 10,000 ksi, and $\nu = 0$. The only parameters that change between the different cases are the boundary conditions and load placement. Similarly, all cases use an identical mesh, either of 1000 shell or 2000 solid elements. Note that significantly coarser mesh densities may be used with no significant loss of accuracy.

5.3.2.1 Case 1: Simple Column

Here, a pinned-end column is considered. The mode of instability is not LTB, but bifurcation due to uniform axial compression, a simpler case of elastic instability. A 1 kip load is applied to the top of the column (two symmetric 0.5 kip loads on either edge of the column in the FEA model to minimize local deformation). The column base is constrained vertically, and the top and bottom edges of the column constrained laterally to prevent a static instability. Results for all models are given in Table 5.1. The shape of the first buckling mode is shown in Figure 5.21.
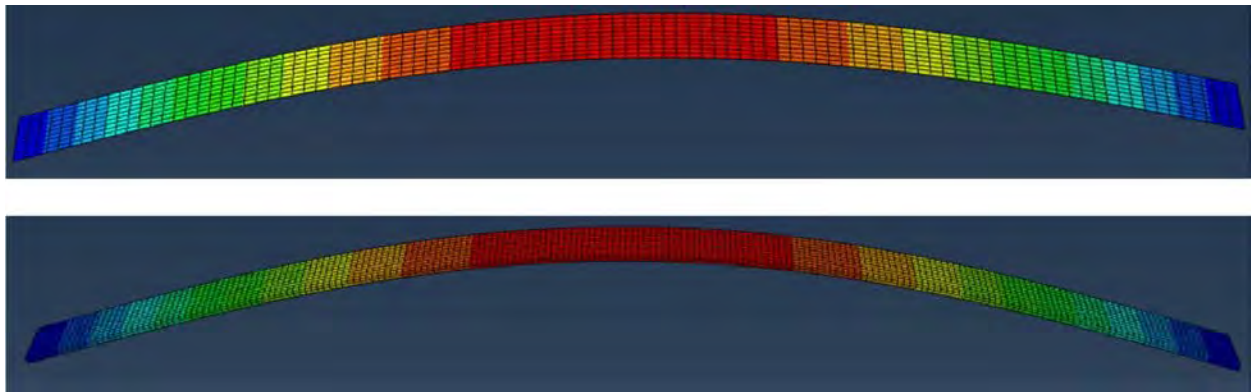
Figure 5.21. Shell and Solid Column Models, Buckled Shape.

5.3.2.2 Case 2: Cantilever Beam

For the cantilever beam, all nodes at one end are completely constrained in translation as well as rotation. As the solution assumes load is applied at the centroid, the load is applied normal to the beam end in two 0.5 kip loads as per the column, one at the top and one at the bottom 'flange' of the beam to provide symmetry. The shape of the first buckling mode is shown in Figure 5.22.
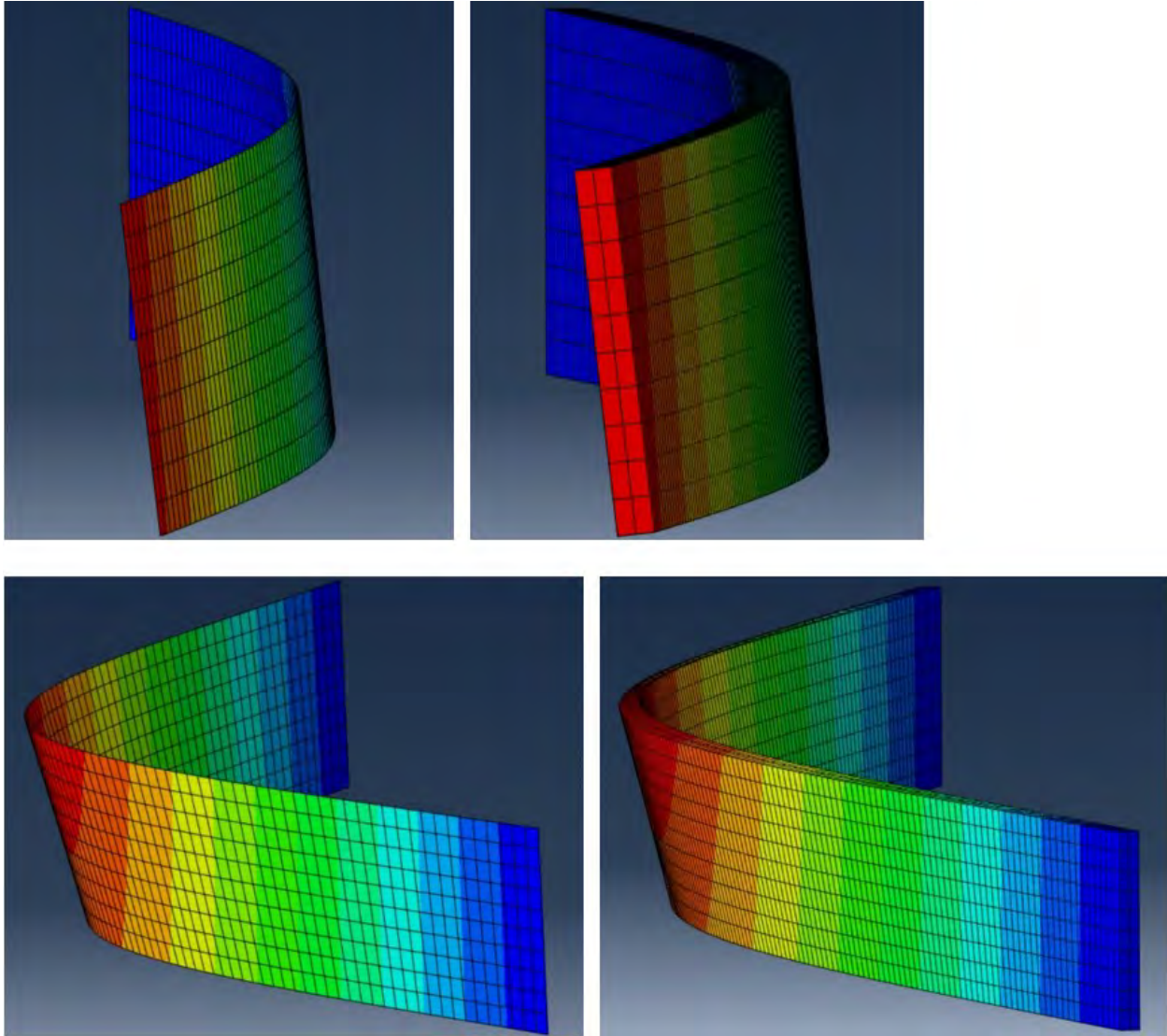
Figure 5.22. Shell and Solid Cantilever (Top) and Simple (Bottom) Beam Models, Buckled Shape.

5.3.2.3 Case 3: Simple Beam

In this case, vertical supports are provided at the centroid of each end of the beam; lateral and torsional constraints are provided across the entire depth of either end, and a longitudinal constraint is provided at the centroid of one end for static stability. A single 1 kip point load is applied at the centroid at midspan.   The shape of the first buckling mode is shown in Figure 5.22.

Table 5.1. Model vs Exact Solutions.

Case	Exact Solution*	Shell Model	Solid Model	% error
Column	0.206	0.206	0.206	0
Cantilever Beam	1.03	1.028	1.029	~ 0
Simple Beam	4.27	4.24	4.23	< 1%

*The first eigenvalue; i.e. in the problems considered, equal to Pcr (kips).

As expected, the classic solutions can be well replicated with the modeling approach used. The problems above were next reconsidered, but now implementing a nonlinear buckling analysis. Here, different degrees of imperfection were imposed on the structures based on factors applied to the first Euler buckling modes found earlier. In the nonlinear analysis, to maintain as much consistency as possible with the Euler approach for comparison, the material is taken as linear elastic; only a geometric nonlinearity is included. Load-displacement results are shown in Figures 5.23-5.28. Note that the results shown for the nonlinear simple beam shell model in Figure 5.27 are based on slightly changed boundary conditions from the solid model. Here, to illustrate the effect of altering boundary conditions, a single torsional constraint was applied at the beam centroid at each end rather than constraining the entire beam height as in the initial Euler and solid model analysis. This change resulted in the Euler critical buckling load to be reduced from 4.27 to 3.78. As shown in the figures, as expected, as the imperfection is increased, the transition from the stable to instable condition becomes more smooth, whereas as the imperfection decreases, the point of instability begins to converge to the Euler solution. The nonlinear stiffening response past the onset of instability is due to the use of an ideal linear elastic material and would not occur if a more realistic material model were used. Also seen is that both shell and solid element approaches give nearly identical results.
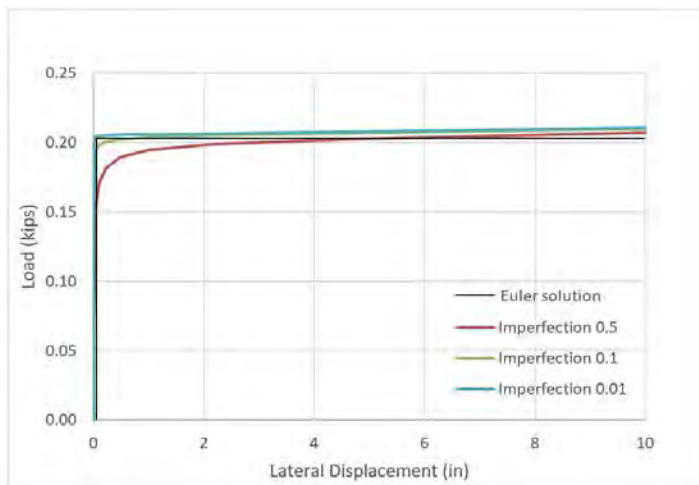
Figure 5.23. Load Displacement Response of Column, Shell Model.
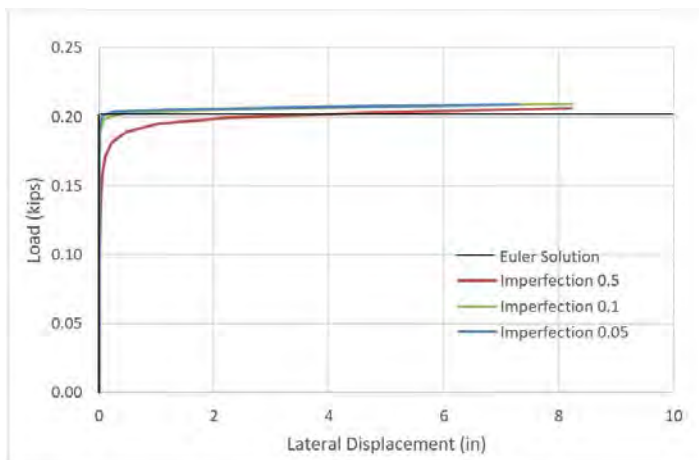
Figure 5.24. Load Displacement Response of Column, Solid Model.
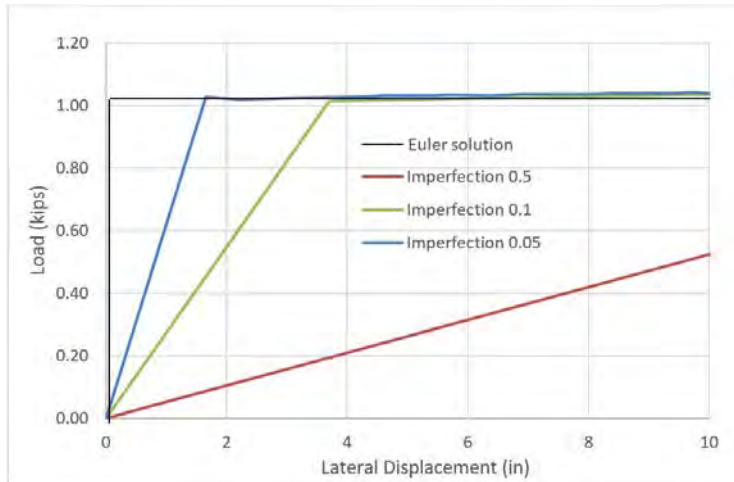
Figure 5.25. Load Displacement Response of Cantilever Beam, Shell Model.
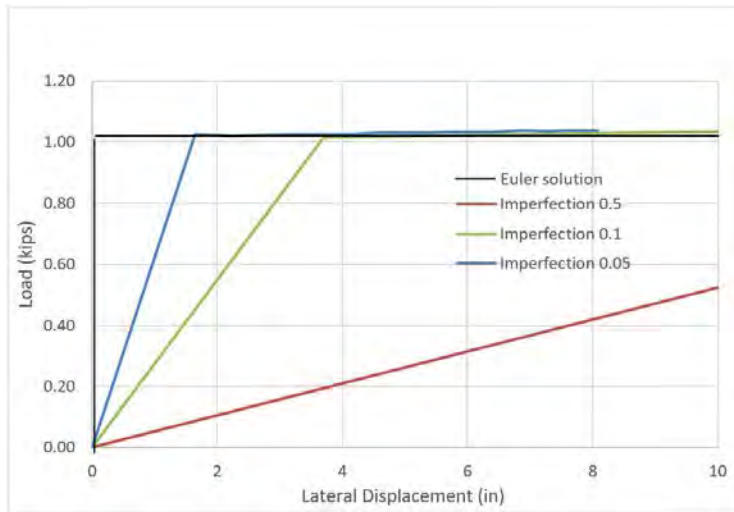
Figure 5.26. Load Displacement Response of Cantilever Beam, Solid Model.
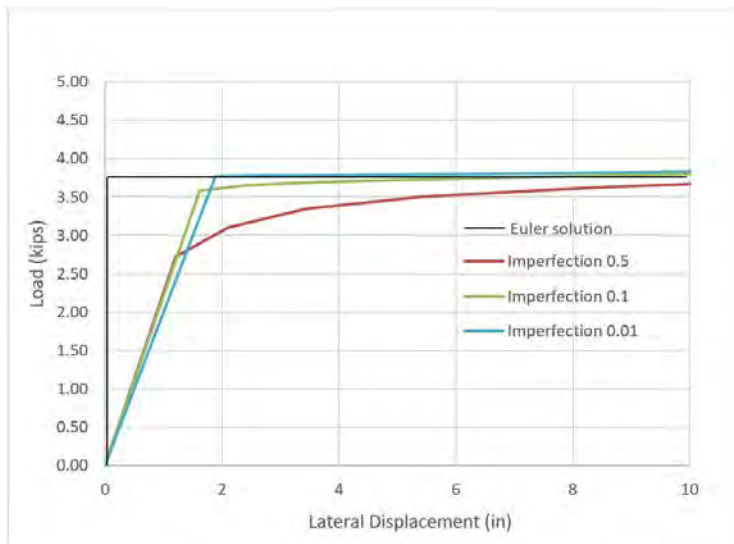
Figure 5.27. Load Displacement Response of Simple Beam, Shell Model.
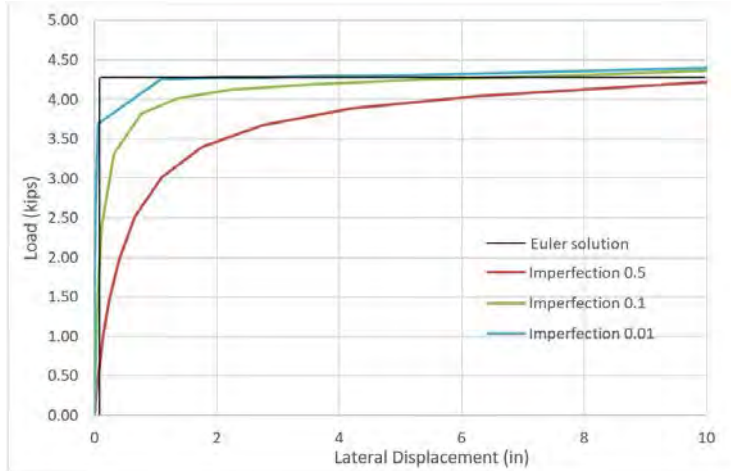
Figure 5.28. Load Displacement Response of Simple Beam, Solid Model.

5.3.3 Validation Model 2: Reinforced Concrete Beam

Prior to considering prestressed specimens, a simpler reinforced concrete beam was modeled.

5.3.3.1 Test Specimen

This beam is taken from Zureick et al. (2009), and is a reinforced concrete specimen with total height of 36 in, width of 3 in, and length of 39 ft (specimen B36-L2). The uncracked E is given as 4500 ksi, Poisson ratio as 0.15, and midspan sweep was recorded as 0.38 in. The ends of the beam were constrained vertically and laterally to represent torsionally fixed supports, and the beam was loaded at the top of the section with a vertical point load at midspan. The cross-section and load-displacement response are shown in Figure 5.29. The critical buckling load was reported as 21.6 kips. The Euler LTB load is 36.3 kips, while the nominal flexural capacity is estimated to be 39.5 kips.
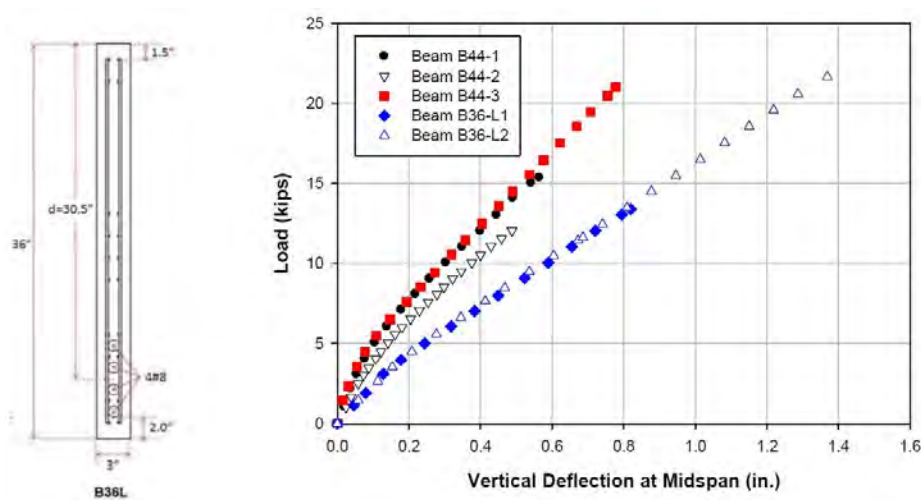
Figure 5.29. RC Test Beam (from Zureick et al. 2009).

5.3.3.2 FEA Model

Several different approaches were considered, with the goal to produce a simple but effective model. The first model explored the possibility of using an Euler analysis with a reduced E value to account for the beam imperfection and cracking. In this model, the E value was proportionally decreased to correspond to the change in stiffness from the first to second slopes on the load displacement relationship shown in Figure 5.29. The model is composed of approximately 20,500 solid elements and supported and loaded as in the test set-up, as shown in Figure 5.30. No reinforcement was modeled.

The second approach considered a geometrically-only nonlinear analysis, using the reduced E value as in the first model. The recorded sweep value of 0.38 in. was imposed on the first buckling mode to represent the initial imperfection.

The third approach is similar to the second, but here a bi-linear material model was used. The bi-linear stress strain curve was specified to correspond to the expected flexural stresses and strains corresponding to the load displacement response of the specimen.
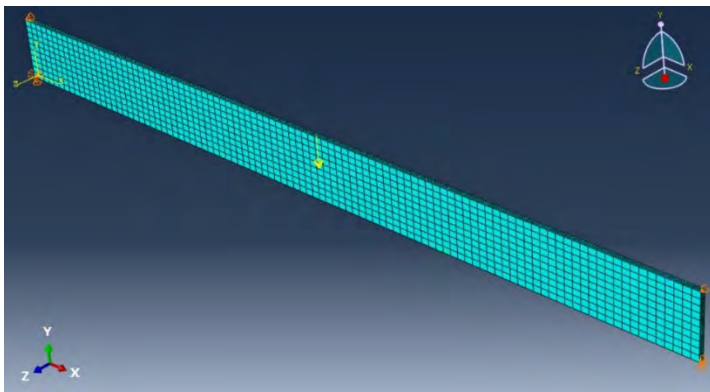
Figure 5.30. RC Beam Model.

5.3.3.3 Results

Using the reduced E value, the first model resulted in an Euler LTB load of 21.0 kips, which is close to the experimental value of 21.6 kips. An image of the buckled shape is given in Figure 5.31.

The load deflection response of the second model is given in Figure 5.32, along with the actual critical load. As shown in the figure, there is no clear way to obtain the actual buckling load from the vertical deflection curve, although the horizontal curve does appear to converge to the test result, although at an unrealistically large value of deflection.

Results of the third approach are given in Figure 5.33. As shown, reasonable agreement between the model and experimental values were obtained. Note a horizontal line was added at the peak of the experimental capacity (where the test was stopped) when considering vertical deflection for ease of comparison to the FEA result, which captured post-peak response.
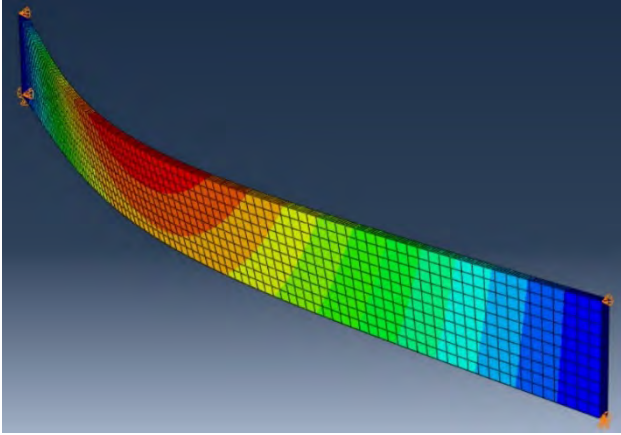
Figure 5.31. Buckled Shape.
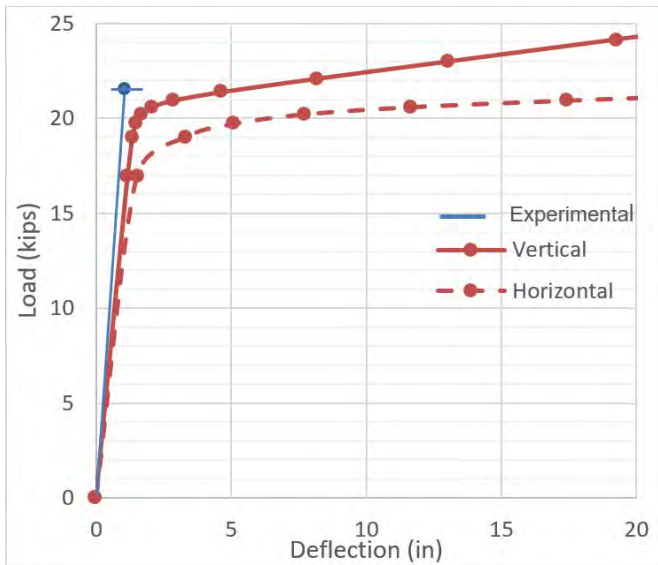
Figure 5.32. Load Deflection Response of Linear Material Model Approach.
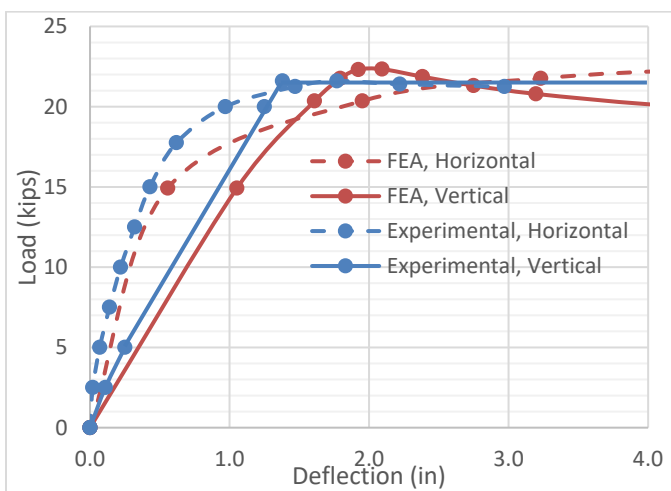
Figure 5.33. Load Deflection Response of Bi-Linear Material Model Approach.

Although reasonable critical load results were obtained with all simplified models, a remaining need for each of these approaches was to determine an effective post-cracked E value based on section and material properties rather than the specimen load displacement response, which of course would be unavailable for a hypothetical beam. However, these simplified approaches were not pursued further, as discussed below.

5.3.4 Validation Model 3: Zureick PC Beam

<u>5.3.4.1 Test Specimen</u>

This beam is also taken from Zureick et al. (2009), and has a height of 40 in, width of 4 in, and spans 32 ft (specimen 40B1A). Concrete has properties f'_c = 10,133 psi, E = 4713 ksi, and ν = 0.19, while midspan sweep was recorded as 0.403 in. and initial rotation approximately zero. The beam has five #8 longitudinal bars (1 at top; 4 at bottom) and was prestressed with a single ½ in (nominal) diameter strand to 33.37 kips. The ends of the beam were constrained and load applied as per the RC beam above. The cross-section and load-displacement responses are shown in Figures 5.34 and 5.35, respectively. The peak buckling load is approximately 36.5 kips. The Euler LTB load is approximately 133 kips, where the ultimate flexural capacity is estimated to be reached at 74.3 kips (with 60 ksi nonprestressed steel and 270 ksi prestress steel).
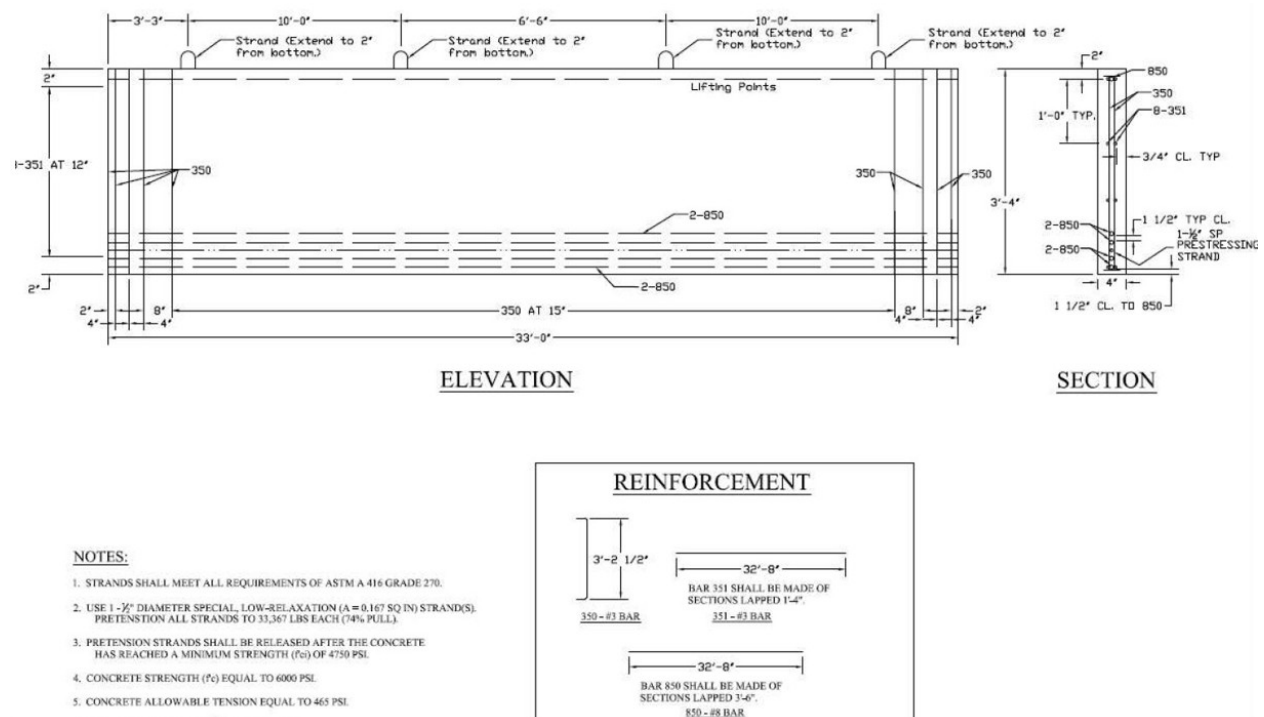
Figure 5.34. Zureick PC Test Beam (from Hurff 2010).
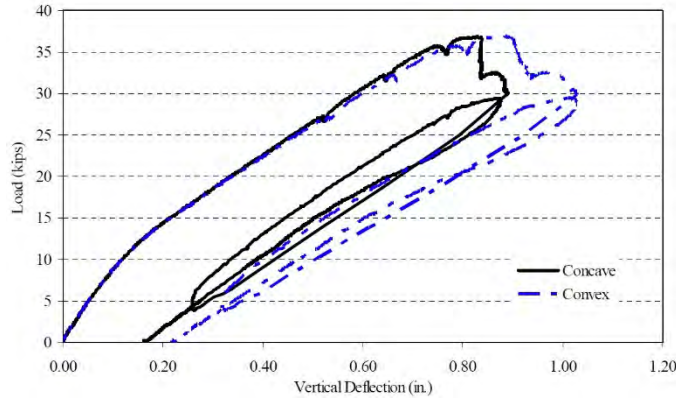
Figure 5.35. Zureick PC Test Beam Load Displacement Response (from Hurff 2010).

<u>5.3.4.2 FEA Model</u>

This model has similar constraints and load application as the RC model discussed above (see Figure 30), and uses approximately 6200 elements. Unfortunately, the model simplifications used for the RC beam (i.e. based on an effective reduced E value) could not produce adequate results for the PC beam. This is likely because there is a more gradual loss of stiffness as the LTB load is approached, as seen near the peak load in Figure 5.35, where stiffness gradually approaches zero before the ultimate load is reached. Neither bi- nor tri-linear material models were effective here.

Therefore, a more complex approach was required. The first adjustment was the use of a concrete-specific material model that softens to account for cracking, the Concrete Damage Plasticity Model (CDP). Material parameters were based on the recommendations of Nguyen and Livaoglu (2020), and adjusted to correspond to the concrete strength of the test specimen. Other material model parameters are: $\psi = 35$; $\varepsilon = 0.1$; $f_{b0}/f_{c0} = 1.16$, $k = 0.667$, and $\mu = 0$. A full description of the meaning of these parameters and how to calibrate them to experimental data is given elsewhere (Alfarah et al. 2017; Tomasz and Tomasz 2013; Sumer and Aktas 2015; Wahalathantri et al. 2011), but in general, ψ is the dilation angle (in the p-q plane) at high confining pressure and accounts for changes in Poisson ratio as pressure increases; k is the ratio of deviatoric stresses in uniaxial tension and compression, and varies from 0.5 using a Rankine yield surface to 1.0 using von Mise theory; ε is the eccentricity of the plastic potential surface; f_{b0}/f_{c0} is the ratio of initial biaxial to uniaxial compressive yield stress; and μ is the viscosity parameter, which is used to increase numerical convergence by allowing stresses to extend beyond the specified yield surface. The concrete compressive inelastic ("yield stress") stress-strain relationship is given in Figure 36, while the post-cracking tensile behavior is given by Figures 5.37 and 5.38, where a strain-based concrete tension damage model is used. The tensile damage parameter refers to the ratio of cracking strain to total strain, and is used to degrade elastic stiffness during unloading. Note that although the beam was loaded monotonically, as cracks grow and disrupt the stress field, some areas previously loaded may unload, activating the damage parameter.
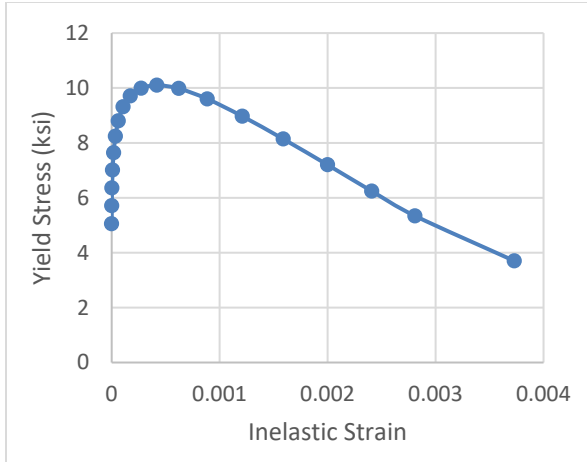
Figure 5.36. Concrete Inelastic Compressive Stress-Strain Behavior.
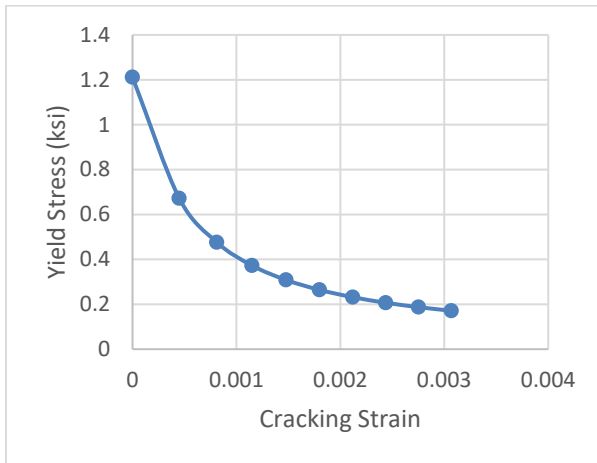
Figure 5.37. Concrete Inelastic Tensile Stress-Strain Behavior.
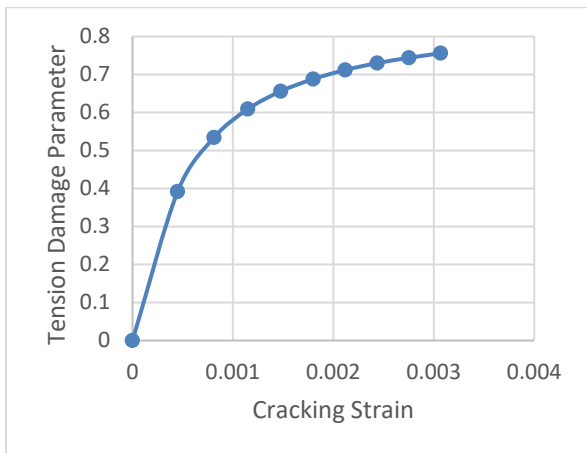
Figure 5.38. Concrete Inelastic Tensile Damage Function.

Next, the primary longitudinal steel was included; the prestress strand and the four #8 tension bars and single #8 compression bar, as shown in Figure 5.39. The steel was assumed to be completely bonded with the concrete, with no slip. Shear reinforcement was not modeled.
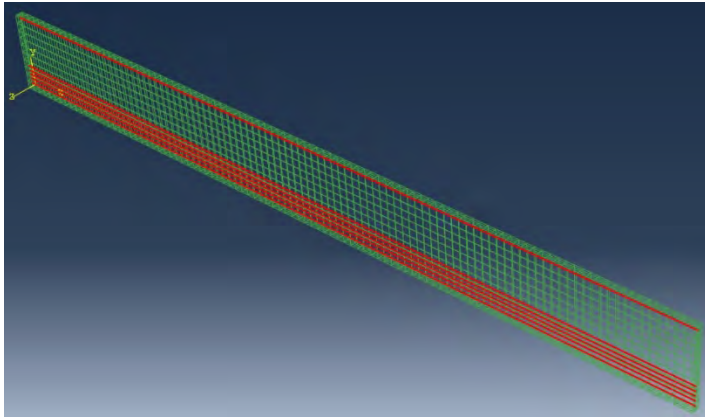
Figure 5.39. Model with Primary Longitudinal Steel Reinforcement.

Next, the analysis was decomposed into three stages to better represent the deformed geometry and response of the specimen:

1) A prestress stage, where a reduction in temperature was applied to the strand to cause an equivalent prestrain associated with the actual prestress force applied and resulting camber.
2) A dead load stage, where gravity load was applied. Here concrete density was taken as 145 PCF and steel density as 495 PCF.
3) The LTB stage, where the nonlinear analysis is conducted by first imposing the 1st Euler buckling mode onto the beam. Because it is not possible to precisely represent the recorded imperfections of zero rotation with non-zero sweep using the Euler buckling mode, which will also provide rotation, some judgement must be used as to the magnitude of the imperfection imposed. Because rotation was found to be the most important parameter with regard to LTB (Zuerick et al. 2009), the value of sweep was ignored, and a much smaller imperfection imposed just to allow the nonlinear instability analysis to progress. In this case, a value of 0.05 in. was used; it was found that 0.1 in. gave nearly identical LTB results.

Due to the use of the CDP material model, the analysis could not converge using an implicit analysis procedure, even when increasing the viscosity parameter to a reasonable level. Thus, an explicit solution was conducted using linear (8-node solid) elements. In this procedure, the prestress and dead load stages were run over (model) time periods of 1.0 seconds each, while the buckling stage was run over 50 seconds. All loads were applied as smooth steps to avoid discontinuities, while the buckling stage was conducted as a displacement-controlled analysis. Note that the actual computational time was much longer than the model time, on the order of several hours when using four CPUs in parallel.

A second approach was considered as well, where all of the nonprestressed reinforcement was modeled, as shown in Figure 5.40. This included shear reinforcement as well as four layers of longitudinal #3 bars on either side of the stirrups. Interestingly, it was found that adding this steel

prevented the concrete on the beam faces from properly cracking during the analysis, resulting in a much too stiff response and a significantly over-predicted LTB load. Various versions of this model were studied, including changes in material and solution parameters, mesh density, time of load application, as well as other factors. As shown in the results, an effective solution was to conservatively assume that nearly all tension is carried by the steel and that the concrete has no significant tension capacity (note: maximum tension capacity was reduced to a small value, on the order of 10 – 100 psi, rather than zero, to provide stability to the model). It is not clear why the interaction of the complete steel cage and a realistic value for concrete tension capacity produced poor results. It should be noted that the research team could find no studies in the literature that modeled experimentally validated PC LTB using the CDP model, nor does such an application appear in the ABAQUS validation manual. However, given that two alternative workable solutions were found, the further exploration of this issue was considered beyond the scope of this project and not further studied.
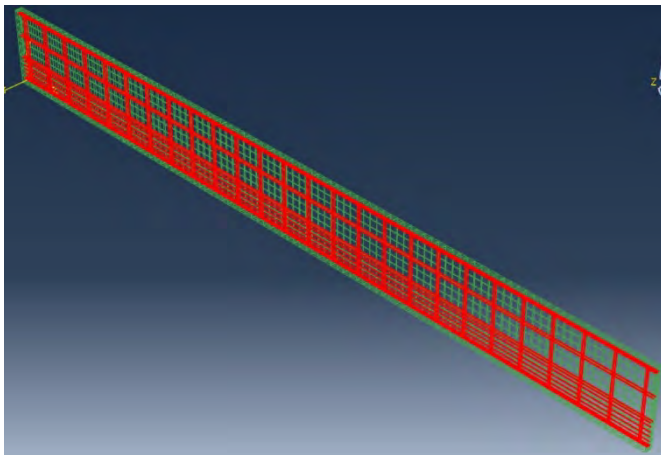
Figure 5.40. Complete Steel Model.

5.3.4.3 Results

For stages 1 and 2 in both models (prestress and dead load), model results closely matched theoretical expectations. For stage 3, the load-displacement curve of the first approach (i.e. using primary longitudinal steel with concrete tension) is shown in Figure 5.41. Although the post-cracked stiffness prior to the instability is somewhat off, the model provides a close approximation to the experimental buckling load: the peak reported load is 36.5 kips, while the model load is 35.7 kips (within 3%). A picture of the deformed shape at the peak load is shown in Figure 5.42. The load displacement response of the second approach (using all steel, no concrete tension) is given in Figure 5.43. Here, the stiffness prediction worsens, perhaps expected since concrete tension capacity is relieved. However, the ultimate LTB load is nearly identical to the first model, with 35.8 kips as the result.
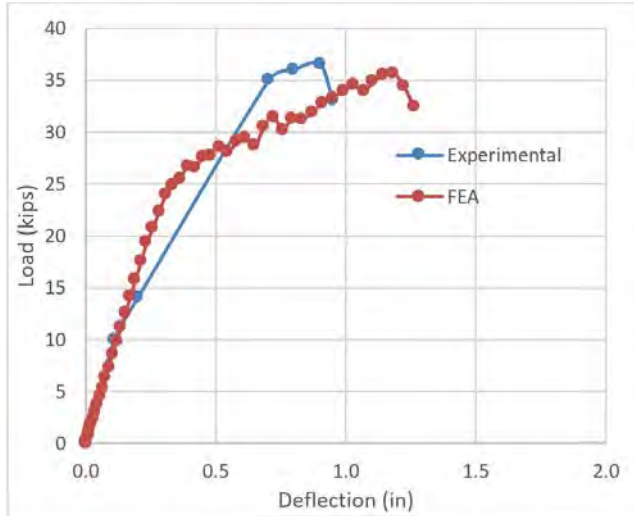
Figure 5.41. Load Deflection Response of First LTB Modeling Approach.
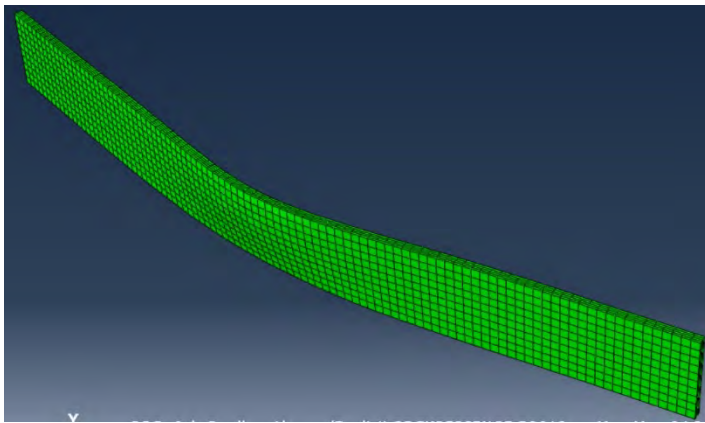
Figure 5.42. Buckled Shape at Peak Load.
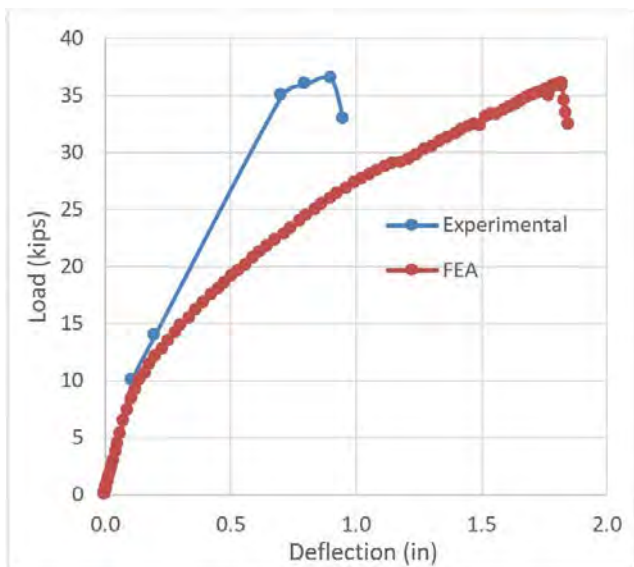
Figure 5.43. Load Displacement Curve of Second LTB Modeling Approach.

Although both approaches produce good agreement to the critical LTB load, the second approach, despite its larger discrepancy in stiffness, is more desirable for the purposes of this project. This is because the results of the first approach were found to be rather sensitive to the tension model used for the concrete, where using reasonable alternative tension stress-strain and damage relationships produced significant variance in the LTB load. This is problematic because the actual concrete tension constitutive relationship is generally unknown, and since making alternatively reasonable assumptions produces inconsistent results, the reliability of the model for wider parametric use becomes questionable. That is, although the particular material parameters, based on Nguyen and Livaoglu (2020), work well for the particular concrete mix used in the test specimen, there is no guarantee that they will similarly work well for other mix designs, such as those used by MDOT. The second approach eliminates these uncertainties by removing these unknown parameters from the model. Thus, it is this approach that will be further considered.

5.3.5 Validation Model 4: Konig and Pauli PC Beam

5.3.5.1 Test Specimen

This beam is taken from Konig and Pauli (1990), has a height of 53 in. and spans 84 ft (specimen #6). Concrete has properties f'_c = 5940 psi and E = 4493 ksi, while average midspan sweep was recorded as 0.43 in. with an initial midspan rotation of 0.40 radians. The beam has 20 nonprestressed steel longitudinal bars and 24 prestress strands, each stressed to 22.47 kips. The ends of the beam were constrained similarly to the other validation tests above, but here two point loads were applied at the beam 3rd points. The cross-section is shown in Figure 5.44. No vertical load-deflection curve is available, only the final LTB load and associated (vertical) displacement, which were reported as 50.9 kips and 5.51 in., respectively. The total Euler LTB load is approximately 281 kips.
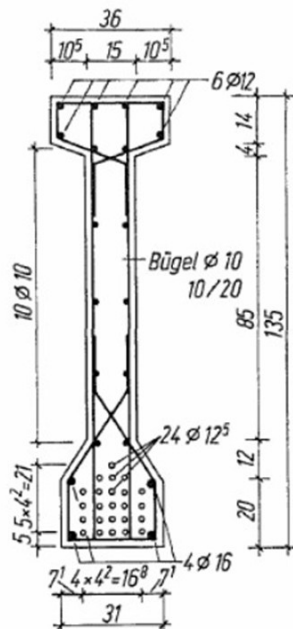
Figure 5.44. Konig and Pauli Test Beam (from Konig and Pauli 1990).

5.3.5.2 FEA Model

To confirm the validity of the FEA approach used for validation model #3, the modeling approach used here was identical to that previously developed (approach 2). This model is composed of approximately 25,400 elements, and is shown in Figure 5.45. Solution time for this model was relatively long, approximately 10 hours on 4 CPUs in parallel.
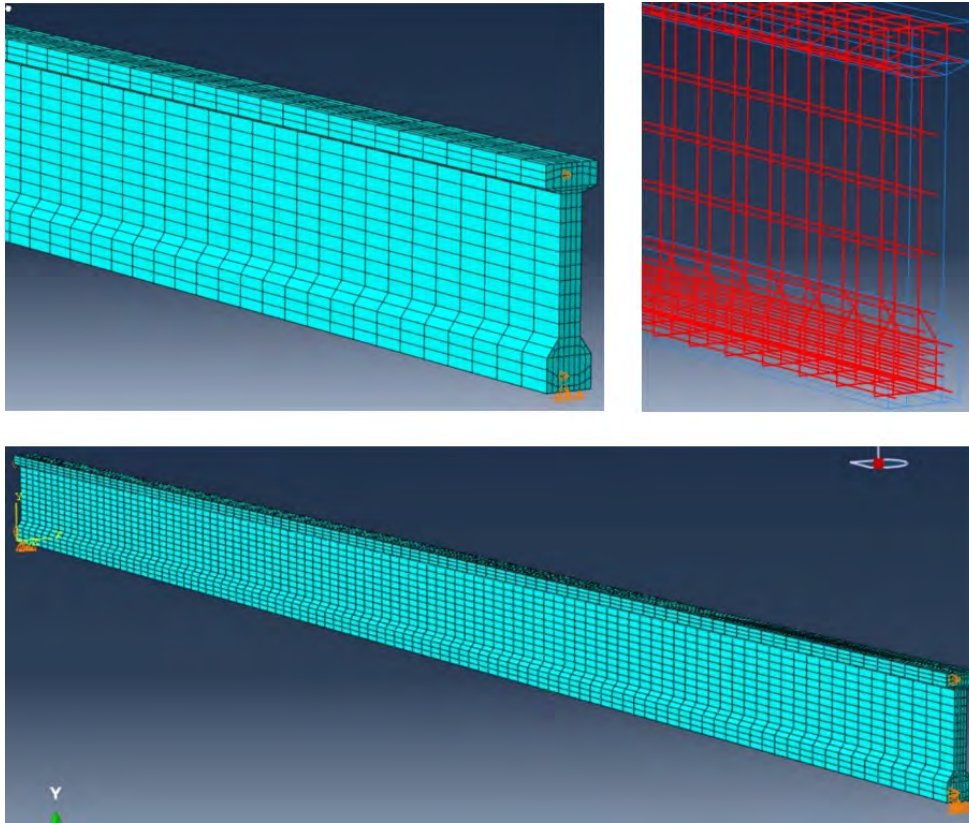
Figure 5.45. Validation Model Four.

5.3.5.3 Results

The load-displacement response of the model is given in Figure 5.46, while the available experimental LTB data point is also provided. The peak load is 49.4 kips, while the experimental value was reported as 50.9 kips (within 3%). Oscillating drops and increases in load may indicate concrete cracking and the recovery of stiffness as steel is engaged. However, it is not clear why the response is so markedly jagged in this model and not in the previously studied case, which may be a result of applying the load too quickly or a numerical instability, among other possibilities. It is also interesting that this model appears to be more stiff than the experimental result despite reducing concrete tensile strength nearly to zero, since the LTB load is reached at a lower value of deflection. Regardless, the peak capacity is well matched by the approach. The deformed shape of the model at peak load is shown in Figure 5.47.
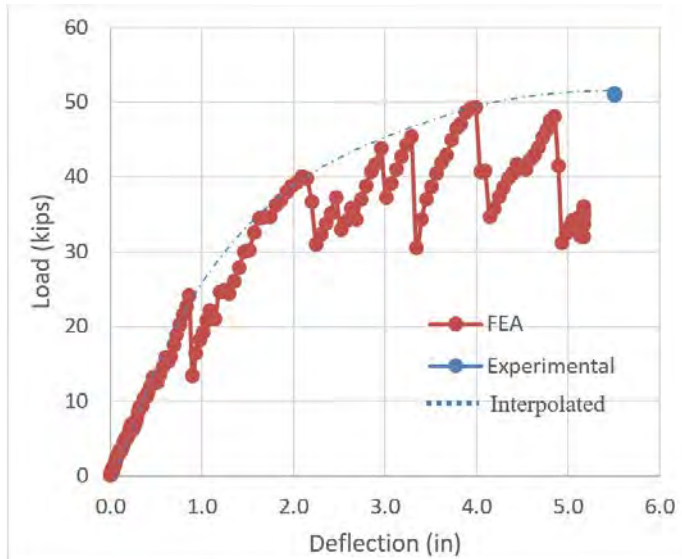
Figure 5.46. Load Displacement Curve for Validation Model Four.
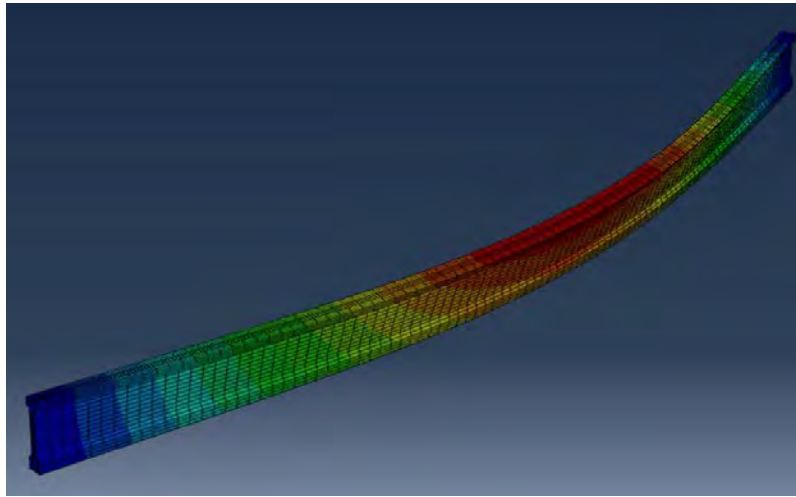
Figure 5.47. Buckled Shape at Peak Load.

5.4 Model Validation: Girder Rollover

5.4.1 Modeling Considerations

Although idealized simple and continuous supports are often assumed for design, various studies have indicated that girder instability during construction, particularly with regard to rollover, is significantly influenced, if not a primary function of, the bearing properties (Osterle et al. 2007; Garlich et al. 2015). Therefore, a more refined consideration of support conditions rather than the idealized pin and roller constraints typically used are critical to accurately evaluate stability. Influential bearing factors include slope, tilt angle, skew, and stiffness. In particular, PC girder rollover was found to be caused by an initial girder rotation, compounded by a deviation in flatness of the bottom flange and bearing roll flexibility (Garlich et al. 2015). Bearing pad properties and expected tilt and rotational performance limits are available in in NCHRP Reports 298 (Roeder et al. 1987) and 596 (Stanton et al. 2008).

Various studies have examined the rollover behavior of PC beams on elastic supports with analytical approaches (Mast 1993; Zureick et al. 2009; Plaut and Moen 2014; Krahl et al. 2020), but few have used an FEA approach. In fact, only one study could be found in the literature that used an FEA approach implemented within a commercial code that was validated with experimental data (Krahl 2017). Thus, as with the LTB modeling, guidance is limited.

5.4.2 Test Specimen

Only one test specimen was found in the literature that considered the rollover of a PC girder placed on elastomeric bearing pads and had the girder and support imperfections documented (Zureick et al. 2009), a BT-54 girder as shown in Figure 5.48. The beam spans 100 ft, and has 44 straight and harped prestress strands carrying a total prestress force of approximately 1800 kips. Concrete has properties of E = 4493 ksi and v = 0.22. The top sweep of the girder at midspan was recorded as 2.46 in. when placed on the bearing pads. The bearing pads were purposely placed on a sloped ground surface of 0.051 radians to encourage rollover. The elastomeric pads were 24 in x 14 in x 2-7/8 in. The rotational stiffness of the pad, its most critical property relevant to the rollover analysis, was reported to be 219,500 k-in/rad, while the shear stiffness was given as 4.7 kips/in and the compressive stiffness was found to nonlinear (Hurff 2010). A diagram of the beam is shown in Figure 5.48. The beam was loaded with a point load at midspan until rollover instability resulted. The resulting load-horizontal displacement curve is shown in Figure 5.49. The test was stopped at a load level of approximately 107 kips due to safety concerns.
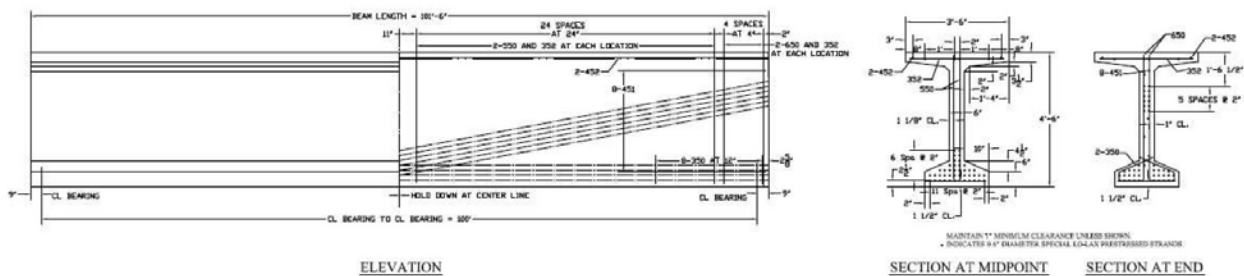
Figure 5.48. BT-54 Rollover Specimen (from Hurff 2010).
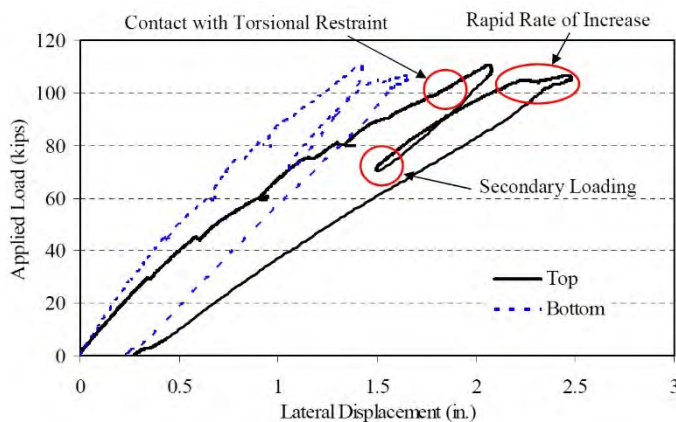
Figure 5.49. BT-54 Load Displacement Curve (from Hurff 2010).

5.4.3 FEA Model

The modeling approach was similar to that used for the LTB analysis, with several exceptions. First, since no cracking was reported, concrete was taken as linear elastic, and the only steel modeled was the prestress strands. These were included to impart the proper camber, and to validate that model deflections at the prestress and dead load stages.

Second, no single point constraints were imposed on the girder. Rather, the bearing pads were modeled explicitly and served as the supports. Here, a contact surface was specified between the bearing pad surface and the bottom of the girder flange. The bearing pads were supported vertically across their entire bottom surface, and supported horizontally and longitudinally by truss elements with equivalent stiffness to properly represent the pad shear stiffness. Various bearing pad modeling approaches were investigated, including explicitly modeling the steel shims; the use of a nonlinear elastic (hyperelastic) rubber material model; and representing the entire pad with a grid of vertical nonlinear springs, among others. However, using a solid modeling approach, it was not possible to match the specified values of rotational, vertical, as well as shear stiffness. Thus, a hybrid approach was used, which implemented a homogeneous linear elastic solid model ($E = 24.4$ ksi, $v = 0.48$, no shims), and the truss (spring) elements for shear stiffness. This approach could exactly match the specified shear and rotational stiffness properties of the bearing pad.

Third, adjustments were made in beam positioning during the analysis stages to better represent the actual sequence of loading. During the first stage, the beam was placed slightly above the bearing pad, without touching, and prestressed without constraint. Next, the dead load was applied, slowly pushing the beam down into the bearing pad. Finally, the nonlinear buckling analysis was conducted. The model has approximately 8000 elements and is shown in Figure 5.50.
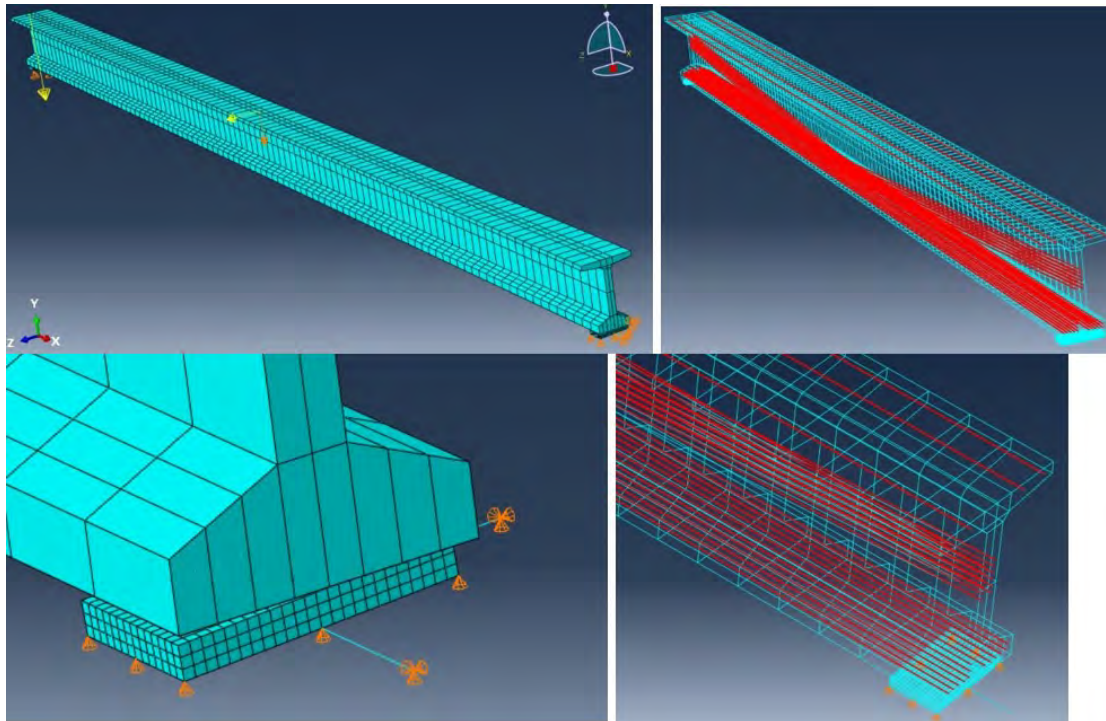
Figure 5.50. FEA Model of Rollover Beam.

5.4.4 Results

The load–horizontal displacement curve of the model is shown in Figure 5.51. The peak load applied to the model was 111.9 kips. The load on the test beam was stopped at approximately 107 kips, so the precise peak capacity is unknown. Thus, in Figure 5.51, two bounds are given to represent the test results: a lower bound taken at 107 kips, when the test was stopped, and an upper bound of approximately 116 kips, based on a linear extrapolation (dotted red line) from the recorded results (solid red line). In either case, the model result is within about 5% of the test value. Illustration of the beam rollover sequence is given in Figures 5.52 and 5.53.
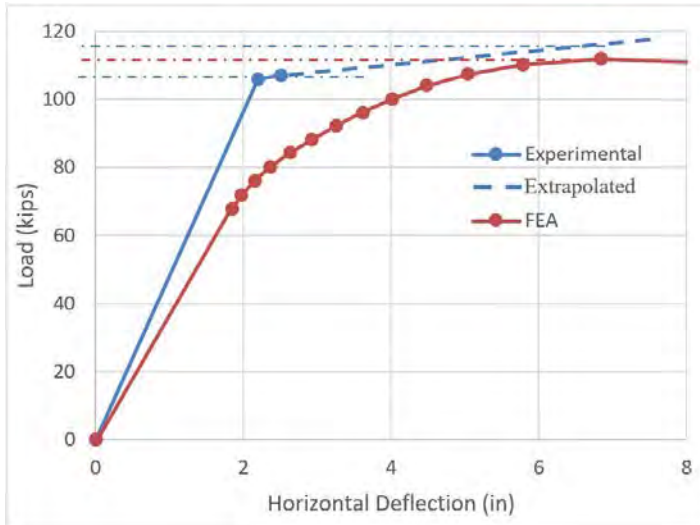
Figure 5.51. Load Displacement Curve for Rollover Model.
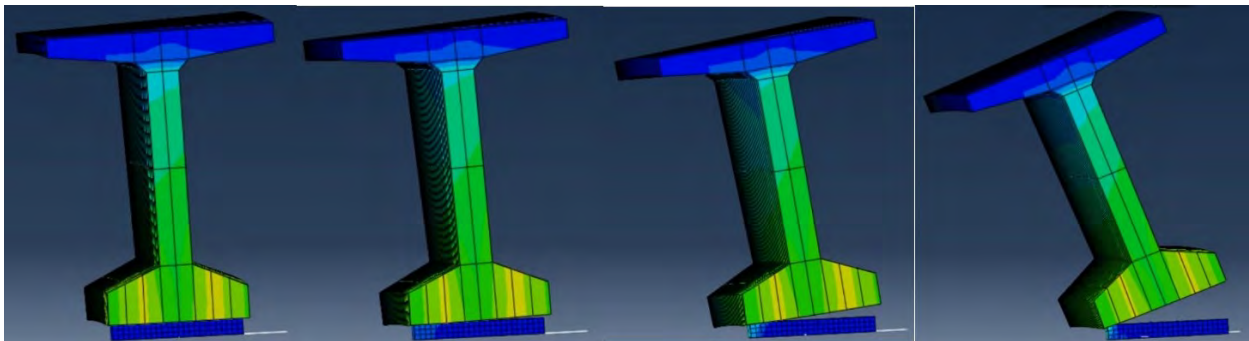
Figure 5.52. Beam Rollover, End View.
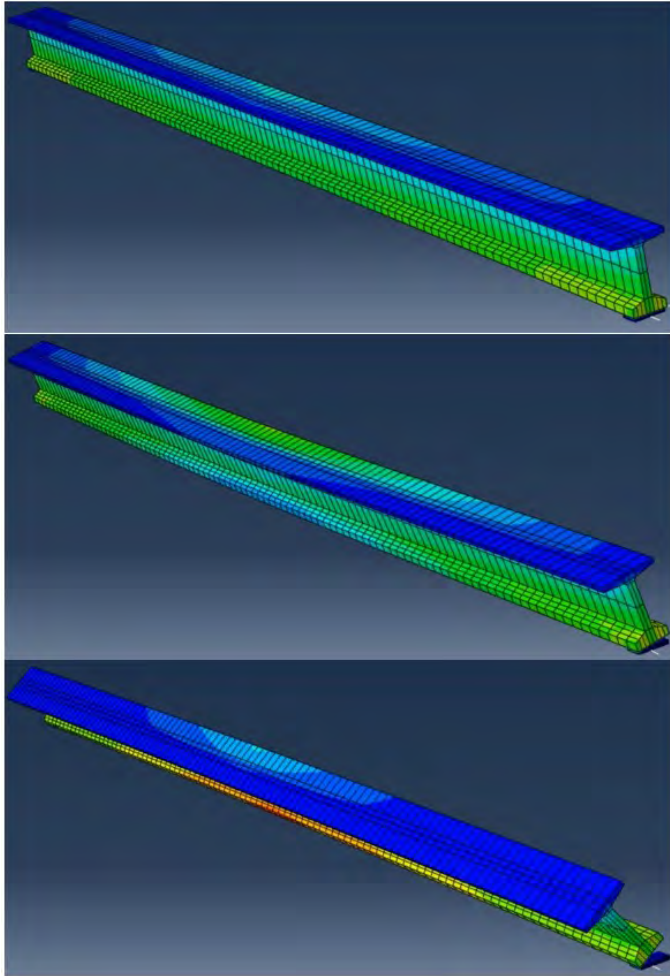
Figure 5.53. Beam Rollover, Side View.

5.5 Summary and Recommendations

The validation effort considered three bridges for diaphragm and structural system model verification (two laboratory bridges and one field structure); three theoretical buckling cases (one axial and two LTB) and three beam tests (one RC, two PC) for LTB model verification; and one test for beam rollover stability model verification. In each case, reasonable agreement between the model and experimental data were found. From these results, the following modeling approaches are recommended:

1. The bridge deck and girders can be modeled with either solids or shells per the convenience of the analyst, as either of these approaches work adequately. Diaphragms may be represented with truss elements. The mesh densities considered above can be used with quadratic elements. It is likely that the mesh may be coarsened if needed for larger structures. In this case, however, the adequacy of the coarser mesh must be compared to the results of the original mesh.

   This analysis will be used to assess the contribution on IDs on the performance of the in-service structure under vehicular live load.

2. PC girder LTB can be modeled using the second approach detailed above. This involves a three-stage analysis including the application of prestressing, dead load, and then the buckling load(s), with the model load time periods considered. The CDP model can be used for concrete considering LTB provided that all reinforcing steel is explicitly included and concrete tensile strength is set to near zero.

   The LTB model will be used to assess the need for IDs during construction and deck replacement, prior to deck curing, after at least one end wall or diaphragm has been placed. Prior to the placement of any lateral bracing, beam instability will be assessed with rollover rather than LTB.

3. PC girder rollover can be modeled using the approach given above. However, concrete strains are to be monitored throughout the analysis to ensure that cracking does not occur and the assumption of a linear elastic material response is valid. If cracking is indicated, the CDP modeling approach suggested for LTB can be included in the rollover model. Given the sensitivity of girder rollover to bearing properties, it is critical that a realistic assessment of bearing rotational stiffness be used in the analysis. Similarly, appropriate values for girder sweep and length must be considered. In addition to the procedure given by PCI, various studies have suggested such procedures. These must be assessed in relationship to the available experimental data for bearing stiffness properties prior to use in the parametric analysis.

   The rollover model will be used to assess girder stability prior to the placement of any lateral supports.

CHAPTER 6: EFFECT OF DIAPHRAGMS ON LIVE LOAD DISTRIBUTION

6.1 Introduction

The in-service performance of a bridge is of significant concern. In this study, the interest in this stage of the life cycle is the effect of diaphragms on the distribution of traffic load effects to the girders. In particular, it is desired to determine whether IDs alter live load distribution to an extent that their removal is unwarranted. To make this determination, two pieces of information are needed: quantitative data regarding the effect of IDs on live load distribution, and the degree of change in load distribution that would be unacceptable if IDs were removed. Such information can be used to assess their effectiveness on the in-service bridge as well as to compare resulting distribution factors (DFs) to AASHTO LRFD values, which have been developed without including the effect of IDs. As IDs are generally at or close to midspan, where moment effect rather than shear is generally critical, the evaluation conducted concerns moment effects rather than shear.

6.2 Structures Considered

A variety of hypothetical bridges were considered, with variations in span, girder spacing, number of lanes, type and number of diaphragms, live load configuration, and girder type. Although most structures were representative of MDOT design practice, some configurations exceeded current MDOT requirements (in particular, in terms of HL93-mod deflection limits) to explore further bounds of diaphragm performance. Variations include skew, curvature, and two span continuous structures. Note for continuous structures, since the models are linear elastic, the application of dead load will have no effect on live load distribution or ID behavior under live loads. Thus a distinction cannot be made between continuity for all load or live load only. However, full continuity is assumed under the live loads applied. The range of structures considered is summarized in Table 6.1. Note that not all combinations of parameters were studied. Typical cross-sections are given in Figure 6.1.

Table 6.1. Range of Bridges Considered.

Parameter	Range
Span length	40-200 ft
Girder spacing	5-13 ft
Skew angle	0, 30 degrees
Radius of curvature	0, 800 ft
Deck width	1, 2, 4 lanes
Diaphragm type	steel & CIP as specified in MDOT Design Guide
Diaphragm location	midspan, quarterspan
Number of spans	1, 2 (two span continuous over piers)
Beam type	bulb-tee, I-beam, box beam
Live load	single lane and two lane HS20 and truck trains

For all structures, deck thickness was taken as 9 in. and Young's modulus for the girders and deck of 5000 ksi and 4000 ksi, respectively (Poisson ratio taken as 0.19). These moduli roughly correspond to concrete compressive strengths of 8000 psi and 5000 psi, respectively. Although a minimum f'_c = 4000 psi was traditionally specified for decks, it was found that a Grade D mix

(now f'_c = 4500 psi) generally results in significantly higher strength than required (Eamon et al. 2014). CIP diaphragm strength was taken as 3000 psi (E ~ 3000 ksi).
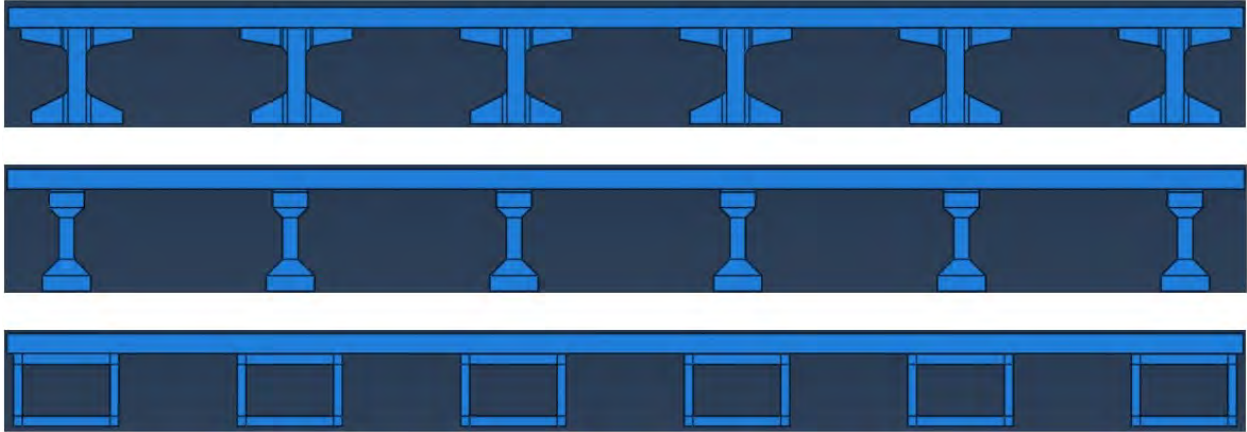
Figure 6.1. Typical Idealized Bridge Cross-Sections.

A set of available MDOT PC bridge construction drawings indicated most modern PC bridges appear to be of the bulb-tee type, with (single) spans from 100-150 ft and girder spacing from about 6 – 9 ft. Additionally, results of the MDOT bridge database survey conducted in Task 1 indicated that the most typical PC structures are single span, from 40-50 ft wide, 90-110 ft long (each span), and zero skew. From these results, the base bridge type was taken as a two lane, 8 ft girder spacing (5 girder), 100 ft span structure with zero skew and zero curvature. The default deck width was taken as 47 ft total, assuming a non-freeway bridge with ADT > 2000, resulting in two 12 ft lanes and 10 ft wide shoulder regions (8 ft shoulder + 2 ft), and a 1.5 ft wide barrier base. However, width was slightly adjusted in some cases to produce a typical overhang close to 2.5 ft from the girder centerline to the deck edge, though the overhang was allowed to vary somewhat depending on the bridge width and girder spacing.

A summary of the bridge geometries considered is given in Tables 6.1-6.4. Girder sizes were chosen based on span tables (PCI 2011; Eamon et al. 2018) and nearly all met HL93-mod deflection criteria. For intermediate spans, and longer spans beyond the range of the available tables, needed girder stiffness characteristics were interpolated and extrapolated, respectively. If girder stiffness was needed that was beyond the largest PC girder size given in the MDOT Design Guide, a haunch was added to appropriately increase stiffness. This is identified by the symbol "3h", indicating a 3 in. haunch. In a few cases, girder modulus of elasticity was also increased as needed. For these cases, however, it was found that this stiffness change no significant effect on the performance of the diaphragm. "Overhang" refers to the distance from the centerline of the fascia girder to the deck outer edge. Diaphragms were chosen as specified in the MDOT Design Guide, where for the beam sizes considered, either a single channel, cross-bracing (with L6x4x1/2 angle members), or concrete diaphragms were used.

Table 6.2. Bulb-Tee Bridge Geometries.

Label	Span (ft)	Girder Spacing (ft)	Girder Size	Width ft (lanes)	Over-hang (ft)	Diaphragm
40-6	40	6.0	36BT	47 (2)	2.5	C12x20.7
40-10.5	40	10.5	36BT	47 (2)	2.5	C12x20.7
100-5	100	5.0	36BT	45 (2)	2.5	C12x20.7
100-8.5 (1L)	100	8.5	42BT	23 (1)	3.0	C12x20.7
100-7 (4L)	100	7.0	42BT	75 (4)	2.5	C12x20.7
100-8 (45w)	100	8.0	42BT	45 (2)	2.5	C12x20.7
100-8	100	8.0	42BT	47 (2)	3.5	Crossbracing
100-8 (72BT)	100	8.0	72BT	47 (2)	3.5	Crossbracing
100-12 (72BT)	100	12.0	72BT	45 (2)	4.5	Crossbracing
200-6	200	6.0	72BT - 3h	47 (2)	2.5	Crossbracing
200-8 (45w)	200	8.0	72BT - 3h	45 (2)	2.5	Crossbracing
200-8.5	200	8.5	72BT - 3h	47 (2)	2.25	Crossbracing
200-8.5 (1L)	200	8.5	72BT - 3h	23 (1)	3.0	C12x20.7
200-8.5 (4L)	200	8.5	72BT - 3h	75 (4)	3.5	Crossbracing
200-10.5	200	10.5	72BT - 3h	47 (2)	2.5	Crossbracing
200-13	200	13.0	72BT - 3h	47 (2)	4.0	Crossbracing

Table 6.3. AASHTO Girder Bridge Geometries.

Label	Span (ft)	Girder Spacing (ft)	Girder Size	Width ft (lanes)	Over-hang (ft)	Diaphragm
40-6	40	6.0	Type 1	47 (2)	2.5	C10x15.3
40-6 (CD)	40	6.0	Type 1	47 (2)	2.5	concrete
40-11	40	11.0	Type 2	47 (2)	1.5	C12x20.7
40-11 (CD)	40	11.0	Type 2	47 (2)	1.5	concrete
100-6	100	6.0	Type 3	47 (2)	2.5	MC18x42.7
100-6 (CD)	100	6.0	Type 3	47 (2)	2.5	concrete
100-8.5	100	8.5	Type 3 - 1.5h	47 (2)	2.25	MC18x42.7
100-8.5 (23w)	100	8.5	Type 3 - 1.5h	23 (1)	3.0	MC18x42.7
100-8.5 (75w)	100	8.5	Type 3 - 1.5h	75 (4)	3.5	MC18x42.7
100-11	100	11.0	Type 4	47 (2)	1.5	MC18x42.7
100-11 (CD)	100	11.0	Type 4	47 (2)	1.5	concrete
100-11 (CB)	100	11.0	Type 4	47 (2)	1.5	Crossbracing
150-6	150	6.0	Type 4 - 1.5h	47 (2)	2.25	MC18x42.7
150-6 (CD)	150	6.0	Type 4 - 1.5h	47 (2)	2.25	concrete
150-8.5	150	8.5	Type 4 - 1.5h	47 (2)	2.5	MC18x42.7
150-8.5 (CD)	150	8.5	Type 4 - 1.5h	47 (2)	2.5	concrete

Table 6.4. Box Beam Bridge Geometries.

Label	Span (ft)	Girder Spacing (ft)	Girder Size	Width ft (lanes)	Over-hang (ft)	Diaphragm
40-6	40	6.0	36 x 17	47 (2)	2.5	concrete
40-11	40	11.0	36 x 17	47 (2)	1.5	concrete
60-6	60	6.0	48 x 21	47 (2)	2.5	concrete
60-10.5	60	10.5	48 x 21	47 (2)	2.5	concrete
100-6	100	6.0	48 x 33	47 (2)	2.5	concrete
100-8.5	100	8.5	48 x 33	47 (2)	2.25	concrete
100-10.5	100	10.5	48 x 33	47 (2)	2.5	concrete

Table 6.5. Continuous, Curved, and Skewed Bridge Geometries.

Label	Span (ft)	Girder Spacing (ft)	Girder Size	Width ft (lanes)	Over-hang (ft)	Diaphragm	Feature
40-11 (Cont)	40	11.0	Type 2	47 (2)	1.5	C12x20.7	Continuous
100-11 (Cont)	100	11.0	Type 3	47 (2)	1.5	MC18x42.7	Continuous
40-8.5 (Skew)	40	8.5	Type 2	47 (2)	1.5	C12x20.7	Skew (30 deg)
100-8.5 (Skew)	100	8.5	Type 3 - 1.5h	47 (2)	1.5	MC18x42.7	Skew (30 deg)
150-8.5 (Skew)	150	8.5	Type 4 - 1.5h	47 (2)	1.5	MC18x42.7	Skew (30 deg)
40-8.5 (Curve)	40	8.5	Type 2	47 (2)	1.5	C12x20.7	Curved (800 ft rad)
100-8.5 (Curve)	100	8.5	Type 3 - 1.5h	47 (2)	1.5	MC18x42.7	Curved (800 ft rad)
150-8.5 (Curve)	150	8.5	Type 4 - 1.5h	47 (2)	1.5	MC18x42.7	Curved (800 ft rad)

6.3 Modeling Approach

6.3.1 Geometry Idealization

Although barriers are known to lower girder distribution factor (DF), since they are not designed to carry gravity loads, they are conservatively not included in the bridge models. For modeling simplicity, the deck thickness is taken to be constant across the entire deck width. Similarly, the deck is modeled as a perfectly flat volume, with no crown, slope, or girder camber, as girder camber and deck slope have no significant effect on live load distribution.

As shown in Figure 6.2, girders were modeled to closely resemble the actual cross-sectional shapes rather than using simpler geometric approximations. This is because it is difficult to accurately capture all of the multiple primary stiffness properties of the girder as well as the behavior of the diaphragm with simpler representations. Flange and web thicknesses were adjusted slightly such that the primary stiffness properties of the idealized shapes matched those of the actual girder. Although beam elements could be used, in which the cross-sectional properties could be explicitly specified, this idealization has been found to negatively influence the accuracy of results when diaphragms are considered.
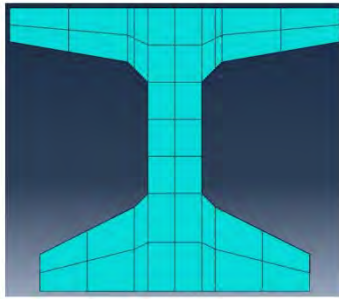
(a) 42" Bulb Tee.
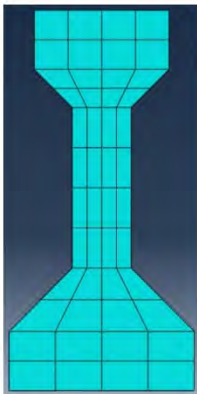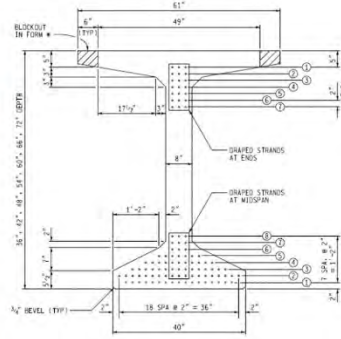
(b) AASHTO Type III Girder.
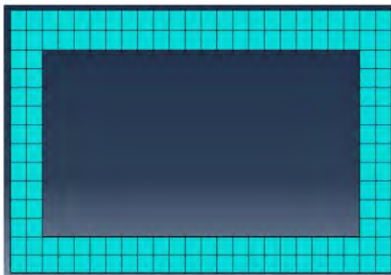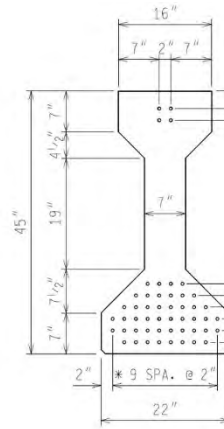
(c) 48 x 33 Box Beam.
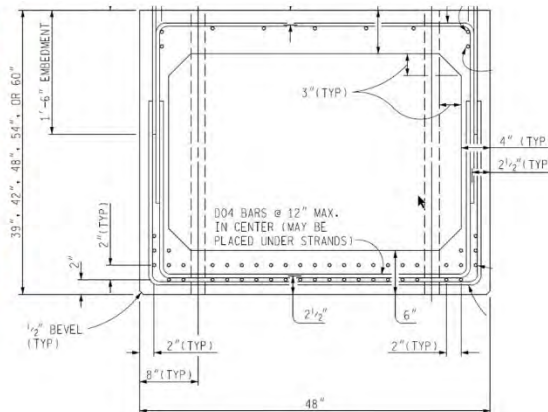
Figure 6.2. Example Idealized Bridge Girders (figures on right from MDOT BDG).

6.3.2 Boundary Conditions

Each girder is constrained vertically at both ends to represent roller supports, while the bridge system model as a whole is given sufficient but minimal symmetric longitudinal (parallel to girder span) and lateral (normal to girder span) constraints at girder vertical support points on one end of the bridge to provide stability. This generally involved one end of two girders constrained longitudinally and one end of one girder constrained laterally (see Figure 6.3a). Note that since

solid elements are used (see below), all constraints are translational. Bearing flexibility was not considered nor were end walls or additional longitudinal constraints included.

6.3.3 Element Type and Mesh Density

Guided by the validation models developed earlier, the deck and girders for all models were represented with quadratic (20-node) hexahedral (solid) elements, which potentially represents the most accurate approach. Mesh density varied depending on the model type and size, but in general, girders were approximately discretized on the order of 10 elements throughout the depth, 100 elements along the length, and 4-10 elements laterally, depending on the beam type modeled (see Figures 6.2 and 6.3 for typical mesh densities). The deck was approximately discretized with 10 elements between girders, 100 elements along the length, and 2-3 elements through the thickness. A mesh sensitivity study revealed that further discretization produced no significant changes in results. Example of typical models are shown in Figure 6.3. Components with different mesh densities and nodal alignments (girder, deck, diaphragm) were linked together using ties (a type of multi-point constraint).

6.3.4 Diaphragm Representation

Diaphragms are assumed to be perfectly connected to the girders (and deck, when CIP IDs are used) without slip. This results in a conservative evaluation of the need for diaphragms if less than ideal connections exist, as the model provides the upper bound of diaphragm effectiveness. Regardless of type, diaphragms were modeled with 8-node quadratic shell elements, and were discretized using approximately 10-20 elements between girders and from 4-10 elements deep, depending on model type. All diaphragms were modeled to recover the primary stiffness properties of the components as specified in the MDOT Bridge Design Guide for the girder size chosen. The large majority of IDs considered for bulb-tee and AASHTO-type girders were steel. Concrete diaphragms were used in selected cases for comparison, as well as for all box beams bridges. Typical diaphragm models are shown in Figure 6.4.

6.3.5 Live Load

Bridges were loaded with a single HS20 truck configuration (with axles spaced 14 ft and wheel lines spaced 6 ft apart) as well as two HS20 trucks placed side-by-side, where the vehicles were placed longitudinally on the bridge to maximize moment. Here, wheel loads were represented by concentrated loads applied on the deck (see Figure 6.3a). A program was written that automatically generates multiple load steps in the analysis that increments the trucks transversely across the deck (typically at 0.5 – 1 ft increments), such that the concentrated wheel load is placed from 3.5 ft of the deck edge (i.e. 2 ft from the edge of an assumed barrier width of 1.5 ft), until the truck is centered on the bridge. For the two truck case, the trucks are moved together with a constant space between the adjacent wheel lines of 4 ft. An additional load configuration is considered where multiple trucks are placed in a line that spans across the entire bridge (i.e. "line load" case). For the continuous bridge case, a single vehicle in each lane was placed to maximize positive moment on one span.
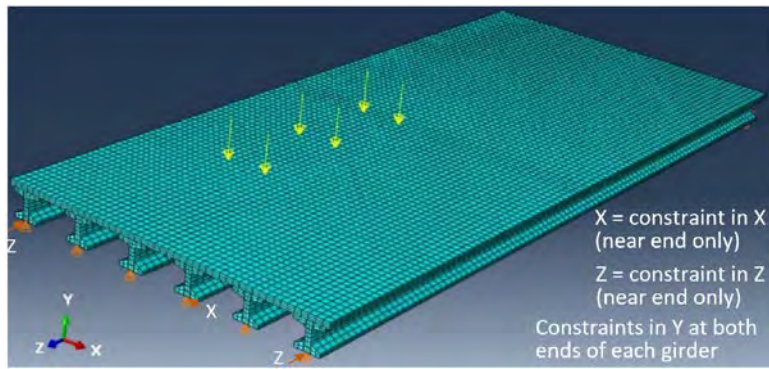
(a) Example Complete Model and Typical Boundary Conditions.
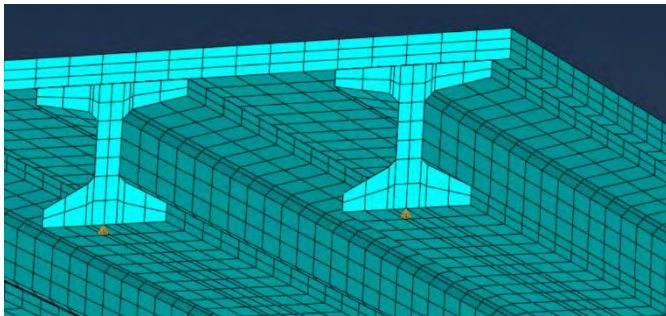
(b) Example Bulb-Tee Model.
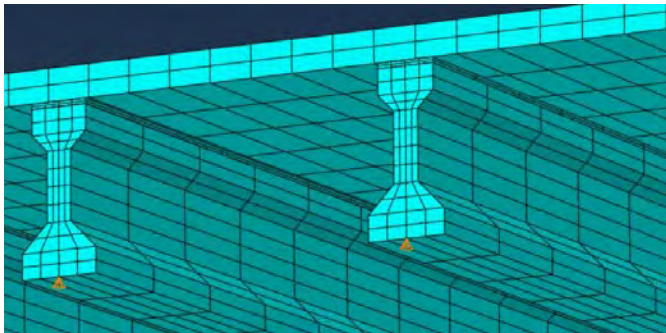
(c) Example AASHTO Girder Model.
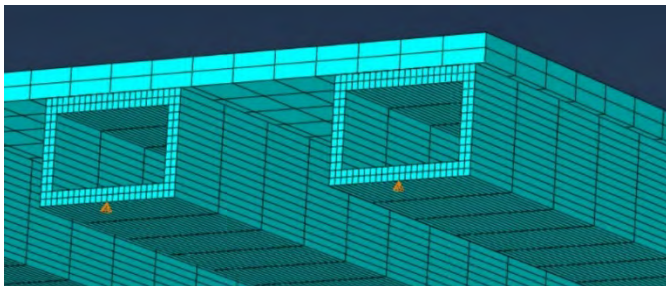
(d) Example Box Beam Model.

Figure 6.3. Typical FEA Models.
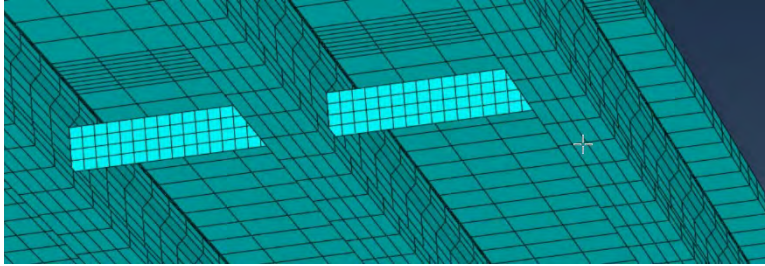
(a) Example Channel Diaphragm Model.
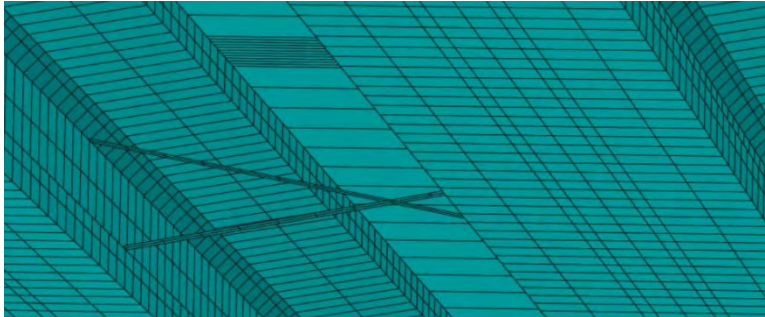
(b) Example Cross-bracing Diaphragm Model.
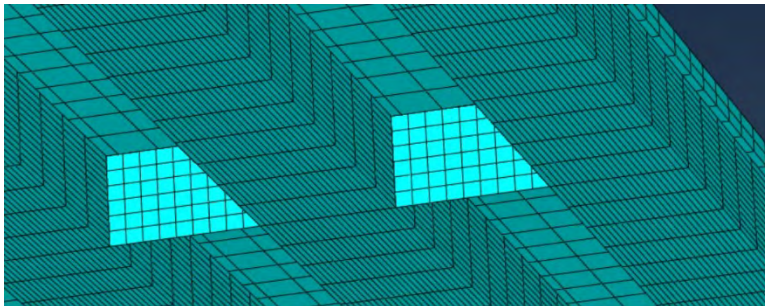
(c) Example Concrete Diaphragm Model.

Figure 6.4. Typical Diaphragm Models.

6.3.6 Solution Process

Models are linear elastic. Change in girder DF is used to quantify diaphragm effectiveness, as it normalizes results regardless of girder capacity, bridge geometry, and load level. For each load configuration (i.e. one lane, two lane, and line load cases), results of all runs are recorded, and DF is computed for all girders for all load increments. From this set of results, the maximum DF is reported for the exterior and the governing interior girder. For n total girders on the bridge, DF for girder k is computed as:

$$DF_k = \frac{v_k}{\sum_{i=1}^{n} v_i} \qquad (6.1)$$

where v is the deflection of girder k. Accounting for the alternative base bridge geometries, girder sizes, and ID configurations, approximately 140 models were developed. The one and two lane load cases resulted in approximately 280 scenarios. As the loads were incremented an average of

roughly 30 locations across (half) of the deck transversely to determine maximum DF, approximately 8400 analyses were conducted.

6.4 Results

6.4.1 Introduction

Figures 6.5-6.7 show typical deformed shapes of the bridge models (where color contours are used to illustrate changes in vertical deflection). Detailed results are given in Tables 6.6-6.13, while a summary of results is given in Tables 6.14-6.16, where maximum and average DF values are given for all cases and for typical cases. The typical case is that of a two lane structure using one line of steel diaphragms at midspan, and with expected girder stiffness. For comparison, DF values for moment effect given by AASHTO LRFD are provided.

When bulb tee girders are considered, the AASHTO DF values are calculated using two alternate deck thickness values; one value considering just the thickness of the deck, as originally defined, and another where deck thickness is taken as the sum of the deck and upper girder flange thickness. Although not code-specified, this latter approach is provided for reference, as it was found to provide a better match to the FEA results.

For consistent comparison to the DF values determined from the FEA models, when presented in the Tables, the one lane AASHTO DF value is divided by 1.2 to remove the included multiple presence factor (other than for the exterior girder case, in which the lever rule governs), while the two lane AASHTO value is divided by 2.0 to account for the fact that the AASHTO DF value is meant to be applied to the weight of a single design truck rather than to the weight of two trucks as used in the two lane loaded FEA model results.
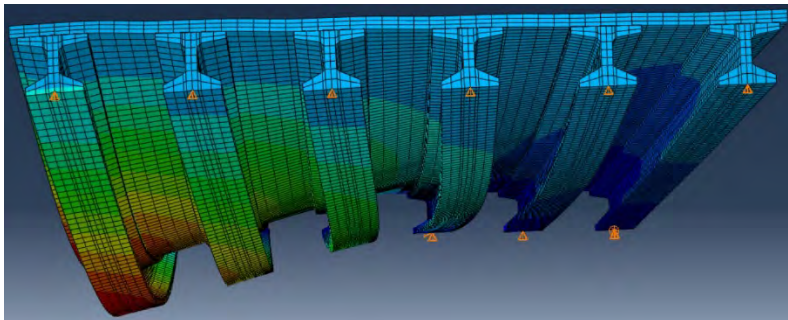
a) No diaphragms.
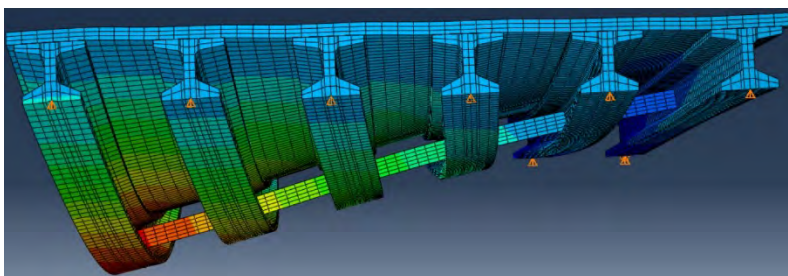
b) Midspan diaphragms.
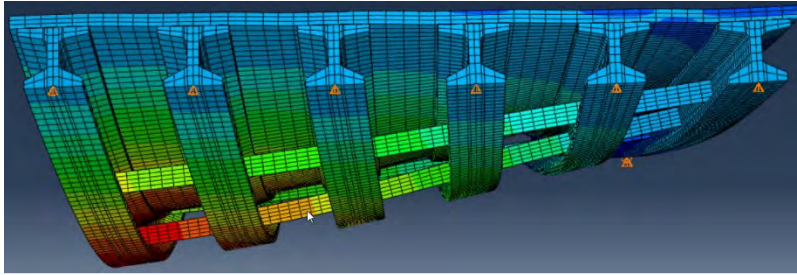
c) Mid and quarterspan diaphragms.

Figure 6.5. Typical Deflection of Bulb Tee Bridge, Load on Edge Girder.
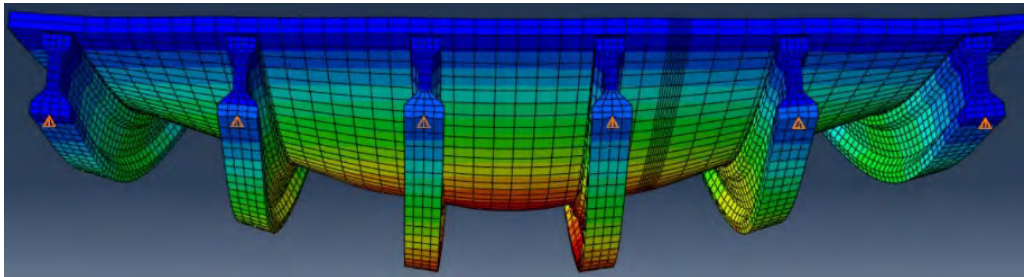
a) No diaphragms.
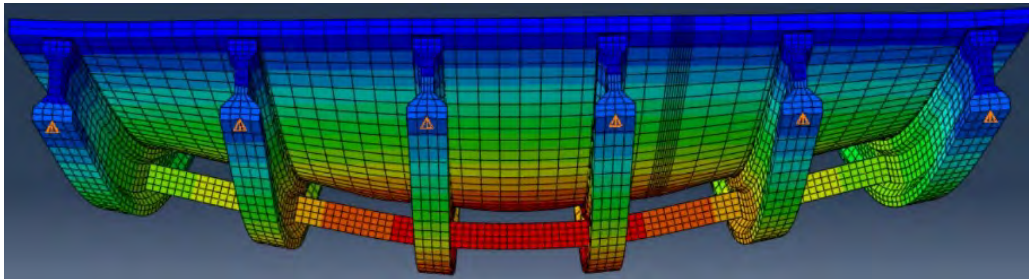
b) Midspan diaphragms.

Figure 6.6. Typical Deflection of AASHTO Beam Bridge, Load on Center Girder.
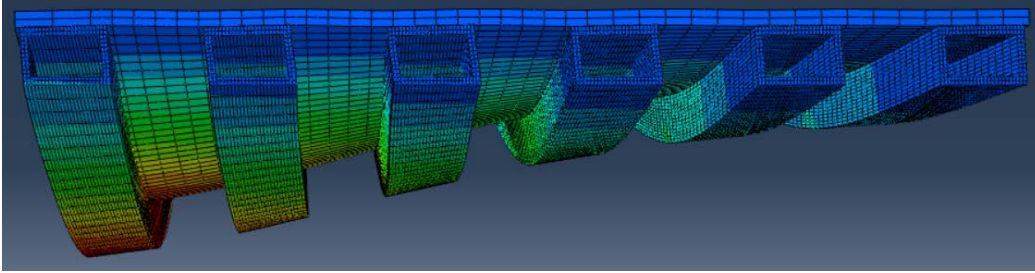
a) One lane loading at edge, no diaphragms.
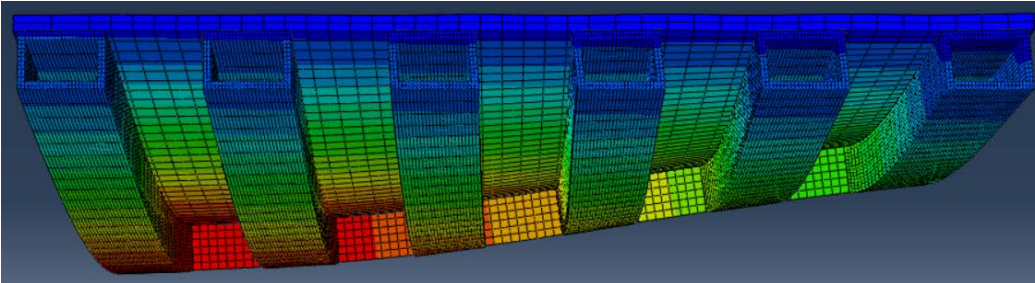
b) One lane loading at edge, with midspan diaphragms.
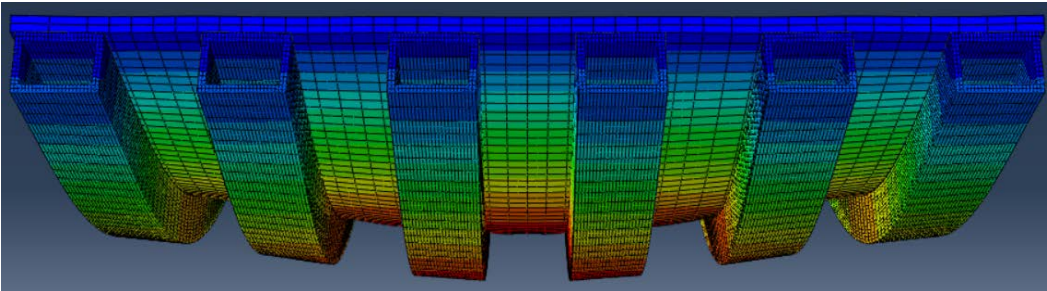
c) Two lane loading at center, no diaphragms.
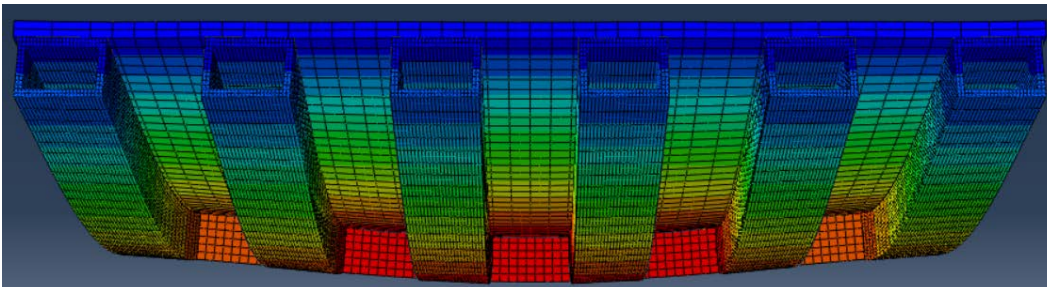
d) Two lane loaded at center, with midspan diaphragms.

Figure 6.7. Typical Deflection of Box Beam Bridge.

Table 6.6. Interior Girder DFs for Bulb Tee Bridges.

| Bridge | Load Case | AASHTO (deck) | AASHTO (flange) | Girder DF | | | DF (none) / DF (ID) | | AASHTO / None |
				None	1 ID	3 IDs	1 ID	3 IDs	
40-6	1-HS20	0.41	0.36	0.34	0.32	0.32	1.04	1.06	1.22
	2-HS20	0.32	0.27	0.26	0.26	0.25	1.03	1.04	1.20
40-10.5	1-HS20	0.59	0.50	0.39	0.37	0.36	1.05	1.08	1.50
	2-HS20	0.47	0.41	0.44	0.41	0.39	1.07	1.12	1.08
100-5	1-HS20	0.28	0.24	0.22	0.21	0.21	1.01	1.01	1.29
	2-HS20	0.23	0.20	0.18	0.18	0.18	1.00	1.00	1.27
100-7 (4L)	1-HS20	0.34	0.30	0.28	0.27	0.27	1.03	1.04	1.21
	2-HS20	0.29	0.25	0.24	0.24	0.24	1.02	1.01	1.18
100-8 (45w)	1-HS20	0.37	0.32	0.30	0.30	0.29	1.01	1.01	1.23
	2-HS20	0.31	0.27	0.27	0.26	0.26	1.02	1.02	1.18
	1-Axle	0.37	0.32	0.30	0.30	0.30	1.01	1.01	1.23
	2-Axle	0.31	0.27	0.27	0.26	0.26	1.02	1.02	1.18
	1-Line	0.37	0.32	0.30	0.29	0.29	1.01	1.01	1.23
	2-Line	0.31	0.27	0.26	0.26	0.26	1.02	1.02	1.19
100-8	1-HS20	0.37	0.32	0.30	0.30	0.30	1.01	1.01	1.23
	2-HS20	0.31	0.27	0.27	0.26	0.26	1.02	1.03	1.16
100-8 (72BT)	1-HS20	0.41	0.35	0.34	0.31	0.31	1.08	1.09	1.22
	2-HS20	0.35	0.30	0.30	0.29	0.29	1.05	1.06	1.15
100-8.5 (1L)	1-HS20	0.38	0.33	0.34	0.34	0.34	1.01	1.01	1.13
100-12 (72BT)	1-HS20	0.53	0.45	0.38	0.35	0.35	1.07	1.07	1.40
	2-HS20	0.47	0.40	0.38	0.35	0.34	1.08	1.09	1.24
200-6	1-HS20	0.27	0.23	0.23	0.23	0.23	1.01	1.02	1.18
	2-HS20	0.24	0.20	0.20	0.20	0.20	1.01	1.01	1.21
200-8 (45w)	1-HS20	0.32	0.27	0.28	0.27	0.27	1.01	1.01	1.17
	2-HS20	0.29	0.24	0.25	0.24	0.24	1.01	1.02	1.20
	1-Line	0.32	0.27	0.27	0.27	0.27	1.00	1.00	1.19
	2-Line	0.29	0.24	0.24	0.24	0.24	1.01	1.01	1.20
200-8.5	1-HS20	0.34	0.28	0.28	0.28	0.28	1.01	1.01	1.19
	2-HS20	0.31	0.25	0.25	0.25	0.25	1.02	1.02	1.21
200-8.5 (1L)	1-HS20	0.34	0.28	0.33	0.33	0.33	1.00	1.00	1.02
200-8.5 (4L)	1-HS20	0.34	0.28	0.29	0.28	0.28	1.02	1.03	1.16
	2-HS20	0.31	0.25	0.25	0.24	0.24	1.03	1.04	1.23
200-10.5	1-HS20	0.38	0.32	0.31	0.31	0.31	1.00	1.00	1.23
	2-HS20	0.36	0.29	0.29	0.28	0.28	1.02	1.03	1.23
200-13	1-HS20	0.44	0.36	0.33	0.33	0.33	1.00	1.00	1.32
	2-HS20	0.42	0.34	0.32	0.32	0.32	1.02	1.02	1.28

Table 6.7. Interior Girder DFs for AASHTO Beam Bridges.

| Bridge | Load Case | AASHTO | Girder DF | | | DF (none) / DF (ID) | | AASHTO |
			None	1 ID	3 IDs	1 ID	3 IDs	/ None
40-6	1-HS20	0.36	0.33	0.32	0.32	1.03	1.04	1.09
	2-HS20	0.28	0.26	0.25	0.25	1.04	1.03	1.08
40-6 (CD)	1-HS20	0.36	0.33	0.32	0.31	1.05	1.06	1.09
	2-HS20	0.28	0.26	0.25	0.25	1.04	1.05	1.08
40-11	1-HS20	0.56	0.42	0.39	0.38	1.06	1.09	1.34
	2-HS20	0.46	0.46	0.43	0.41	1.07	1.12	1.00
40-11 (CD)	1-HS20	0.56	0.42	0.38	0.36	1.11	1.15	1.34
	2-HS20	0.46	0.46	0.40	0.38	1.16	1.23	1.00
100-6	1-HS20	0.30	0.28	0.27	0.27	1.02	1.03	1.08
	2-HS20	0.25	0.23	0.23	0.23	1.02	1.02	1.09
100-6 (CD)	1-HS20	0.30	0.28	0.27	0.27	1.03	1.04	1.08
	2-HS20	0.25	0.23	0.23	0.22	1.02	1.02	1.09
100-8.5	1-HS20	0.37	0.32	0.32	0.32	1.02	1.02	1.15
	2-HS20	0.32	0.29	0.28	0.28	1.03	1.04	1.11
100-8.5 (23w)	1-HS20	0.37	0.34	0.34	0.34	1.01	1.01	1.09
100-8.5 (75w)	1-HS20	0.37	0.31	0.31	0.30	1.02	1.04	1.18
	2-HS20	0.32	0.29	0.28	0.27	1.04	1.06	1.11
100-11	1-HS20	0.46	0.36	0.35	0.35	1.03	1.03	1.29
	2-HS20	0.41	0.35	0.33	0.32	1.06	1.08	1.18
100-11 (CB)	1-HS20	0.46	0.36	0.35	0.35	1.03	1.03	1.29
	2-HS20	0.41	0.35	0.32	0.32	1.08	1.10	1.18
100-11 (CD)	1-HS20	0.46	0.36	0.34	0.34	1.04	1.05	1.29
	2-HS20	0.41	0.35	0.32	0.31	1.09	1.12	1.18
150-6	1-HS20	0.28	0.25	0.24	0.24	1.02	1.02	1.12
	2-HS20	0.24	0.21	0.21	0.21	1.01	1.01	1.14
150-6 (CD)	1-HS20	0.28	0.25	0.24	0.24	1.02	1.03	1.13
	2-HS20	0.24	0.21	0.21	0.21	1.01	1.02	1.15
150-8.5	1-HS20	0.34	0.30	0.29	0.29	1.01	1.01	1.14
	2-HS20	0.31	0.26	0.26	0.26	1.02	1.02	1.17
150-8.5 (CD)	1-HS20	0.34	0.30	0.29	0.29	1.01	1.02	1.15
	2-HS20	0.31	0.26	0.26	0.26	1.03	1.03	1.18

Table 6.8. Interior Girder DFs for Box Beam Bridges.

Bridge	Load Case	AASHTO	Girder DF			DF (none) / DF (ID)		AASHTO
			None	1 ID	3 IDs	1 ID	3 IDs	/ None
40-6	1-HS20	0.29	0.28	0.27	0.27	1.04	1.06	1.03
	2-HS20	0.25	0.22	0.22	0.22	1.02	1.04	1.12
40-11	1-HS20	0.42	0.36	0.34	0.33	1.04	1.06	1.18
	2-HS20	0.39	0.36	0.34	0.33	1.05	1.09	1.09
60-6	1-HS20	0.25	0.23	0.22	0.22	1.03	1.04	1.10
	2-HS20	0.23	0.19	0.19	0.19	1.02	1.03	1.18
60-10.5	1-HS20	0.35	0.31	0.30	0.30	1.03	1.03	1.13
	2-HS20	0.35	0.30	0.29	0.29	1.05	1.07	1.15
100-6	1-HS20	0.21	0.19	0.19	0.18	1.02	1.03	1.11
	2-HS20	0.22	0.17	0.17	0.17	1.02	1.02	1.30
100-8.5	1-HS20	0.26	0.25	0.24	0.24	1.03	1.03	1.05
	2-HS20	0.28	0.23	0.22	0.22	1.03	1.03	1.22
100-10.5	1-HS20	0.30	0.28	0.27	0.27	1.02	1.02	1.07
	2-HS20	0.33	0.27	0.26	0.26	1.04	1.04	1.23

Table 6.9. Exterior Girder DFs for Bulb Tee Bridges.

Bridge	Load Case	AASHTO	Girder DF			DF (none) / DF (ID)		AASHTO / None
			None	1 ID	3 IDs	1 ID	3 IDs	
40-6	1-HS20	0.42	0.42	0.42	0.42	1.00	1.01	1.00
	2-HS20	0.42	0.24	0.25	0.25	0.97	0.96	1.76
40-10.5	1-HS20	0.62	0.58	0.58	0.58	1.00	1.00	1.07
	2-HS20	0.62	0.34	0.36	0.36	0.96	0.95	1.81
100-5	1-HS20	0.40	0.25	0.25	0.25	1.01	1.01	1.58
	2-HS20	0.40	0.20	0.20	0.20	0.99	0.99	2.04
100-7 (4L)	1-HS20	0.43	0.37	0.36	0.36	1.04	1.03	1.16
	2-HS20	0.43	0.28	0.28	0.28	1.01	1.00	1.54
100-8 (45w)	1-HS20	0.63	0.40	0.39	0.39	1.02	1.02	1.57
	2-HS20	0.63	0.30	0.31	0.31	0.99	0.98	2.09
	1-Axle	0.63	0.40	0.39	0.39	1.02	1.02	1.57
	2-Axle	0.63	0.30	0.30	0.31	0.99	0.98	2.10
	1-Line	0.63	0.39	0.39	0.39	1.00	1.01	1.60
	2-Line	0.63	0.30	0.30	0.31	0.99	0.98	2.09
100-8	1-HS20	0.63	0.42	0.40	0.40	1.03	1.05	1.51
	2-HS20	0.63	0.32	0.32	0.32	0.99	0.99	1.99
100-8 (72BT)	1-HS20	0.63	0.39	0.39	0.39	0.99	1.00	1.61
	2-HS20	0.63	0.34	0.35	0.35	0.97	0.97	1.84
100-8.5 (1L)	1-HS20	0.59	0.45	0.46	0.46	0.98	0.98	1.31
100-12 (72BT)	1-HS20	0.83	0.55	0.55	0.55	1.00	1.00	1.51
	2-HS20	1.25	0.48	0.49	0.49	0.98	0.98	2.60
200-6	1-HS20	0.42	0.28	0.27	0.27	1.02	1.02	1.50
	2-HS20	0.42	0.22	0.23	0.23	0.99	1.00	1.87
200-8 (45w)	1-HS20	0.50	0.36	0.35	0.35	1.02	1.02	1.40
	2-HS20	0.50	0.29	0.29	0.29	0.99	0.99	1.75
	1-Line	0.50	0.35	0.35	0.35	0.99	1.00	1.44
	2-Line	0.50	0.29	0.29	0.29	0.99	0.99	1.75
200-8.5	1-HS20	0.50	0.37	0.36	0.36	1.02	1.02	1.36
	2-HS20	0.50	0.30	0.30	0.30	1.00	1.00	1.67
200-8.5 (1L)	1-HS20	0.59	0.42	0.42	0.42	1.00	1.00	1.39
200-8.5 (4L)	1-HS20	0.65	0.39	0.36	0.35	1.07	1.09	1.69
	2-HS20	0.62	0.30	0.29	0.28	1.03	1.05	2.09
200-10.5	1-HS20	0.62	0.43	0.43	0.43	1.02	1.02	1.43
	2-HS20	0.62	0.35	0.36	0.36	0.99	0.99	1.76
200-13	1-HS20	0.81	0.53	0.52	0.52	1.02	1.02	1.52
	2-HS20	1.21	0.44	0.44	0.44	0.99	1.00	2.78

Table 6.10. Exterior Girder DFs for AASHTO Beam Bridges.

Bridge	Load Case	AASHTO	Girder DF			DF (none) / DF (ID)		AASHTO / None
			None	1 ID	3 IDs	1 ID	3 IDs	
40-6	1-HS20	0.42	0.42	0.42	0.42	1.00	1.01	1.00
	2-HS20	0.42	0.24	0.25	0.26	0.96	0.94	1.75
40-6 (CD)	1-HS20	0.42	0.42	0.42	0.41	1.01	1.02	1.00
	2-HS20	0.42	0.24	0.25	0.26	0.99	0.93	1.71
40-11	1-HS20	0.55	0.55	0.55	0.56	0.99	0.99	1.00
	2-HS20	0.55	0.32	0.34	0.35	0.95	0.91	1.73
40-11 (CD)	1-HS20	0.55	0.55	0.55	0.55	0.99	0.99	1.00
	2-HS20	0.55	0.32	0.35	0.37	0.90	0.87	1.73
100-6	1-HS20	0.42	0.35	0.34	0.34	1.03	1.05	1.20
	2-HS20	0.42	0.25	0.26	0.26	0.98	0.98	1.66
100-6 (CD)	1-HS20	0.42	0.35	0.34	0.33	1.04	1.06	1.20
	2-HS20	0.42	0.25	0.26	0.26	0.98	0.98	1.66
100-8.5	1-HS20	0.50	0.44	0.43	0.43	1.03	1.04	1.12
	2-HS20	0.50	0.32	0.33	0.33	0.98	0.97	1.54
100-8.5 (23w)	1-HS20	0.59	0.49	0.49	0.49	1.00	1.00	1.20
100-8.5 (75w)	1-HS20	0.65	0.46	0.43	0.42	1.07	1.11	1.40
	2-HS20	0.65	0.34	0.34	0.33	1.01	1.03	1.91
100-11	1-HS20	0.55	0.52	0.51	0.51	1.01	1.02	1.07
	2-HS20	0.55	0.37	0.38	0.39	0.96	0.95	1.48
100-11 (CB)	1-HS20	0.55	0.52	0.51	0.50	1.02	1.03	1.07
	2-HS20	0.55	0.37	0.39	0.39	0.95	0.94	1.48
100-11 (CD)	1-HS20	0.55	0.52	0.50	0.49	1.02	1.04	1.07
	2-HS20	0.55	0.37	0.39	0.39	0.95	0.95	1.48
150-6	1-HS20	0.40	0.31	0.30	0.29	1.02	1.03	1.31
	2-HS20	0.40	0.23	0.24	0.24	0.99	0.99	1.70
150-6 (CD)	1-HS20	0.40	0.30	0.29	0.29	1.03	1.04	1.32
	2-HS20	0.40	0.23	0.24	0.24	0.99	0.99	1.71
150-8.5	1-HS20	0.53	0.39	0.39	0.38	1.02	1.03	1.35
	2-HS20	0.53	0.31	0.31	0.31	0.99	0.99	1.73
150-8.5 (CD)	1-HS20	0.53	0.39	0.38	0.38	1.02	1.03	1.35
	2-HS20	0.53	0.31	0.31	0.31	0.99	0.99	1.73

Table 6.11. Exterior Girder DFs for Box Beam Bridges.

Bridge	Load Case	AASHTO	Girder DF			DF (none) / DF (ID)		AASHTO /
			None	1 ID	3 IDs	1 ID	3 IDs	None
40-6	1-HS20	0.42	0.35	0.34	0.34	1.02	1.04	1.20
	2-HS20	0.42	0.23	0.23	0.24	0.98	0.98	1.82
40-11	1-HS20	0.55	0.51	0.50	0.50	1.01	1.01	1.09
	2-HS20	0.55	0.35	0.36	0.36	0.97	0.95	1.59
60-6	1-HS20	0.42	0.27	0.26	0.26	1.02	1.03	1.56
	2-HS20	0.42	0.21	0.21	0.21	0.99	0.99	2.04
60-10.5	1-HS20	0.60	0.44	0.43	0.43	1.03	1.04	1.36
	2-HS20	0.60	0.34	0.34	0.34	0.99	0.99	1.78
100-6	1-HS20	0.50	0.22	0.21	0.21	1.01	1.02	2.31
	2-HS20	0.50	0.18	0.18	0.18	1.00	1.01	2.77
100-8.5	1-HS20	0.41	0.30	0.30	0.30	1.03	1.03	1.35
	2-HS20	0.41	0.25	0.25	0.25	1.00	0.99	1.64
100-10.5	1-HS20	0.52	0.37	0.36	0.35	1.04	1.04	1.41
	2-HS20	0.52	0.30	0.30	0.30	1.00	1.00	1.72

Table 6.12. Interior Girder DFs for Special Cases.

Bridge	Load Case	AASHTO	Girder DF		DF (none) / DF (ID)	AASHTO / None		
			None	1 ID				
40-11 (Cont)	1-HS20	0.56	0.43	0.40	1.07	1.30		
	2-HS20	0.46	0.46	0.44	1.04	1.00		
100-11 (Cont)	1-HS20	0.46	0.36	0.35	1.04	1.27		
	2-HS20	0.41	0.36	0.33	1.08	1.13		

Bridge	Load Case	AASHTO	Girder DF			DF (none) / DF (ID)		AASHTO /
			None	1 ID	3 IDs	1 ID	3 IDs	None
40-8.5 (Skew)	1-HS20	0.48	0.41	0.40	0.38	1.04	1.07	1.17
	2-HS20	0.38	0.37	0.36	0.35	1.04	1.08	1.01
100-8.5 (Skew)	1-HS20	0.37	0.32	0.31	0.31	1.01	1.01	1.17
	2-HS20	0.32	0.28	0.28	0.27	1.02	1.03	1.14
150-8.5 (Skew)	1-HS20	0.34	0.29	0.29	0.29	1.00	1.01	1.16
	2-HS20	0.31	0.26	0.26	0.26	1.01	1.02	1.19

Bridge	Load Case	AASHTO	Girder DF			DF (none) / DF (ID)		AASHTO /
			None	1 ID	3 IDs	1 ID	3 IDs	None
40-8.5 (Curve)	1-HS20	0.48	0.39	0.37	0.36	1.05	1.07	1.23
	2-HS20	0.38	0.37	0.35	0.34	1.06	1.10	1.03
100-8.5 (Curve)	1-HS20	0.37	0.33	0.32	0.32	1.02	1.02	1.13
	2-HS20	0.32	0.29	0.28	0.28	1.04	1.05	1.11
150-8.5 (Curve)	1-HS20	0.34	0.29	0.29	0.29	1.01	1.01	1.16
	2-HS20	0.31	0.26	0.25	0.25	1.03	1.03	1.20

Table 6.13. Exterior Girder DFs for Special Cases.

Bridge	Load Case	AASHTO	Girder DF		DF (none) / DF (ID)	AASHTO / None		
			None	1 ID				
40-11 (Cont)	1-HS20	0.55	0.55	0.55	0.99	1.01		
	2-HS20	0.55	0.31	0.33	0.94	1.77		
100-11 (Cont)	1-HS20	0.55	0.52	0.51	1.01	1.06		
	2-HS20	0.55	0.37	0.38	0.95	1.51		
Bridge	Load Case	AASHTO	Girder DF			DF (none) / DF (ID)		AASHTO / None
			None	1 ID	3 IDs	1 ID	3 IDs	
40-8.5 (Skew)	1-HS20	0.41	0.47	0.48	0.48	0.99	0.98	0.87
	2-HS20	0.41	0.26	0.27	0.28	0.96	0.92	1.59
100-8.5 (Skew)	1-HS20	0.41	0.43	0.42	0.42	1.02	1.03	0.96
	2-HS20	0.41	0.31	0.32	0.32	0.98	0.98	1.32
150-8.5 (Skew)	1-HS20	0.41	0.38	0.38	0.37	1.01	1.03	1.07
	2-HS20	0.41	0.30	0.30	0.30	1.00	0.99	1.36
Bridge	Load Case	AASHTO	Girder DF			DF (none) / DF (ID)		AASHTO / None
			None	1 ID	3 IDs	1 ID	3 IDs	
40-8.5 (Curve)	1-HS20	0.41	0.52	0.52	0.52	1.00	1.00	0.79
	2-HS20	0.41	0.29	0.31	0.32	0.95	0.92	1.39
100-8.5 (Curve)	1-HS20	0.41	0.43	0.43	0.43	1.01	1.02	0.95
	2-HS20	0.41	0.31	0.32	0.32	0.97	0.96	1.32
150-8.5 (Curve)	1-HS20	0.41	0.38	0.38	0.38	1.01	1.02	1.07
	2-HS20	0.41	0.29	0.30	0.30	0.99	0.99	1.40

Table 6.14. Summary of DF Results, Bulb Tee Bridges.

DF (none) / DF (ID)	Interior		Exterior	
	1 ID	3 IDs	1 ID	3 IDs
1 Lane				
max ALL	1.09	1.09	1.07	1.09
max TYP	1.05	--	1.03	--
ave	1.02	1.03	1.01	1.02
2 Lane				
max ALL	1.09	1.13	1.03	1.05
max TYP	1.07	--	1.00	--
ave	1.03	1.04	0.99	0.98

Table 6.15. Summary of DF Results, AASHTO Beam Bridges.

DF (none)	Steel IDs			
	Interior		Exterior	
/ DF (ID)	1 ID	3 IDs	1 ID	3 IDs
1 Lane				
max ALL	1.08	1.14	1.07	1.04
max TYP	1.08	--	1.03	--
ave	1.03	1.04	1.02	1.01
2 Lane				
max ALL	1.08	1.10	1.01	1.01
max TYP	1.06	--	0.99	--
ave	1.04	1.05	0.98	0.99
DF (none)	Concrete IDs			
	Interior		Exterior	
/ DF (ID)	1 ID	3 IDs	1 ID	3 IDs
1 Lane				
max ALL	1.11	1.15	1.04	1.02
max TYP	--	--	--	--
ave	1.04	1.06	1.02	1.01
2 Lane				
max ALL	1.16	1.23	0.99	1.00
max TYP	--	--	--	--
ave	1.07	1.09	0.96	0.98

Table 6.16. Summary of DF Results, Box Beam Bridges.

DF (none)	Interior		Exterior	
/ DF (ID)	1 ID	3 IDs	1 ID	3 IDs
1 Lane				
max ALL	1.04	1.06	1.04	1.05
max TYP	1.04	--	1.04	--
ave	1.03	1.04	1.02	1.03
2 Lane				
max ALL	1.05	1.09	1.00	1.01
max TYP	1.05	--	1.00	--
ave	1.03	1.05	0.99	0.99

6.4.2 Overall Results

As shown in Table 6.14, the average DF (none) / DF (ID) ratio (hereafter referred to as "DFr") for all bulb tee structures is approximately 1.03 for interior girders and 1.0 for exterior girders. Note that this ratio represents the penalty to DF, in terms of a factor, that would occur if IDs were removed from the structure. The maximum interior girder DFr for all bulb tees is 1.13, and occurs for structure 100-12 (72BT) for both the one lane and two lane cases. For exterior girders, results

are similar, but with a slightly reversed trend, where maximum DFr (DFrmax) ratios tend to occur for the one lane loaded case. Differences in effect are small, however. For exterior girders, maximum DFr occurs for structure 200-8.5 (4L) for both the one and two lane cases (with DFrmax values of 1.09 and 1.05, respectively).

However, considering typical structures only (two lane, one diaphragm at midspan, and expected girder stiffness), DFrmax for interior girders is 1.07 for the two lanes loaded case, and occurs on structure 40-10.5. Note that the average DFr (DFrave) for the two lane case for exterior girders is slightly less than one (0.99). That is, the presence of IDs penalizes exterior girders for this case. That is, adding IDs results in an increase in DF by a factor of 1/0.99 = 1.01. This occurs because the IDs stiffen the deck transversely, such that the deck acts to some extent as a lever, where the exterior girders are pulled further down when load is applied on the deck that is not directly over the exterior girder. The highest penalty that occurs for midspan exterior girders is 0.87, and occurs on structure 40-10.5 for the two lanes loaded case. Note that AASHTO LRFD specifies that DFs for steel exterior girders with diaphragms are to be taken no less than that assuming rigid-body rotation of the bridge cross-section, but this provision is not specified for PC beams.

As shown in Table 6.15, when AASHTO beams are coupled with steel diaphragms, very similar results were found as for bulb tees (DFrave approximately 1.04 and DFrmax = 1.08 for one ID and 1.14 for quarter span IDs). Here, maximum DFr for interior girders occurred for structure 100-8.5 (75w). When considering typical bridges only, maximum DFr occurred at structures 40-11 (single lane loaded), and 100-11 (two lanes loaded). The maximum penalty for IDs for exterior girders occurred at structure 40-6 for the two lane load case (0.96), whereas there was no penalty for the one lane loaded case.

Table 6.16 presents the box beam cases. Here, a similar average effect for IDs was found as for the bulb tee and AASHTO beam cases. However, maximum effects were generally lower, with DFrmax for any case of 1.09 (1.05 for typical cases). For the one lane loaded case, maximum DFr occurred on structures 40-6 and 40-11 for interior girders and 100-10.5 for exterior girders. For the two lane case, maximum DFr occurred on structures 40-11 for interior girders, while no benefit occurred for exterior girders. Moreover, no penalty occurred for exterior girders for the one lane case, while the maximum penalty for the two lane case was 0.96 and occurred on structures 40-6 and 40-11.

6.4.3 Girder Position and Number of Lanes Loaded

Considering the typical case of a two lane bridge with midspan IDs of steel for bulb tees and AASHTO girders and concrete IDs for box beams, the following observations can be made.

For interior girders, a DFrave value from 1.03-1.04 occurs for all girders types, whether one or two lane load cases are considered, with the slightly higher average (1.04) for the two lane case. DFrmax for interior girders ranges from 1.04-1.08.

For exterior girders, DFrave is approximately 1.0 for both one lane and two lane cases, where the one lane case is slightly greater than 1 (1.0-1.02) and the two lane case slightly less than 1 (0.98-0.99).

There is less variation in DFrmax in exterior girders relative to interior girders, where DFrmax for the typical single lane case ranges from 1.03-1.04. For the two lane case, DFrmax is 0.99-1.0 for all girder types.

6.4.4 Bridge Geometry

For interior girders, DFrmax tends to occur on the shortest spans with the widest girder spacing. For exterior girders, DFrmax has little variation, but tends to peak at the midspan length (100 ft). Highest penalties for exterior girders tend to occur on the shortest spans (40 ft) with wide girder spacing (10 ft and greater). Note that the shortest spans and wider girder spacing configurations correspond to structures with the largest ratios of girder to (transverse) deck stiffness.

When bridge width was considered, slight increases in DFr occur as bridge width increases. For interior bulb tee girders, for both 100 ft and 200 ft spans, DFr decreased from 1.03 to 1.0 as bridge width changed form 75 ft wide to 23 ft wide. A similar decrease occurred for exterior girders, from 1.04-0.98 as width decreased. A similar trend occurred for AASHTO girders (100 ft span), where DFr slightly fell from 1.024 to 1.009 and 1.04 to 1.03 for one and two lane loaded interior girders and from 1.07 to 1.0 and 1.01-0.98 for one and two lane loaded exterior girders.

Compared to simple span structures, continuous bridges show a slight to no increase in (positive) DFr when 1 lane loading is considered for both interior and exterior girders (1% or less), and a small increase in DFr when two lane loads are considered, with a maximum change from 1.05 to 1.10 for structure 40-11 for interior girders.

Similarly, skewed (30 deg.) structures have a slight to no increase in DFr for interior and exterior girders when compared to straight structures (see 100-8.5 and 150-8.5 cases). Curved structures resulted in no significant differences in DFr from straight bridges.

6.4.5 Girder Type

Girder type has no significant effect on DFrave, and a minor effect on DFrmax. Considering typical cases, for interior girders, one lane loaded, DFrmax was 1.05, 1.08, and 1.04 for bulb tee, AASHTO, and box beam bridges, respectively, while DFrmax ranged from 1.07 to 1.05 for the typical two lane cases. These generally occurred at the 40-11 (or 40-10.5) structures. Note that box beams had a concrete diaphragm while the other beam types were paired with steel.

Considering exterior girders, the typical one lane load case resulted in minor differences in DFr max, from 1.03-1.04. The two lane case produced a DFmax ratio of 0.99-1.0 for all girder types. The highest penalty for typical exterior girders (0.87) was for the 40-10.5 bulb tee case, while AASHTO girders produced a maximum penalty of 0.96 and typical box beams had no penalty for IDs. The remaining bulb tees produced nearly no penalty, however.

As expected, increasing girder stiffness while other parameters remain constant increases DFr for interior girders. For example, changing the originally sized 42BT to a 72BT for structure 100-8 resulted in an increase in DFr for interior girders from 1.01 to 1.08 for the single lane case and from 1.02 to 1.05 for the two lane case. For exterior girders, DFr decreased from 1.03 to 0.99 for

the one lane case and from 0.99 to 0.97 for the two lane case. This behavior is expected based on the transverse deck behavior discussed previously.

6.4.6 Diaphragm Type and Number

Increasing diaphragm stiffness by a reasonable amount consistently increases DFr, but not by a substantial amount. For the AASHTO girders, a series of models were reconsidered with concrete IDs. In this case, maximum and average DFr increased slightly for the one lane case and somewhat more for the two lane case. When replacing steel channel sections with concrete IDs, the largest difference was found for structure 40-11, where for interior girders, DFr increased from 1.08 to 1.16 (by a ratio of 1.07) for the two lane loaded case. For all other cases, however, DFr was changed by a ratio of 1.01-1.03.

For exterior girders, concrete ID results were similar to those of steel, with slight decreases in DFr. Here, the largest change in DF was by a factor of 0.93 (DFr concrete / DFr steel), for structure 40-11, for the two lane loaded case. For all other cases, the change ratio varied from 1.04 to 0.99.

Similarly, the average penalty on exterior girders for concrete IDs did not substantially vary from that of steel IDs. Maximum DFr for exterior girders occurred on structures 100-6 and 150-6 for the one lane loaded case, while no benefit was found for IDs for the two lanes loaded cases. The maximum penalty occurred on structure 100-11 for the two lane case (0.95), where no penalty was associated with the 1 lane case.

Changing the ID type from a steel channel to the steel cross bracing specified by MDOT for larger bulb tee sections (only done for structure 100-11) resulted in no significant change in DFr for all cases except for the case of an interior girder subjected to two lanes loaded, where DFr increased slightly from 1.06 to 1.08.

Changing the number of IDs from one at midspan to three at quarter span points generally resulted in minor differences. For bulb tees, most cases experienced increases in DFr within 1%. An exception was case 40-10.5, where DFr increased by 5% and decreased by 3% for interior and exterior girders, respectively. Case 100-12 (72BT), had DFr change by 3% for interior girders.

For AASHTO girders, most cases experienced minor changes, as with bulb tees. Here an exception is structure 40-11, where DFr increased from 5-6% for interior girders when a concrete diaphragm was considered (two lane loaded case). Considering exterior girders throughout all cases, the range of results tended to be more variable than for interior girders. The maximum change for exterior girders was for structures 40-6 and 40-11 with concrete diaphragms (2 lane loaded cases), where DFr changed by approximately 6% when IDs were increased from one to three. Diaphragm number had little effect on box beam bridges as well, where most DFr changes were within 1% and none were greater than 3%.

6.4.7 Load Configuration

Loading the bridge with a HS20 truck configuration, a single axle, or a line of point loads across the span representing a truck train resulted in no significant change in DFr for any case (less than 1% change).

6.4.8 Comparison to AASHTO LRFD DF Values

As expected, it was found that that AASHTO DFs are nearly always conservative with regard to model results (with no IDs). For all bulb tee interior girders, the average ratio of AASHTO to model DF (A/Mr) was 1.21. Note this ratio is labeled as "AASHTO / None" in the Tables. This was fairly consistent, with most results between 1.15-1.23, and a coefficient of variation (COV) of 0.07. The maximum discrepancy was 1.50 (for the one lane loaded case of structure 40-10.5), with no unconservative results. If the deck thickness was taken as the deck plus the girder upper flange, the average A/Mr ratio dropped to 1.03, with a maximum ratio of 1.29. However, this resulted in several unconservative cases. For exterior girders, larger inconsistencies (COV = 0.22) and very conservative results in general were obtained with the AASTHO procedure. Here, the average A/Mr was 1.69, with a maximum ratio of 2.78 (case 200-13), where most fell between 1.5 and 2.0.

Similar results were obtained from the AASHTO girder bridges, with slightly lower A/Mr values. For interior girders, the average A/Mr was 1.15, with no unconservative cases. For exterior girders, A/Mr was 1.41, with a maximum ratio of 1.91 (and COV of 0.20). Box beam interior girder results were very similar to the AASHTO girders, but more consistent, with slightly reduced average and maximum A/Mr values of 1.14 and 1.30, respectively (COV 0.07). For exterior girders, average and maximum A/Mr values were 1.69 and 2.77, respectively (COV 0.27). For two special cases of 1-lane DF for skewed and curved exterior girders, the AASHTO DF values were found to be 4-20% less than the FEA results (skewed and curved structures 40-8.5 and 100-8.5).

The general conservativeness of the AASHTO results is expected, since the modeling approach used to develop the interior girder AASHTO expressions modeled all girders with beam elements (i.e. zero thickness lines), and hence did not account for the girder flange width that stiffens the deck, substantially in some cases. Similarly, the lever rule approach for exterior girders does not account for bridge geometry (other than girder spacing and overhang length) and stiffness parameters, producing a large variance in results.

6.5 Summary

Overall, DFrave is small, approximately 1.03, whereas DFrmax is about 1.08 among the typical cases (bridges with typical girder sizing and diaphragm type, with midspan IDs), and tends to peak on the shortest spans with the widest girder spacing for interior girders, and on moderate span lengths for exterior girders. Thus, for interior girders, IDs appear to be most effective on bridges with larger girder to transverse deck stiffness ratios. Although not always the case, exterior girders typically experienced a decrease in DFr when two lanes were loaded. That is, adding diaphragms penalized exterior girders in this case.

For all cases considered, DFrmax was found to be 1.13 for the interior girders of a bulb tee bridge (case 40-10.5 using 3 IDs with one lane loaded). and 1.16 and 1.23, for an AASHTO beam bridge

(case 40-11 using 1 and 3 concrete diaphragms, respectively, with two lanes loaded). The maximum penalty found on exterior girders when IDs were added was approximately a DFrmax of 0.87 (case 40-10.5 for a bulb tee bridge with 3 IDs).

Changing bridge width, continuity, skew, and curvature generally produced minor differences on the effect of IDs. In summary, slight increases in DFr occur as bridge width increases, while continuous bridges showed a slight to no increase in (positive) DFr when one lane loading was considered and a small increase in DFr when two lane loads were considered. Similarly, skewed and curved structures developed a slight to no increase in DFr. Changing the load configuration had no significant effect on DFr.

Girder type has no significant effect on DFrave, and a minor effect on DFrmax for most cases. Considering typical cases, for interior girders, changing girder type resulted in a DFrmax variation from 1.04-1.08, and typically occurred at the short span, large girder spacing structures. For exterior girders, changing girder type resulted in no significant maximum DFr changes.

As expected, increasing girder stiffness while other parameters remain constant increases DFr for interior girders, where a maximum increase of about 8% was found when changing a 42BT to a 72BT for structure 100-8. For exterior girders, increasing girder size tends to decrease DFr, but to a lesser extent than the change seen for interior girders.

Increasing diaphragm stiffness (by changing type of diaphragm) by a reasonable amount had a minor effect on DFr for nearly all cases. Similarly, changing the number of IDs from one at midspan to three at quarterspan points generally resulted in minor differences (within 1%). A few exceptions were found, with the largest changes in DFr at about 5%.

As expected, it was found that that AASHTO DFs are nearly always conservative with regard to model results when no IDs were considered. For interior girders, the average ratio of AASHTO to model DF (A/Mr) was from about 1.14-1.23, depending on girder type. Significantly conservative results were obtained for a few cases. For exterior girders, greater conservatism and inconsistency in results were found than for interior girders, with average A/Mr values from 1.7-1.9.

CHAPTER 7: ASSESSMENT OF BEAM ROLLOVER

7.1 Introduction

Before any lateral constraints are applied to the beam, rollover potential exists. This may occur when it is first seated during construction, or if all lateral constraints (including end walls) are removed during reconstruction. In this chapter, the ability of typical bridge beams to resist rollover is determined.

7.2 Beams Considered

As with the in-service analysis presented in the previous chapter, three PC beam types are considered: bulb tees (BTs), AASHTO girders, and box beams. All bulb tee sections given in the MDOT Bridge Design Guide are evaluated (depths of 36, 42, 48, 54, 60, 66, and 72 in, with a 61 in. top flange width as well as a 49 in. top flange width). Similarly, all AASHTO Beam sections (Types I-IV), and all box beam sections that have greater depth than width (39x36; 42x36; 54x48; 60x48) are analyzed.

As beam length is an important parameter with regard to instability, maximum spans appropriate for the section were used to encompass reasonable possibilities. In this study, two beam lengths were chosen for evaluation: those that meet HL93-mod and HS25 deflection (L/800), and flexural stress and strength criteria, with prestress force and eccentricity chosen such that AASHTO LRFD tension and compression stress limits for concrete and prestressing steel at transfer and in-service are also satisfied. That is, the span of a two-lane bridge with beams composed of the given section was chosen such that the beam just met HL93-mod deflection criteria, then the beam prestressing design parameters were chosen such that the flexural strength and stress limit requirements were met. This process was repeated to create a second, longer span based on HS25 criteria. The latter was considered to enable assessment of beams on pre-LRFD structures subjected to deck removal. Note that (in most cases) the beams were not specifically designed for construction loads.

These hypothetical structures were based on the geometry and material properties used for the in-service live load distribution analysis discussed above (Chapter 6). For calculation of DF and top flange width of the composite section needed to evaluate girder live load and stiffness, beam spacing was usually taken as 8 ft, a representative value based on the summary of available PC bridge plans in Chapter 3.

Here it should be noted that changing beam spacing effects DF as well as composite section stiffness. Thus, choosing a spacing other than 8 ft will generate a different maximum beam length. For the beams considered, it was found that increasing beam spacing beyond 8 ft caused increases in DF at a greater rate than beam stiffness. Thus, a beam with spacing greater than 8 ft generally need not be analyzed for rollover if the 8 ft spacing case survived, since the wider spacing would result in a shorter, less-critical beam length. However, longer beams would be possible with more closely-spaced girders. Therefore, beams that passed rollover criteria at 8 ft spacing were resized (i.e. with regard to span) using 4-6 ft girder spacing. Although atypical, particularly for longer spans, this check was meant to produce a relatively long beam to enable assessment of stability across a wide range of girder spacings. Similarly, beams that failed at 8 ft spacing were reconsidered at 10-12 ft spacing.

7.3 Modeling Approach

7.3.1 Analytical Procedure

Although the FEA procedure developed in Chapter 5 well-matched the available experimental data for rollover, as the research progressed, it was determined that this model was impractical for the size of the parametric study deemed necessary for this study (approximately 150 different beam and bearing cases) due to its complexity of construction and lengthy time for solution. Therefore, an alternative solution process was considered.

This process is based on a modified form of the analytical procedure first introduced by Mast (1989), which, for greater accuracy, was calibrated to a selection of rollover runs using the FEA rollover model developed in this study. The original Mast procedure was first introduced in 1989, and underwent several revisions and additions by other investigators over the last several decades to account for more complex rollover scenarios (Mast 1993; Cojoaru and Moen 2013; PCI 2016). The general method is published by PCI and is fully described in *CB-02-16-E, Recommended Practice for Lateral Stability of Precast, Prestress Concrete Bridge Girders* (PCI 2016). A brief description of the approach is as follows.

The fundamental idea of the method is to compute a factor of safety (FS) for rollover as the ratio of the resisting (M_r) and applied (M_a) moments on the beam. Due to beam camber and/or bearing tilt and bearing eccentricity, the applied moment is due to the centroid of beam self-weight being eccentric to the roll center (taken as the centerline of the bearings), as well as due to any gravity loads similarly eccentric to the supports, as well as that caused by lateral wind loads. The resisting moment is supplied by the rotation of the bearings, which are treated as rotational springs.

Based on different limits, the FS can be computed for cracking and rollover. PCI specifies minimum acceptable FS as 1.0 for cracking and 1.5 for rollover. Note that this FS is equivalent to the AASHTO construction load factors of 1.35 for non-wearing surface dead load (DC) and construction dead load (CDL) with a resistance factor of 0.9 (1.35/0.9) = 1.5. Note that, because the model treats the bearing as a rotational spring rather than a surface separate from the girder, full contact is implicitly assumed between the bottom of the girder flange and the top of the bearing pad. Such an assumption can often produce unrealistically high rollover loads for seated girders, since beyond a certain roll angle, the rotational stiffness required of the bearing exceeds its ability to deform in a planar manner, and thus the beam may begin to lift off of the bearing. To guard against this possibility, PCI has introduced a third check to limit the rotation to be within the kern of the bearing (i.e. such that no tensile stresses would be predicted between the two surfaces). Based on requirements specified in the *AASHTO Guide Design Specifications for Bridge Temporary Works* (AASHTO 2008), PCI specifies this minimum acceptable factor of safety as 1.2.

Assuming small rotations, such that $\sin \theta \approx \theta$ and $\cos \theta \approx 1$, the FS in general can be developed as the ratio of resisting (M_r) and applied (M_a) moments:

$$FS = \frac{M_r}{M_a} = \frac{K_\theta(\theta - \alpha)}{W[(\bar{z}_o + y)\theta + z_w + e_i] + M_{OT}} \tag{7.1}$$

where:

K_θ = equivalent rotational stiffness of the bearing(s);

θ = angle of the beam from the vertical in its equilibrium state;

α = initial slope of the bearing surface, such that $(\theta - \alpha)$ is the total angle through which the bearing was deformed once the beam was set;

W = self-weight of the beam;

$\bar{z}_o$ = theoretical lateral displacement of the center of gravity of the deflected shape of the beam if it was loaded laterally with self weight. That is, if the beam was positioned to bend about its weak axis under self weight, $\bar{z}_o$ represents the distance that the center of gravity of the deflected shape of the beam moved from the beam's undeformed position (i.e. the mean lateral deflection of the beam across its entire length due to self weight);

y = height of mean center of gravity of beam above roll center;

z_w = lateral deflection of the center of gravity of the deflected shape of the beam due to wind load;

e_i = lateral eccentricity of the center of gravity of the deflected shape of the beam to the roll center, accounting for sweep and bearing eccentricity;

M_{OT} = overturning moment due to wind, taken about the roll center.

An illustration of some of these variables is given in Figure 7.1
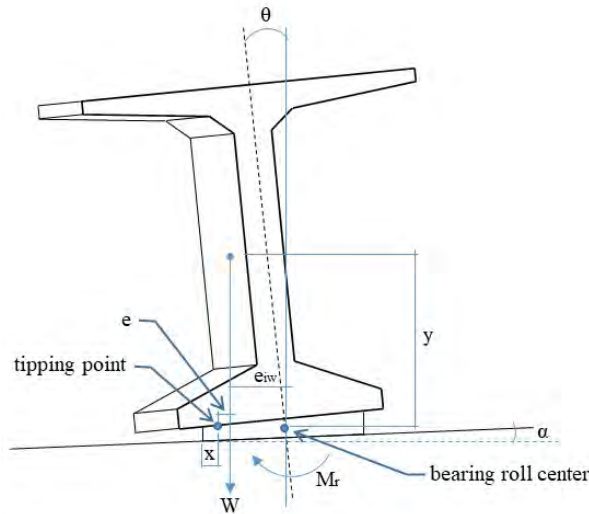
Figure 7.1. Rollover Model Parameters.

To account for the lateral stiffness loss of the section due to possible cracking as the beam deflects laterally, Mast (1993) introduced an empirical modification $(1 + 2.5\theta)$ to magnify the lateral displacement of the beam, which is applied to the terms $\bar{z}_o$ and z_w. This results in a generalized FS expression considering cracking as:

$$FS = \frac{M_r}{M_a} = \frac{K_\theta(\theta - \alpha)}{W[(\bar{z}_o(1 + 2.5\theta) + y)\theta + z_w(1 + 2.5\theta) + e_i] + M_{OT}} \qquad (7.2)$$

94

Based on this formulation, FS for the three modes of failure (cracking, rollover, and leaving the bearing kern) discussed above can be developed as:

$$FS_{crack} = \frac{K_\theta(\theta_{cr} - \alpha)}{W[(\overline{Z_o} + y)\theta_{cr} + Z_w + e_i] + M_{OT}}$$ (7.3)

where θ_{cr} = the angle at which cracking in the top flange is expected, which if assuming small rotations, becomes: $\theta_{cr} = M_{ycr} / M_g$. Here, M_{ycr} is the lateral moment needed to cause cracking, accounting for the cracking stress and the imposed flexural stresses on the beam, and M_g is the self-weight moment.

$$FS_{roll} = \frac{K_\theta(\theta - \alpha)}{W[(\bar{z}_o(1 + 2.5\theta) + y)\theta + z_w(1 + 2.5\theta) + e_i] + M_{OT}}$$ (7.4)

In this expression, θ is initially unknown, and is increased with an iteration from a starting value of α until FS_{roll} is maximized. This is because the resisting moment increases with increased bearing rotation, and the bearing must pass through all rotation values until it topples, and thus the largest governs rollover resistance.

$$FS_{kern} = \frac{K_\theta(\theta_{max} - \alpha)}{W[(\bar{z}_o(1 + 2.5\theta_{max}) + y)\theta_{max} + z_w(1 + 2.5\theta_{max}) + e_i] + M_{OT}}$$ (7.5)

where θ_{max} is the maximum angle of rotation such that the beam reaction remains within the bearing kern. This is found from a balance of resisting and applied moments, where the beam reaction is placed at the kern limit, and for the beams in this study, again assuming small rotations, is taken as:

$$\theta_{max} = \frac{W\left(\frac{b_w}{6} - \frac{b_h}{2}\alpha - e_b\right) + M_{OT}}{K_\theta} + \alpha$$ (7.6)

where b_w is the width of the bearing, b_h the height of the bearing, and e_b the eccentricity of the bearing.

Although good results have been reported with this method (Mast 1989; 1993), a validation was conducted by comparing outcomes of this approach to the results of the FEA rollover model developed in Chapter 5. In particular, a 72 in. bulb tee was modeled with a typical bearing designed using Method A per AASHTO LRFD (2020). Four different scenarios were considered: girders with and without sweep (see below for sweep limit discussion), paired with bearings with and without slope (taken as 2%; see below for additional discussion). Following the rollover modeling procedure described in Chapter 5, the beam was first prestressed, then subjected to dead

load and set onto the bearings. A horizontal displacement was then imposed on the top flange of the beam at midspan and increased until tipping occurred.

The analytical procedure was appropriately modified to include the horizontal load. For use in the analytical procedure, the equivalent (lateral) rotational stiffness of the bearing used in the FEA model was determined by applying a unit moment couple on the edges of a rigid block attached to the top of the bearing, and the corresponding edge deflections of the bearing were measured. Assuming plane sections remain plane during rotation about the center of the bearing, a constraint which was enforced with the rigid block attached to top of the bearing surface, the rotational stiffness can be developed as: $K_\theta = PL^2/(2\Delta)$, where P is the edge force applied (taken as P=1.0), L the bearing length (i.e. width) in the direction of rotation, and Δ the measured vertical edge deflection. This value (K_θ) is then multiplied by 2 in the analytical model since two bearings support the beam.

The ability of the analytical method to predict cracking was first considered. In this case, the horizontal load was increased in the analytical procedure until cracking occurred, which must occur when $FS_{crack} = 1.0$. The value of this load was then compared to that found in the FEA model when the same assumed cracking stress, measured at the top flange of the beam, was obtained (taken as $0.24f'_c{}^{0.5}$). Results are given in Table 7.1.

Table 7.1. Predicted Cracking Load.

Case	FEA Model (kips)	Analytical Procedure (kips)
No sweep, Sloped	17.0	15.5
No sweep, Flat	19.2	18.1
Sweep, Sloped	10.2	8.61
Sweep, Flat	12.5	11.2

As shown in the Table, the analytical procedure is consistently conservative as compared to the FEA model, from approximately 1 – 1.5 kips in each case. Thus, cracking check seems reasonably conservatively predicted by the analytical procedure and no adjustments were made to the cracking model.

The process above was repeated, but now comparing when the beam begins to lift from the bearing (i.e. when $FS_{kern} = 1.0$) and when the beam rolls over (when $FS_{roll} = 1.0$). The force required for initiation of lift-off (i.e. the kern limit) in the FEA model corresponds to the horizontal load when stresses across far edge of the bearing are zero, whereas tipping represents the maximum horizontal load that the beam can resist prior to toppling. It was found that both limits in the analytical procedure were inconsistent with the FEA model results, and were sometimes unconservative. The rollover prediction of the analytical model was particularly poor, suggesting rollover loads much greater than those found from the FEA model. As discussed above, this is not surprising since it is assumed in the analytical approach that the beam does not leave contact with the bearing and no lift-off occurs.

Therefore, the analytical model was deemed unreliable for rollover prediction and a modified procedure was developed for this study based on overturning of the girder at its toe. This avoids problem of assuming the bearing surface remains in contact with the girder flange throughout any

angle of rotation. The difficulty in the suggested procedure is determining the effective toe point, since the bearing is elastic and this point is inbound of the actual bearing edge. That is, the bearing surface deforms in a non-planar manner as the girder begins to tip, compressing the most heavily loaded edge of the bearing more than the unloaded surface. This can be seen in Figure 7.2, where the tipping (toe) point is clearly inbound of the bearing edge due to the non-uniform compression of the bearing. Note that, although more difficult to detect visually, this non-uniform compression occurs much earlier in the rollover process, soon after lift-off begins, placing the effective tipping point significantly closer to the bearing center than shown in Figure 7.2. The solution to identify this point for the modified procedure used in this study is discussed below.
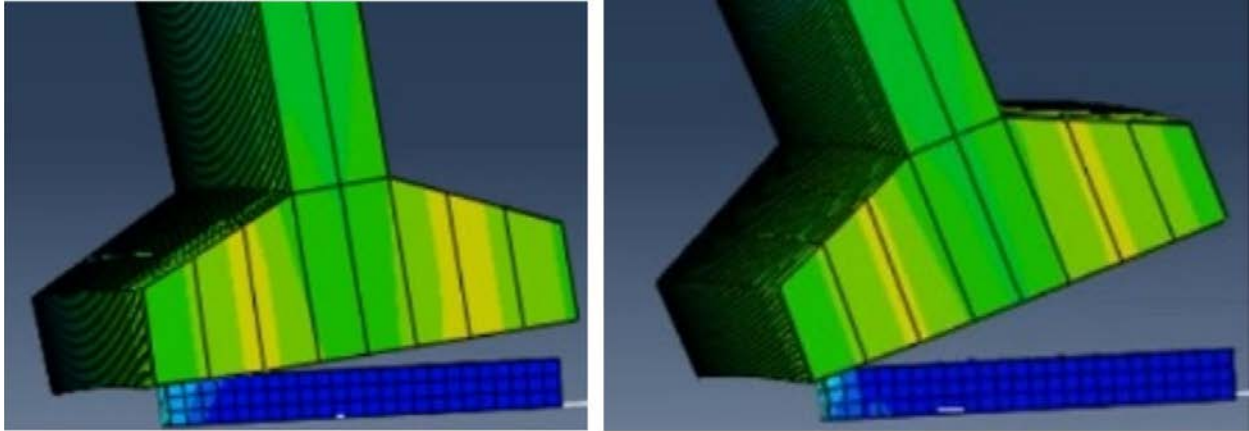
Figure 7.2 Nonlinear Bearing Compression During Tipping.

7.3.2 Development of Modified Rollover Procedure

7.3.2.1 Tipping Factor of Safety

The factor of safety for the modified procedure is conceptually computed in a manner consistent with the PCI/Mast analytical method presented above (i.e. Eq. 7.1), where it is taken as the ratio of resisting moment to overturning moment. However, because uplift is modeled and it is assumed that the bearing does not remain in contact with the girder flange, the bearing rotational resistance is not taken as the resisting moment. Rather, resisting moment is caused by the weight of the girder and the centroidal distance of this weight inbound of the effective toe (tipping) point. Here the toe is not taken at the roll center (i.e. bearing centerline) as in the PCI model, which is an inaccurate assumption at the onset of overturning due to the flexible surface of the bearing. This effective toe location is unknown, as it will vary with bearing, load, and girder characteristics. To determine this position, an assessment of the FEA rollover model results was conducted, as discussed below. The factor of safety associated with the proposed procedure is referred to as the tipping FS, and is taken as:

$$FS_{tip} = \frac{M_r}{M_{OT}} = \frac{W \cdot e}{M_w + M_b + M_p} \tag{7.7}$$

In this expression, the following notation is used:

e = lateral eccentricity of the center of gravity of the deflected shape of the beam to the effective toe, accounting for sweep, bearing rotation, and bearing eccentricity;

M_w = overturning moment caused by wind (taken about the effective toe);

M_b = overturning moment caused by fascia jacks attached to girder prior to setting;

M_p = overturning moment caused by a lateral load applied at midspan (used for model calibration purposes only and taken as zero for assessment of beam stability during construction).

Lateral eccentricity e is computed as:

$$e = b_w / 2 - e_{iw} - x \tag{7.8}$$

where:

e_{iw} is the lateral distance the center of gravity of the deflected shape of the beam to the roll center, accounting for sweep, bearing eccentricity, and applied loads, and is computed as:

$$e_{iw} = (\bar{z}_o + y - b_h / 2) \, \theta_e \, (1 + 2.5 \theta_e) + z_{wp} \, (1 + 2.5 \theta_e) + e_i \tag{7.9}$$

$\bar{z}_o$ is defined above and is computed as:

$$\bar{z}_o = [w_b / (12 \, E_c \, I_y \, L) \,] \, (L_1{}^5 / 10 - a^2 L_1{}^3 + 3 a^4 L_1 + (6/5) a^5) \tag{7.10}$$

w_b = unit weight of beam (force/length)
E_c = Young's modulus of beam concrete at time of seating
L = total length of beam, end to end
L_1 = center to center distance between bearing pads, given as: $L_1 = L - 2 \, a$
a = distance from the center of bearing pad to beam end

y is the height of the center of gravity of the deflected shape of the beam above the roll center, given as:

$$y = b_h / 2 + y_b + t_s + e_{i0} \, v_c \tag{7.11}$$

y_b = distance from the bottom of the beam section to the section centroid
t_s = thickness of sole plate (taken as 0.75 in.)
e_{i0} = ratio of mean center of gravity of beam in deflected shape to maximum deflection under uniform load, given by: $e_{i0} = (L_1/L)^2 - 1/3$
v_c = beam camber at seating (under self weight)
b_h = bearing thickness

θ_e is the girder tilt equilibrium angle when the girder is seated and loaded (found by adjusting the angle θ within Eq. 7.4 until FS=1.0; requires iteration)

z_{wp} is the sum of displacements from wind and load P: $z_{wp} = z_w + z_p$

z_p is the lateral displacement of the center of gravity of the deflected shape of the beam due to point load P (similar to $\bar{z}_o$ except under load P not self-weight). This is computed as:

$$z_p = \frac{\bar{z}_{ab} \, A_{ab} + \bar{z}_{bc} \, A_{bc}}{A_{ab} + A_{bc}} \tag{7.12}$$

$$\bar{z}_{ab} = \frac{1}{3}\left(\frac{PaL_1^2}{16E_cI_y}\right)$$

$$A_{ab} = \frac{a}{2}\left(\frac{PaL_1^2}{16E_cI_y}\right)$$

$$\bar{z}_{bc} = \frac{L_1\left(\frac{k_1^2 L_1^4}{112} - \frac{k_1 k_2 L_1^2}{10} + \frac{k_2^2}{3}\right)}{2\left(\frac{k_1 L_1^2}{8} - k_2\right)}\left(\frac{1}{E_cI_y}\right)$$

$$A_{bc} = \frac{L^2}{8E_cI_y}\left(\frac{k_1 L_1^2}{8} - k_2\right)$$

$$k_1 = P/12 \; ; \; k_2 = PL_1^2 / 16$$

z_w is the lateral deflection of the center of gravity of the deflected shape of the beam due to wind, taken as:

$$z_w = [w_w /(12 \, E_c \, I_y \, L)] \, (L_1^5/10 - a^2 L_1^3 + 3a^4 L_1 + (6/5)a^5) \tag{7.13}$$

$$w_w = \text{wind load on beam (force/length)}$$

e_i = total eccentricity of the girder centroid to the roll center due to sweep and bearing eccentricity, computed as:

$$e_i = sw * e_{i0} + e_b \tag{7.14}$$

$$sw = \text{girder sweep}$$
$$e_b = \text{bearing eccentricity}$$

x is the effective tipping point, measured inward from the bearing edge, computed as:

$$x = b_w/2 - L_{tip} \, b_w - e_b - Z_{wp} \tag{7.15}$$

b_w = bearing width (perpendicular to beam span)
L_{tip} = ratio of tipping point (measured from the center of gravity of the laterally deflected shape of the girder to the end of the bearing), to the bearing width b_w. This ratio was calibrated from FEA results, and is taken as 0.22.

M_w is computed as:

$$M_w = L\, w_w\, (h/2 + b_h/2 + v_c\, e_{i0} + t_s) \tag{7.16}$$

h = girder height

M_b is computed as:

$$M_b = -\, w_{br}\, L_1\, z_{br} \tag{7.17}$$

w_{br} = equivalent uniform weight of fascia jacks (in units of force/length along beam; note (-) sign due to how z_{br} is calculated, which is taken as negative)

z_{br} = distance from bracket cg to tipping point, beam in deformed state, computed as:

$$z_{br} = b_w/2 - x - z_{brc} \tag{7.18}$$

z_{brc} = horizontal distance from the bracket centroid to the roll center, while the girder is in the laterally deflected shape, compute as:

$$z_{brc} = (\,(\bar{z}_o + y - b_h/2)\, \theta_e)\,(1 + 2.5\theta_e) + z_{wp} + e_i + d_b \tag{7.19}$$

d_b = horizontal distance from the centroid of weight of the attached brackets to the undeformed girder centroid

M_p is computed as:

$$M_p = P\,(\, d_p + b_h/2 + v_c(L_1/L)^2 + t_s) \tag{7.20}$$

P = the lateral load applied at midspan (for model calibration purposes only)

d_p = height of load P above the bottom girder flange

Because this process (in particular, the critical toe position ratio L_{tip}) was calibrated to match the rollover loads found from the FEA rollover models, FS_{tip} is taken as the most reliable and critical.

7.3.2.2 Determination of L_{tip}

Using the FEA rollover modeling approach detailed in Chapter 5, eight rollover models were constructed based on a BT72 with different bearing widths, girder sweep, bearing slope conditions, and bearing eccentricities. Further details of model construction are given in the section Modeling Assumptions below. A horizontal displacement at the top of the beam flange was applied at midspan and increased until the beam toppled, while the corresponding load at this point was recorded. Next, each rollover model was represented in the modified rollover (tipping) procedure described above. Setting the horizontal tipping load in the analytical procedure equal to that found from the FEA model, the required effective tipping point location, x (Eq. 7.15) was determined. Then, the value for L_{tip} was determined by solving Eq. 7.15. These results are summarized in Table 7.2.

Table 7.2. Comparison Models to Determine Ltip.

Case		Bearing Eccentricity (in)	Tipping Load P (k) from FEA	Z_{wp} (in)	Required x (in)	$L_{tip}*b_w$ (in)	L_{tip}
37" Bearing*							
No sweep,	Sloped	1.34	18.4	2.06	6.50	8.60	0.23
No sweep,	Flat	0.83	20.5	2.29	7.40	7.98	0.22
Sweep,	Sloped	0.75	14.6	1.63	7.85	8.27	0.22
Sweep,	Flat	0.99	17.2	1.92	6.30	9.29	0.25
32" Bearing*							
No sweep,	Sloped	1.48	16.1	1.80	4.60	8.12	0.25
No sweep,	Flat	1.51	18.5	2.07	4.80	7.62	0.24
Sweep,	Sloped	0.80	13.4	1.50	4.10	9.60	0.30
Sweep,	Flat	1.53	14.5	1.63	4.19	8.65	0.27

*Bearing widths correspond to a 1.5" and 3" overhang of the bottom girder flange (40" wide) to the bearing, respectively.

As shown, the range of L_{tip} varies from 0.22 – 0.30, and all but two cases (sweep cases with 32" bearing width) fall within 0.22-0.25. As a smaller L_{tip} value is more conservative, bringing the effective tipping point closer to the deflected girder center of mass, the minimum value found of 0.22 is used throughout this study to evaluate rollover capacity. The results of using a constant L_{tip} value of 0.22 are given in Table 7.3. As shown, ratios of FEA to the proposed procedure rollover loads (which are approximately equal to the ratios of predicted factors of safety for tipping) range from 1.0 to a maximum of 1.46, with an average ratio of 1.14. Removing the single outlier of 1.46 results in a range from 1.0 – 1.24, with an average ratio of 1.09, or less than 10% conservative. Thus, the proposed approach appears to have a reasonably conservative approximation of rollover load.

Table 7.3. Comparison of FEA and Proposed Procedure Rollover Loads.

Case	FEA Model (k)	Proposed Procedure (k)	FEA / Proposed (k)
37" Bearing, No sweep, Sloped	18.4	17.2	1.07
37" Bearing, No sweep, Flat	20.5	20.9	1.02
37" Bearing, Sweep, Sloped	14.6	14.3	1.02
37" Bearing, Sweep, Flat	17.2	14.4	1.19
32" Bearing, No sweep, Sloped	16.1	16.1	1.00
32" Bearing, No sweep, Flat	18.5	17.0	1.09
32" Bearing, Sweep, Sloped	13.4	9.15	1.46
32" Bearing, Sweep, Flat	14.5	11.7	1.24

The effect of the degree of conservatism can be illustrated by using a L_{tip} value of 0.22 vs 0.30 (i.e. using the minimum and maximum degrees of conservatism) was explored for an AASHTO Type III beam using a standard bearing width, which did not meet the minimum recommended FS of 1.5 for tipping with an L_{tip} value of 0.22 (FS= 1.12). Increasing L_{tip} to 0.25 still resulted in noncompliance (FS = 1.37), while increasing L_{tip} to the maximum value found of 0.30 resulted in FS=1.81. However, given that 6 out of the 8 validation cases resulted in L_{tip} values from 0.22-0.25, the value of 0.22 remains recommended and was used for assessment. This conservatism is later addressed in Chapter 9 when recommendations are made.

7.4 Modeling Assumptions

Beyond the girder section and material (E) properties, several parameters influence girder rollover. These include: girder length, sweep, and camber; bearing width, slope, eccentricity, and rotational stiffness; and loads. Of these, camber has very minor influence; beam length, sweep, and loads have moderate influence (using reasonable values for the section and construction scenario); and bearing properties have great significance. Due to lateral deflection from wind, bearing slope under self-weight, and sweep, the beam will develop convex and concave sides, where rolling in the direction of the former the beam has the least resistance. All of these parameters are considered in the modeling process, with values as follows.

7.4.1 Beam Geometry and Loads

Beam Length: As noted above, two lengths were considered, based on meeting in-service HL93-mod and HS25 deflection (and strength) criteria for the bridge to which the girder would belong.

Loads: It is assumed that no construction loads are placed on the girder until some form of bracing is placed, such that the only load on the girder for evaluation of rollover is the crane-lifted weight and wind.

Beyond self-weight, the crane-lifted weight includes a provision for temporary brackets (fascia jacks) attached on the side of an exterior beam to support the deck overhang and a worker walkway during construction, as these brackets are often attached to the beam prior to seating. Based on a review of commercially available steel brackets (Gomaco (n.d.)), these are taken as 50 lbs. each and assumed to be spaced 2.5 ft apart along the beam length. This load is approximated as a 20 lbs/ft uniform gravity load along the beam length, and to account for a large overhang, is conservatively applied 5 ft away from the girder centerline.

Wind load is based on provisions taken from the *AASHTO Guide Specifications for Wind Loads on Bridges During Construction* (AASHTO 2017). In these provisions, wind load (KSF) is given as:

$$P_z = 2.56x10^{-6} \; V^2 \, R^2 \, K_z \, G \, C_D \tag{7.21}$$

where:

V = base wind speed (3 second gust), specified as 20 MPH for active work zones
R = wind speed reduction factor, taken as 1.0 for active work zones
K_z = pressure exposure and elevation coefficient, taken as 1.15. This assumes a girder that is ≤ 33 ft from the ground and surface roughness D (worst case; flat, unobstructed ground)
G = gust effect factor, taken as 1.0 (default value, unless a structure-specific wind analysis is conducted)
C_D = drag coefficient, specified as 2.1 for box beams and 2.0 for I-beams.

Note for an inactive construction site, wind load is specified to be substantially higher. However, it is assumed that beams will not be left seated and unstabilized when workers leave the site, and

thus the inactive site provisions are not further considered. Using the expression above results in a wind pressure of 2.47 PSF, which is applied to the concave side of the girder.

Beam Sweep: Sweep tolerance is specified in the PCI *Tolerance Manual for Precast Prestressed Concrete Construction* (PCI 2000) as 1/8 in. per 10 ft of length, or L/960. Conservatively, the girder is assumed to have sweep in the direction in conjunction with other factors (such as wind and bearing tilt) that causes maximum lateral displacement.

Beam Camber: Camber is calculated based on the prestress force and eccentricity needed for the girder concrete to meet AASHTO LRFD stress limit criteria at transfer and in-service (per Article 5.5.2). However, as noted above, this has very minor influence on rollover.

7.4.2 Bearing Properties

Bearing width (defined here as the bearing dimension perpendicular to the beam span) has a significant influence on rollover potential. As such, different widths were considered in the analysis: For AASHTO and Box beams, two bearing widths are considered, a "wide" width and a "narrow" width. The wide bearing is based on information provided in the MDOT Bridge Design Guide and Manual and the bearing details shown in SPR-1669 (Eamon et al. 2018), and is taken as a total of 3 in. less than the beam lower flange width, while the narrow bearing is taken as the minimum of 6 in. less than the lower flange width or 33 in. For Bulb tees, three widths are considered: the wide and narrow widths, as defined above, and a "minimum" width, taken as 24 in, as shown in SPR-1669.

Bearings were designed using AASHTO Method A, with MDOT Bridge Design Guide limitations (assumptions: cover layer thickness: 0.25 in; interior layer thickness 0.75-0.50 in; shim thickness 0.125 in. with F_y = 36 ksi; shear modulus (G) = 100 psi; bulk modulus (K) = 450 ksi; design temperature range -10 to 100 ⁰F with assumed installation temperature 63 ⁰F; creep and shrinkage coefficient = 0.0003 (WiDOT 2019); fatigue factor A (ΔF_{TH}) = 24 ksi; temperature service load factor (γ_{TU}) = 1.2).

Generally, bearing designs were used that would result in lower stiffness values if multiple reasonable choices were possible that met all design criteria. In particular, interior layer thickness was typically taken as 0.75 in, as used on the bridge details provided in SPR-1669, an increment which usually provided bearings thicker than the minimum required. As rotational stiffness decreases with thickness, these bearings represent more conservative results with regard to rollover. However, in a few cases, this layer thickness could not produce reasonable bearing designs, and in such cases layer thickness was reduced to 0.5 in. Bearing length (in the direction parallel to girder span) was sized to the nearest 0.5 in. This always exceeded the minimum length required in the MDOT Bridge Design Manual. Typical bearing thickness was from 3.5 to 1.5 in.

Bearing rotational stiffness K_θ is a critical factor needed for rollover assessment in the analytical procedure. Based on the bearing designs above, rotational stiffness was calculated by the procedure given in NCHRP 596 (Stanton et al. 2008). Here, the rotational stiffness of one interior layer is calculated as:

$$K_r = \frac{EI}{t}(A_r + B_r S^2) \tag{7.22}$$

where:

E = Young's modulus of the elastomer, taken as E = 3G
I = moment of inertia of bearing about roll (parallel to bridge span) axis; I = L b_w^3/12
L = bearing length (parallel to bridge span)
b_w = bearing width (perpendicular to bridge span)
A_r = rotational constant, taken as 1.0
B_r = (0.24 – 0.24 λ) + (1.15 – 0.89 λ)(1 – exp(-0.64b_w/L)) (note the ratio b_w/L rather than L/b_w is used because the rotational axis of concern is parallel rather than perpendicular to the bridge span)
λ = bearing compressibility index; λ = S(3G/K)$^{1/2}$
S = shape factor = (L b_w) / (2t_e(L+ b_w)); t_e = thickness of one interior elastomer layer

The rotational stiffness of the entire bearing is then calculated as:

$$K_{\theta r} = \frac{K_r}{n(1 + \propto_{cr})} \tag{7.23}$$

where n is the number of interior elastomer layers and α_{cr} the elastomer creep coefficient, taken as 0.35.

Note that for use in Eqs. 7.2-7.5, $K_{\theta r}$ is multiplied by two since the beam is supported by two bearings:

$$K_\theta = 2\ K_{\theta r} \tag{7.24}$$

To evaluate the accuracy of this expression, the rotational stiffness values of 29 bearings that were experimentally measured in NCHRP 596 were computed in this study and compared to that predicted by Eq. 7.23. Although significant variation was found between (coefficient of variation 0.35), the mean was well predicted, with Eq. 7.23 conservatively under predicting stiffness by about 10% (see Appendix C).

The bearing slope is taken as 2%. This value is a result of the sum of two slope tolerance limits. First, per the MDOT Bridge Design Manual, a 1% slope of the bearing is tolerated until shims are required. However, the lower flange of the girder may also be out-of-square. Although no specific tolerance limits are given for out-of-flatness for girder flanges by PCI, based on measured flange slopes from a factory precast BT54 reported in the literature (Zureick 2009; Hurff 2010), a 1% slope tolerance appears reasonable. Thus, the resulting worst-case slope of 1% (top of bearing) + 1% (lower girder flange) = 2% was used. The beam is sloped toward the convex side.

Bearing eccentricity is taken as a 1 in. offset from the center of bearing to girder, which is the limit given by PCI with regard to variation in plan location for a beam (PCI MNL135, 2000). The beam is offset on the bearing toward the convex side.

For the evaluation of cracking (Eq. 7.3), the tensile stress limit is taken as $0.24(f'_c)^{0.5}$, per AASHTO LRFD (Section 5.4.2.6) as well as PCI Bridge Design Specifications.

7.5 Results

7.5.1 Exterior Girders

Resulting rollover factors of safety for exterior girders, the governing case, are given in Tables 7.3 - 7.18 below. As noted above, the tipping result is calibrated to the FEA model and is considered the most critical, and cases that did not meet a Tipping FS of 1.5 are highlighted. The remaining checks are given for comparison. However, as previously discussed, these are less reliable. Of these, only the kern check (with a required FS $\geq$ 1.2) failed. Such failures were similarly highlighted in the tables. It is worthwhile to note that in all cases where tipping failed, the kern was also violated, a result that appears to further validate the tipping limit state developed. However, as the kern check failed more often than the tipping check, the kern check appears to be a reasonably conservative criteria for most cases, though perhaps overly so for the bulb tee beams, in which various cases failed the kern limit but were satisfactory for tipping.

For the AASHTO girders (Tables 7.3-7.6), instability is a concern for both narrow and wide bearings for beam sizes appropriate for girder spacings from 4 – 12 ft. In general, stability decreases as beam size (i.e. from Type IV to I) decreases. The resulting pattern of FS is due to the interaction of changing loads and beam lateral flexibility with regard to length, as well as required bearing characteristics, the latter of which has a significant impact on results.

No box beam case (Tables 7.7 and 7.8), regardless if sized for HL93-mod or HS25, resulted in a rollover instability concern.

Bulb tees with 61 in. flanges passed all required FS for both wide and narrow bearings when sized to HL93-mod (Tables 7.9 and 7.10), with a single exception of the BT72, which failed the narrow bearing kern check. Similarly, all BTs passed the minimum bearing width check for tipping, again with the BT72 an exception, if increased in length for 6 ft girder spacing. However, all BTs failed the kern check when the minimum bearing width was considered (with a single exception; the BT36 passed). When the HS25 length was considered (Tables 7.11 and 7.12), all 61 in. flange bulb tees met tipping requirements for wide and narrow bearings, although BTs 72, 66, and 60 failed the kern check for these cases. Considering the minimum bearing width, BTs 72, 66, and 60 failed in tipping, and all 61 in. flange bulb tees violated the kern limit.

Considering the 49 in. flange bulb tees, for the HL93-mod length (Tables 7.13 and 7.14), all passed stability requirements for wide and narrow bearings, except the BT72 failed the kern check for a narrow bearing. When paired with minimum width bearings, all bulb tees except the BT72 met tipping requirements, although all 49 in. bulb tees except the BT36 failed the kern.

When sized for HS25 length (Tables 7.15 and 7.16), all 49 in. flange bulb tees passed tipping for wide and narrow bearings, and all but the BT72 and BT66 passed the kern check. For the minimum bearing width, however, the BT72 and BT66 failed tipping and all 49 in. flange bulb tees failed the kern check.

The MI-1800 girder survived tipping but failed the kern for HL93-mod length considering both wide and narrow bearings, and failed both the tipping and kern checks for the minimum bearing width. The HS25-length MI-1800 girder could not meet tipping nor kern FS limits when 8 ft spacing was considered, but passed tipping limits and failed the kern when 10 ft spacing was used.

As shown in Table 7.3, the tipping FS is most conservative for a typical beam (beam with camber on a sloped bearing) when set on more narrow bearings. Cases that might be prematurely flagged for failure due to this conservatism are those which have tipping FS values within the range of approximately 1 – 1.5, where the lower bound was determined by reducing the FS tipping limit of 1.5 by the factor of conservatism 1.46 (1.5 / 1.46 ≈ 1); FS_{tip} values below 1 are still predicted to fail even if removing the potential under prediction of capacity. Four results are potentially affected (limiting those to narrow or minimum bearings only): the AASHTO Type IV on narrow bearings; the BT72-61 and BT72-49 on minimum bearings; and the MI-1800 on minimum bearings, all when sized for HL93-mod length.

In no case was cracking in lieu of rollover a concern for any beam type or span. To prevent rollover, bracing with adequate capacity (see Chapter 8) may be applied at any location along the beam length.

Note that all rollover results assume non-curved girders (other than unintended curvature due to sweep). Girders that are intentionally curved, resulting in a sweep much beyond the limit imposed in the analysis, will result in an instability and require lateral bracing during construction.

Table 7.3. Rollover FS, AASHTO Beams, HL93-mod Length.

Beam	Wide Bearing (S=8')				Narrow Bearing (S=8')			
	Cracking	Roll	Kern	Tipping	Cracking	Roll	Kern	Tipping
Type I	107	145	0.70	0.49	50	68	0.46	0.33
Type II	34	47	0.74	0.67	39	53	0.55	0.47
Type III	9.2	19	0.83	1.12	5.8	12	0.66	0.81
Type IV	7.3	16	0.88	1.67	4.9	11	0.74	1.25

Table 7.4. Rollover FS, AASHTO Beams, HL93-mod Length, Alternative Girder Spacing.

Beam	Wide Bearing (S=4')				Wide Bearing (S=6')				Wide Bearing (S=12')			
	Cracking	Roll	Kern	Tipping	Cracking	Roll	Kern	Tipping	Cracking	Roll	Kern	Tipping
Type I	not run; WB S=8' failure				not run; WB S=8' failure				131	226	0.72	0.51
Type II	not run; WB S=8' failure				not run; WB S=8' failure				41	81	0.58	0.50
Type III	not run; WB S=8' failure				not run; WB S=8' failure				3.4	63	0.89	1.21
Type IV	6.5	7.9	0.76	1.36	8.0	12	0.83	1.55	not run; WB S=8' survived			

Table 7.5. Rollover FS, AASHTO Beams, HS25 Length.

Beam	Wide Bearing (S=8')				Narrow Bearing (S=8')			
	Cracking	Roll	Kern	Tipping	Cracking	Roll	Kern	Tipping
Type I	24	26	0.65	0.46	11	12	0.43	0.29
Type II	25	36	0.69	0.62	14	20	0.50	0.40
Type III	8.9	11	0.70	0.92	5.6	7.3	0.56	0.58
Type IV	9.5	9.4	0.69	1.20	6.3	6.3	0.58	0.73

Table 7.6. Rollover FS, AASHTO Beams, HS25 Length, Alternative Girder Spacing.

Wide Bearing (S=4')				Wide Bearing (S=6')				Wide Bearing (S=12')			
Cracking	Roll	Kern	Tipping	Cracking	Roll	Kern	Tipping	Cracking	Roll	Kern	Tipping
not run; WB S=8' failure				not run; WB S=8' failure				not run; WB S=12' HL93mod failure			
not run; WB S=8' failure				not run; WB S=8' failure				not run; WB S=12' HL93mod failure			
not run; WB S=8' failure				not run; WB S=8' failure				not run; WB S=12' HL93mod failure			
not run; WB S=8' failure				not run; WB S=8' failure				11	13.5	0.78	1.46

Table 7.7. Rollover FS, Box Beams, HL93-mod Length.

Beam	Wide Bearing (S=8')				Narrow Bearing (S=8')				Narrow Bearing (S=6')			
	Cracking	Roll	Kern	Tipping	Cracking	Roll	Kern	Tipping	Cracking	Roll	Kern	Tipping
60x48	80	73	1.95	5.38	29	27	1.35	3.41	24	22	1.31	3.32
54x48	113	101	2.13	5.65	56	50	1.50	3.66	46	41	1.46	3.60
42x36	96	94	1.80	3.10	78	76	1.61	2.72	64	61	1.57	2.68
39x36	237	233	1.91	3.11	192	189	1.72	2.73	68	65	1.64	2.68

Table 7.8. Rollover FS, Box Beams, HS25 Length.

Beam	Wide Bearing (S=8')				Narrow Bearing (S=8')				Narrow Bearing (S=6')			
	Cracking	Roll	Kern	Tipping	Cracking	Roll	Kern	Tipping	Cracking	Roll	Kern	Tipping
60x48	54	43	1.67	4.98	27	21	1.17	3.04	26	24	1.32	3.29
54x48	75	63	1.86	5.25	31	26	1.30	3.29	28	22	1.24	3.18
42x36	81	79	1.66	2.96	73	70	1.49	2.59	54	50	1.44	2.54
39x36	88	86	1.75	2.96	80	78	1.57	2.61	59	54	1.51	2.55

Table 7.9. Rollover FS, 61" Flange Bulb Tees, HL93-mod Length.

Beam	Wide Bearing (S=8')				Narrow Bearing (S=8')			
	Cracking	Roll	Kern	Tipping	Cracking	Roll	Kern	Tipping
BT72-61	18	18	1.25	4.08	15	14	1.10	3.33
BT66-61	22	22	1.38	4.41	17	18	1.21	3.66
BT60-61	42	45	1.54	4.76	31	33	1.35	4.05
BT54-61	56	57	1.69	5.03	41	42	1.48	4.26
BT48-61	70	71	1.85	5.26	52	53	1.61	4.48
BT42-61	90	90	2.02	5.45	68	67	1.76	4.67
BT36-61	239	238	2.26	5.62	182	181	1.97	4.84

Table 7.10. Rollover FS, 61" Flange Bulb Tees, HL93-mod Length, Alternative Girder Spacing.

Beam	Minimum Bearing (S=8')				Minimum Bearing (S=6')			
	Cracking	Roll	Kern	Tipping	Cracking	Roll	Kern	Tipping
BT72-61	6.7	6.6	0.74	1.59	5.31	5.07	0.70	1.31
BT66-61	8.2	8.4	0.82	1.96	6.55	6.45	0.77	1.74
BT60-61	14	15	0.92	2.30	7.56	7.82	0.85	2.07
BT54-61	20	20	1.04	2.57	not run; HS25 MB S=6' survived			
BT48-61	24	24	1.09	2.79	not run; HS25 MB S=6' survived			
BT42-61	33	33	1.19	2.98	not run; HS25 MB S=6' survived			
BT36-61	92	91	1.33	3.16	not run; HS25 MB S=6' survived			

Table 7.11. Rollover FS, 61" Flange Bulb Tees, HS25 Length.

Beam	Wide Bearing (S=8')				Narrow Bearing (S=8')			
	Cracking	Roll	Kern	Tipping	Cracking	Roll	Kern	Tipping
BT72-61	8.5	7.7	0.88	2.74	6.47	5.8	0.76	1.95
BT66-61	17	15	1.08	3.74	13	12	0.95	2.97
BT60-61	20	18	1.24	4.12	16	15	1.09	3.36
BT54-61	28	26	1.44	4.59	22	21	1.26	3.83
BT48-61	58	54	1.66	4.98	43	40	1.45	4.21
BT42-61	69	64	1.85	5.23	58	54	1.62	4.46
BT36-61	94	89	2.08	5.44	71	68	1.81	4.67

Table 7.12. Rollover FS, 61" Flange Bulb Tees, HS25 Length, Alternative Girder Spacing.

Beam	Minimum Bearing (S=8')				Minimum Bearing (S=6')				Minimum Bearing (S=12')			
	Cracking	Roll	Kern	Tipping	Cracking	Roll	Kern	Tipping	Cracking	Roll	Kern	Tipping
BT72-61	3.0	2.7	0.51	0.00	not run; MB S=8' failure				5.2	5.1	0.62	0.86
BT66-61	5.7	5.0	0.64	1.09	not run; MB S=8' failure				8.3	7.7	0.73	1.60*
BT60-61	7.2	6.7	0.73	1.62	3.8	3.1	0.60	0.54	not run; MB S=8' survived			
BT54-61	9.9	9.2	0.85	2.10	8.7	7.8	0.79	1.92	not run; MB S=8' survived			
BT48-61	20	19	0.98	2.53	11	10	0.91	2.33	not run; MB S=8' survived			
BT42-61	27	25	1.09	2.78	23	21	1.06	2.72	not run; MB S=8' survived			
BT36-61	36	34	1.22	2.99	31	28	1.19	2.93	not run; MB S=8' survived			

*Fails tipping at 10' girder spacing

Table 7.13. Rollover FS, 49" Flange Bulb Tees, HL93-mod Length.

Beam	Wide Bearing (S=8')				Narrow Bearing (S=8')			
	Cracking	Roll	Kern	Tipping	Cracking	Roll	Kern	Tipping
BT72-49	17	17	1.21	3.82	14	14	1.06	3.11
BT66-49	not run; MB S=8' survived				not run; MB S=8' survived			
BT60-49	42	41	1.52	4.53	34	33	1.33	3.81
BT54-49	48	50	1.66	4.71	35	41	1.45	4.00
BT48-49	62	70	1.82	4.93	46	52	1.59	4.20
BT42-49	95	93	2.02	5.14	72	70	1.76	4.42
BT36-49	250	250	2.26	5.30	191	191	1.97	4.57

Table 7.14. Rollover FS, 49" Flange Bulb Tees, HL93-mod Length, Alternative Girder Spacing.

Beam	Minimum Bearing (S=8')				Minimum Bearing (S=6')				Minimum Bearing (S=10')			
	Cracking	Roll	Kern	Tipping	Cracking	Roll	Kern	Tipping	Cracking	Roll	Kern	Tipping
BT72-49	6.3	6.3	0.72	1.44	not run; MB S=8' failure				7.6	7.9	0.76	1.64
BT66-49	7.4	7.7	0.80	1.79	5.9	5.9	0.75	1.57	not run; MB S=8' survived			
BT60-49	16	15	0.91	2.22	8.3	7.7	0.84	1.96	not run; MB S=8' survived			
BT54-49	17	20	0.99	2.42	14	15	0.950	2.31	not run; MB S=8' survived			
BT48-49	21	24	1.08	2.61	17	18	1.04	2.52	not run; MB S=8' survived			
BT42-49	35	34	1.19	2.82	27	26	1.16	2.76	not run; MB S=8' survived			
BT36-49	88	88	1.34	2.99	37	37	1.28	2.92	not run; MB S=8' survived			

Table 7.15. Rollover FS, 49" Flange Bulb Tees, HS25 Length.

Beam	Wide Bearing (S=8')				Narrow Bearing (S=8')			
	Cracking	Roll	Kern	Tipping	Cracking	Roll	Kern	Tipping
BT72-49	8.4	7.0	0.81	2.49	6.4	5.4	0.73	1.67
BT66-49	14	12	1.01	3.36	11	9.6	0.88	2.62
BT60-49	not run; MB S=8' survived				not run; MB S=8' survived			
BT54-49	25	24	1.38	4.24	18	18	1.20	3.51
BT48-49	47	46	1.61	4.63	39	38	1.41	3.91
BT42-49	71	66	1.85	4.95	53	50	1.61	4.22
BT36-49	98	92	2.07	5.13	75	70	1.80	4.40

Table 7.16. Rollover FS, 49" Flange Bulb Tees, HS25 Length, Alternative Girder Spacing.

Beam	Minimum Bearing (S=8')				Minimum Bearing (S=6')			
	Cracking	Roll	Kern	Tipping	Cracking	Roll	Kern	Tipping
BT72-49	2.8	2.4	0.47	0.00	not run; MB S=8' failure			
BT66-49	5.3	4.6	0.60	0.80	not run; MB S=8' failure			
BT60-49	7.7	6.5	0.71	1.51	not run; MB S=8' edge of failure			
BT54-49	8.9	8.7	0.82	1.89	7.6	7.0	0.77	1.70
BT48-49	17	17	0.96	2.32	11	9.8	0.89	2.14
BT42-49	26	24	1.09	2.63	24	21	1.05	2.55
BT36-49	34	32	1.22	2.82	32	29	1.18	2.76

Table 7.17. Rollover FS, MI-1800, HL93-mod Length.

Beam	Wide Bearing (S=8')				Narrow Bearing (S=8')				Narrow Bearing (S=6')			
	Cracking	Roll	Kern	Tipping	Cracking	Roll	Kern	Tipping	Cracking	Roll	Kern	Tipping
MI-1800	12	15	1.04	2.37	10	13	0.94	1.97	7.6	9.0	0.87	1.79

Beam	Minimum Bearing (S=8')				Minimum Bearing (S=12')			
	Cracking	Roll	Kern	Tipping	Cracking	Roll	Kern	Tipping
MI-1800	6.0	7.4	0.75	1.20	8.6	11.9	0.82	1.45

Table 7.18. Rollover FS, MI-1800, HS25 Length.

Beam	Wide Bearing (S=8')				Narrow Bearing (S=8')				Wide Bearing (S=10')			
	Cracking	Roll	Kern	Tipping	Cracking	Roll	Kern	Tipping	Cracking	Roll	Kern	Tipping
MI-1800	9	8	0.72	1.48	not run; WB S=8' failure				10.8	11.1	0.8	1.77

7.5.2 Interior Girders

A selection of exterior placed on wide or narrow bearings that failed the tipping rollover requirements were reassessed with loads applicable for an interior girder. The only difference in load is the absence of the fascia jacks. The purpose of this analysis was to determine if interior girders could pass tipping stability requirements. Results are given in Tables 7.19 and 7.20.

As shown in the tables, the AASHTO interior beams passed tipping requirements (but still failed the kern check), except for a Type IV beam at 4 ft girder spacing at HS25 length. Thus, all interior girders, if placed on wide or bearings at reasonable girder spacing, pass the tipping check for rollover. In addition, the BT72-61 was checked for the kern limit at HS25 length while seated on a wide bearing (with 8 ft girder spacing). However, as shown in Table 7.20, the kern isn't significantly affected with changing loads from an exterior to interior girder, and the section still failed the kern (although it passed tipping under both interior and exterior girder loads).

Table 7.19. Rollover FS, Interior Girders, HL93-mod Length.

	Wide Bearing				Narrow Bearing			
Beam	Cracking	Roll	Kern	Tipping	Cracking	Roll	Kern	Tipping
AASHTO Type I (S = 8')	107	145	0.70	6.67	50	68	0.46	4.56
AASHTO Type IV (S = 8')	7.3	16	0.88	7.08	4.9	11	0.74	5.34

Table 7.20. Rollover FS, Interior Girders, HS25 Length.

	Wide Bearing				Narrow Bearing			
Beam	Cracking	Roll	Kern	Tipping	Cracking	Roll	Kern	Tipping
AASHTO Type I (S = 4')	28	29	0.62	5.75	13	13.6	0.41	3.45
AASHTO Type IV (S = 4')	4.5	3.8	0.54	1.76	3.0	2.56	0.45	0.00
AASHTO Type IV (S = 8')	9.5	9.4	0.69	5.14	6.3	6.3	0.58	3.16
BT72-61 (S = 8')	8.5	7.7	0.88	7.65	6.47	5.83	0.76	5.46

7.5.3 Unbraced Girders Subjected to Full Construction Loads

A selection of girders that passed rollover as well as LTB requirements (Chapter 8) were subjected to the full construction loads described in Chapter 8, with no lateral constraints. The purpose of this analysis was to determine if these girders could meet stability requirements without lateral constraints any time during construction. Both exterior and interior girder loads were considered.

7.5.3.1 Exterior Girders

Since load eccentricity as well as load magnitude affects results, checks made for various load configurations, including presence of the formwork and worker live load prior to and after the deck pour, with the uniform worker live load positioned transversely to maximize rollover potential. Generally, loading the worker platform with the edge line load, the worker live load, and a portion of deck formwork with live load prior to deck pour governed, where the deck formwork was loaded with the uniform worker live load from the exterior edge of the slab formwork (at the slab/worker platform boundary), extending close to the center of the girder. Once the deck was poured, this large additional dead load, generally centered on the girder, tended to reduce eccentricity and increase rollover FS. Results are given in Tables 7.21-7.32.

All box beams failed tipping at HL93-mod length (Table 7.21). These sections were reconsidered with a more narrow deck overhang width, reducing the 4 ft typically assumed to 2.5 ft (measured from the center of the girder), as shown in Table 7.22. Although this significantly improved the FS, the sections still failed tipping requirements. Note that for exterior girders subjected to full construction loads, the tipping FS was more often violated than the kern limit, indicating that in this particular load scenario, the tipping model is more conservative than the kern limit model. An additional check was made by applying the 75 lbs/ft line load on the edge of the worker platform (see Figure 8.4) only on the central 20 ft of beam span length, rather than across the entire span length. Although the *AASHTO Design Guide Specifications for Bridge Temporary Works* (2008) specifies that the line load be applied across the entire span, this load placement adjustment was suggested in the commentary if results were thought to be too conservative. It should be noted that these loads are meant for temporary bracing structures used for construction rather than an assessment of beam stability, however. As shown in Table 7.23, making this adjustment allows the 48 in. wide box beams seated on wide bearings using a 2.5 ft overhang to pass the tipping check for HL93-mod length, but the 36 in. wide beams still do not satisfy tipping requirements.

All of the 61 in flange bulb tee sections failed tipping with a 4 ft overhang (Table 7.24) or 2.5 ft overhang (Table 7.25). Appling the 75 lbs/ft line load to the central 20 ft span of the beams, however, results in the sections failing the tipping check at HL93-mod length using a 4 ft overhang (Table 7.26) but all sections survived tipping with a 2.5 ft overhang.

Considering the 49 in. flange BT sections, all failed with a 4 ft overhang (Table 7.27) as well as with a 2.5 ft overhang at 8 ft or larger girder spacing (Table 7.28). However, reducing the line load to a 20 ft length results in all sections passing the tipping check with a 2.5 ft overhang at 8 ft girder spacing (Table 7.29).

The MI-1800 girder failed tipping requirements under full construction loads regardless of overhang length and line load position (Tables 7.30-7.32).

Table 7.21. Rollover FS, Full Construction Loads, Box Beams, HL93-mod Length.

| Beam | Wide Bearing (S=8') | | | | | Narrow Bearing (S=8') | | | |
	Cracking	Roll	Kern	Tipping		Cracking	Roll	Kern	Tipping
60x48	22	18	1.70	0.80		8	7	1.11	0.53
54x48	30	25	1.89	0.81		15	12	1.29	0.62
42x36	20	17	1.57	0.52			N.R.		
39x36	47	41	1.72	0.54			N.R.		

Table 7.22. Rollover FS, 2.5' Overhang, Full Construction Loads, Box Beams, HL93-mod Length.

| Beam | Wide Bearing (S=8', Overhang = 2.5') | | | | Wide Bearing (S=6', Overhang = 2.5') | | | |
	Cracking	Roll	Kern	Tipping	Cracking	Roll	Kern	Tipping
60x48	25	20	1.72	1.39	23.4	19	1.67	1.21
54x48	32	27	1.90	1.42	30.8	25	1.85	1.02
42x36	22	20	1.59	0.67	20	17	1.54	0.60
39x36	54	47	1.73	0.72	37	32	1.67	0.59

Table 7.23. Rollover FS, 20' Line Load, Box Beams, HL93-mod Length.

	Wide Bearing (S=8')				Wide Bearing (S=6')			
Beam	Cracking	Roll	Kern	Tipping	Cracking	Roll	Kern	Tipping
60x48	22	18	1.69	1.38	22	18	1.65	1.11
54x48	31	26	1.88	1.44	29	24	1.84	1.24
42x36	20	17	1.57	1.09	18	15	1.52	0.40
39x36	47	40	1.72	1.16	18	15	1.59	0.40
	Wide Bearing (S=8', Overhang = 2.5')				Wide Bearing (S=6', Overhang = 2.5')			
Beam	Cracking	Roll	Kern	Tipping	Cracking	Roll	Kern	Tipping
60x48	25	20	1.72	2.99	23.4	19	1.67	2.32
54x48	32	27	1.90	2.38	30.8	25	1.85	2.35
42x36	22	20	1.59	1.28	20	17	1.54	1.04
39x36	54	47	1.73	1.26	37	32	1.67	1.02

Table 7.24. Rollover FS, Full Construction Loads, 61" Flange Bulb Tees, HL93-mod Length.

	Wide Bearing (S=8')				Narrow Bearing (S=8')			
Beam	Cracking	Roll	Kern	Tipping	Cracking	Roll	Kern	Tipping
BT72-61	5.7	5	0.96	0.60				
BT66-61		N.R.						
BT60-61		N.R.						
BT54-61	17	15	1.44	0.68		N.R.		
BT48-61		N.R.						
BT42-61		N.R.						
BT36-61	65	59	2.07	0.81				

Table 7.25. Rollover FS, 2.5' Overhang, Full Construction Loads, 61" Flange Bulb Tees, HL93-mod Length.

	Wide Bearing (S=8', Overhang = 2.5')				Wide Bearing (S=6', Overhang = 2.5')			
Beam	Cracking	Roll	Kern	Tipping	Cracking	Roll	Kern	Tipping
BT72-61	6.3	5.6	0.99	0.99		N.R.		
BT66-61		N.R.				N.R.		
BT60-61		N.R.				N.R.		
BT54-61	19	17	1.47	1.17	14	13	1.40	1.03
BT48-61		N.R.				N.R.		
BT42-61		N.R.				N.R.		
BT36-61	71	66	2.08	1.22	59	54	2.03	1.08

Table 7.26. Rollover FS, 20' Line Load, 61" Flange Bulb Tees, HL93-mod Length.

Beam	Wide Bearing (S=8')				Wide Bearing (S=6')			
	Cracking	Roll	Kern	Tipping	Cracking	Roll	Kern	Tipping
BT72-61	5.6	4.9	0.96	1.15				
BT66-61	N.R.							
BT60-61	N.R.							
BT54-61	17	16	1.45	1.13	N.R.			
BT48-61	N.R.							
BT42-61	N.R.							
BT36-61	64	59	2.07	1.11				

Beam	Wide Bearing (S=8', Overhang = 2.5')				Wide Bearing (S=6', Overhang = 2.5')			
	Cracking	Roll	Kern	Tipping	Cracking	Roll	Kern	Tipping
BT72-61	6.3	5.6	0.99	1.95	5.7	4.9	0.94	1.52
BT66-61	N.R.				N.R.			
BT60-61	N.R.				N.R.			
BT54-61	19	17	1.47	2.35	14	13	1.40	1.87
BT48-61	N.R.				N.R.			
BT42-61	N.R.				N.R.			
BT36-61	71	66	2.08	2.43	59	54	2.03	1.91

Table 7.27. Rollover FS, Full Construction Loads, 49" Flange Bulb Tees, HL93-mod Length.

Beam	Wide Bearing (S=8')				Narrow Bearing (S=8')			
	Cracking	Roll	Kern	Tipping	Cracking	Roll	Kern	Tipping
BT72-49	5.2	4.4	0.90	0.46				
BT66-49	N.R.							
BT60-49	12	10	1.22	0.64				
BT54-49	14	13	1.39	0.65	N.R.			
BT48-49	N.R.							
BT42-49	N.R.							
BT36-49	65	58	2.05	0.76				

Table 7.28. Rollover FS, 2.5' Overhang, Full Construction Loads, 49" Flange Bulb Tees, HL93-mod Length.

Beam	Wide Bearing (S=8', Overhang = 2.5')				Wide Bearing (S=6', Overhang = 2.5')			
	Cracking	Roll	Kern	Tipping	Cracking	Roll	Kern	Tipping
BT72-49	5.8	5	0.93	0.91	N.R.			
BT66-49	7.0	6	1.06	0.99	N.R.			
BT60-49	13	12	1.26	1.06	N.R.			
BT54-49	16	14	1.41	1.09	13	12	1.35	0.95
BT48-49	N.R.				N.R.			
BT42-49	N.R.				N.R.			
BT36-49	81	74	2.08	1.15	71	63	2.03	0.70

Table 7.29. Rollover FS, Reduced Overhang, 20' Line Load, 49" Flange Bulb Tees, HL93-mod Length.

Beam	Wide Bearing (S=8', Overhang = 3.5')				Wide Bearing (S=6', Overhang = 3')			
	Cracking	Roll	Kern	Tipping	Cracking	Roll	Kern	Tipping
BT72-49	5.4	4.6	0.91	1.12	4.80	4.1	0.86	1.12
BT66-49	N.R.				N.R.			
BT60-49	N.R.				N.R.			
BT54-49	14	13	1.38	1.29	13	12	1.34	1.38
BT48-49	N.R.				N.R.			
BT42-49	N.R.				N.R.			
BT36-49	67	60	2.05	1.3	45	40	1.93	1.39

Beam	Wide Bearing (S=8', Overhang = 2.5')				Wide Bearing (S=6', Overhang = 2.5')			
	Cracking	Roll	Kern	Tipping	Cracking	Roll	Kern	Tipping
BT72-49	5.8	5.0	0.93	1.82	4.80	4.1	0.86	1.38
BT66-49	N.R.				N.R.			
BT60-49	N.R.				N.R.			
BT54-49	15	14	1.39	2.19	14	13	1.37	1.77
BT48-49	N.R.				N.R.			
BT42-49	N.R.				N.R.			
BT36-49	73	67	2.07	2.26	51	45	2.01	1.78

Table 7.30. Rollover FS, Full Construction Loads, MI-1800, HL93-mod Length.

Beam	Wide Bearing (S=8')				Narrow Bearing (S=8')			
	Cracking	Roll	Kern	Tipping	Cracking	Roll	Kern	Tipping
MI-1800	3.2	2.9	0.70	0.15	N.R.			

Table 7.31. Rollover FS, 2.5' Overhang, Full Construction Loads, MI-1800, HL93-mod Length.

Beam	Wide Bearing (S=8', Overhang = 2.5')			
	Cracking	Roll	Kern	Tipping
MI-1800	3.6	3.3	0.73	0.52

Table 7.32. Rollover FS, 2.5' Overhang, 20' Line Load, MI-1800, HL93-mod Length.

Beam	Wide Bearing (S=8', Overhang = 2.5')			
	Cracking	Roll	Kern	Tipping
MI-1800	3.7	3.5	0.74	0.99

7.5.3.2 Interior Girders

The analysis was repeated with interior girder loads for a selection of girders that failed stability requirements with exterior loads. In this case, no worker platform and associated loads, nor the finishing machine loads, are applied. Results are given in Tables 7.33 and 7.34.

As shown in Table 7.33, all evaluated beams except AASHTO pass tipping at HL93-mod length, although most still fail the kern check. Per Table 7.34, at HS25 length, all box beams pass tipping, and all bulb tee sections pass if seated on wide bearings (except the BT72-49 if girder spacing is reduced less than 8 ft). Note that only the sections within each beam type with the lowest tipping FS for exterior loads were evaluated. Thus, all sections within each beam type for boxes and bulb

tees pass tipping requirements for interior loads at HL93-mod length, as well as interior loads at HS25 length if seated on wide bearings. The MI-1800 nor AASHTO beams do not pass tipping requirements.

Table 7.33. Rollover FS, Full Construction Loads, HL93-mod Length.

Beam	Wide Bearing					Narrow Bearing			
	Cracking	Roll	Kern	Tipping		Cracking	Roll	Kern	Tipping
60x48 Box (S = 6')	28.9	23.6	1.71	15.7		9.6	7.83	1.13	5.62
60x48 Box (S = 8')	26.0	21.6	1.73	8.20		9.6	7.96	1.15	3.46
42x36 Box (S = 6')	23.1	20	1.57	7.78		19.7	16.2	1.39	5.80
BT72-61 (S = 6')	6.43	5.65	0.98	6.03		5.15	4.53	0.85	4.30
BT72-61 (S = 8')	6.75	6.0	1.01	4.06		5.33	4.74	0.87	2.99
MI-1800 (S = 6')	3.8	3.5	0.73	2.84		2.9	2.69	0.64	2.03
MI-1800 (S = 8')	3.8	3.29	0.75	2.01		3.2	2.98	0.66	1.53
AASHTO Type I (S=8')	13.4	11.0	0.52	0.36					
AASHTO Type II (S=8')	12.6	10.0	0.54	0.49			N.R.		
AASHTO Type III (S=8')	7.7	6.25	0.61	0.86					
AASHTO Type IV (S=8')	4.2	3.50	0.63	1.24					

Table 7.34. Rollover FS, Full Construction Loads, HS25 Length.

Beam	Wide Bearing					Narrow Bearing			
	Cracking	Roll	Kern	Tipping		Cracking	Roll	Kern	Tipping
60x48 Box (S = 6')	19.4	13.7	1.41	12.80		9.5	6.7	0.96	4.66
60x48 Box (S = 8')	18.3	13.3	1.47	7.06		9	6.5	1.00	2.95
42x36 Box (S = 6')	24.5	19.4	1.46	7.10		19.5	15.5	1.3	5.31
BT72-61 (S = 8')	2.95	2.45	0.64	2.05		2.24	1.87	0.55	1.19
BT72-61 (S = 6')	2.88	2.37	0.59	2.26		2.19	1.8	0.51	1.02
BT72-49 (S = 8')	2.50	2.05	0.56	1.51		1.9	1.56	0.47	0.71
BT72-49 (S = 6')	2.50	2.00	0.81	1.40		1.9	1.53	0.44	0.26
BT54-61 (S = 8')	9.6	8.04	1.20	5.11		7.7	6.44	1.04	3.77
BT54-61 (S = 6')	10.4	8.3	1.17	9.25		7.6	6.05	1.00	6.39
BT36-61 (S = 6')	33.5	29	1.87	20.5		25.5	22.3	1.62	12.8
BT36-49 (S = 6')	31.9	27.2	1.89	20.1		24.6	21	1.64	12.5
MI-1800 (S = 8')	2.2	1.87	0.46	0.77		not run; wide bearing failure			

CHAPTER 8: ASSESSMENT OF LATERAL TORSIONAL BUCKLING

8.1 Introduction and Beams Considered

Once the girder is braced laterally, it may experience lateral torsional buckling (LTB) between points of support rather than roll over. All of the beam sections considered for LTB are the same as those examined for rollover, where AASHTO beams, bulb tees, and box beams at lengths that meet HL93-mod and HS25 deflection, strength, and stress criteria were analyzed. These hypothetical structures were based on the geometry (i.e. 9 in deck) and material properties used for the in-service live load distribution analysis discussed above (Chapter 6). As when considering beam lengths for rollover, for calculation of DF and top flange width of the composite section needed to evaluate girder live load and stiffness for LTB, general beam spacing was taken as 8 ft, with wider and narrower spacing configurations also considered when necessary.

8.2 Modeling Approach and Assumptions

8.2.1 General Approach

PC girder LTB was modeled using the FEA approach described in Chapter 5. This involves a three-stage analysis including the application of prestressing, dead load, and then the construction loads, with the model load time periods considered. In the prestress stage, beam stresses were monitored to insure damage does not occur to the concrete prior to application of dead load. As detailed in Chapter, 5, prior to load application, an imperfection is imposed onto the beam that allows the potential for nonlinear LTB to occur. The shape of this imperfection is the first Euler buckling mode of the beam, which is given a maximum lateral displacement value equal to the beam sweep limit. As an LTB mode, a slight twisting of the section accompanies this sweep. Similarly following Chapter 5 recommendations, the CDP model was used for concrete with tensile strength set to near zero and all reinforcing steel was explicitly included. Appropriate beam sweep and camber were imposed on the beam as with the rollover analysis, as discussed in Chapter 7.

Positioning of nonprestressed steel longitudinal bars and stirrups is based on MDOT Bridge Design Guide specifications as well as AASHTO requirements as needed. However, to simplify model construction, prestress steel was lumped into two representative strands with eccentricity and total area required to satisfy beam design criteria. Moreover, as shear capacity is not of interest, stirrups were placed with a constant spacing along the beam length.

As noted above, for LTB to be evaluated, support must be provided on the beam. For this analysis, it is assumed that beam is fixed in torsion at both ends, such as provided either from poured end walls or temporary bracing. These torsionally-fixed boundary conditions are represented with lateral constraints at the top and bottom flange midpoints. Other beam boundary conditions are vertical constraints representing the supports at either end (bearings not explicitly modeled), and a longitudinal constraint on one end at the support. As single beams are evaluated, if it was determined that diaphragms were needed for stability, the diaphragm itself was not directly modeled, but rather lateral constraints at the top and bottom flanges were imposed at the midspan of the beam. Here it is assumed that the lateral stiffness of the complete bridge system, with all

beams linked together, is sufficiently rigid such that the system as a whole will not experience LTB. Example beams are shown in Figures 8.1-8.3.
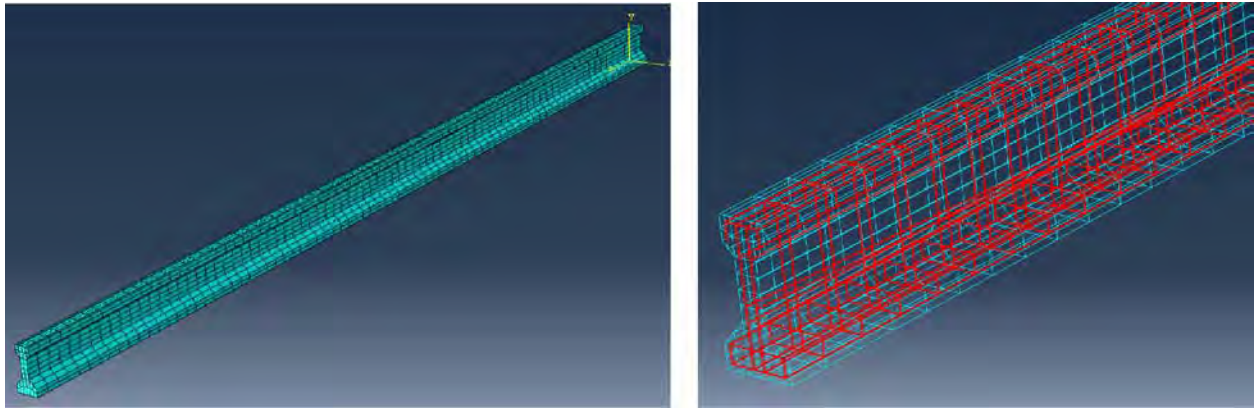
Figure 8.1. Example AASHTO Beam and Reinforcing.
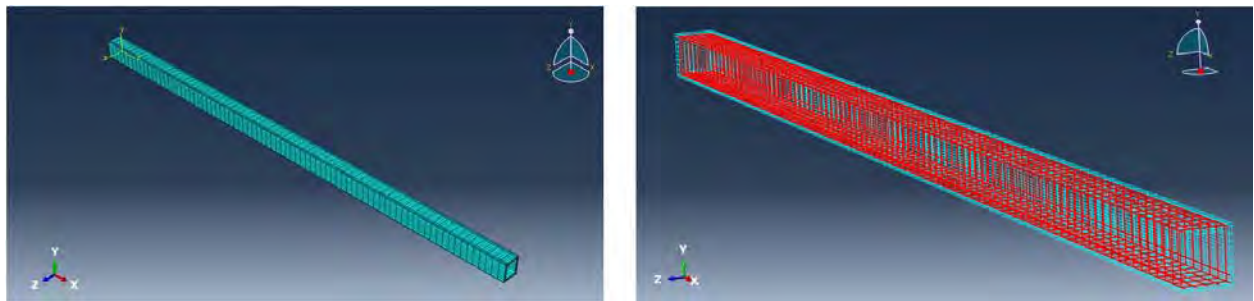
Figure 8.2 Example Box Beam and Reinforcing.
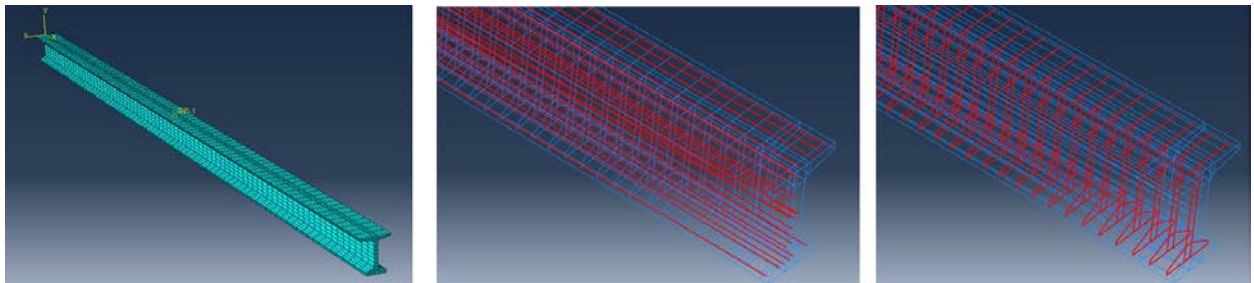
Figure 8.3. Example Bulb Tee and Reinforcing.

8.2.2 Loads

8.2.2.1 Loads Considered

Loads considered are beam dead load (DC), construction dead load (CDL), construction live load (CLL), and wind (W). The loads below are described for an exterior girder, the governing case.

8.2.2.2 General Assumptions

- Conservatively, the weight and eccentricity of a large deck overhang is considered, taken as 4 ft from the center of the exterior girder.

- A temporary walkway extends 2 ft beyond the outer edge of deck (used for formwork CDL and CLL calculations).

- A 3 in. haunch is assumed, such that the slab is taken as 9 in thick inbound of the interior side of the girder flange and 12 in thick from the beginning of the haunch to the edge of the deck.

8.2.2.3 Dead Loads

- Dead loads include the self-weight of the girder and the uncured slab. Although various pour sequences are possible, the worst case with regard to instability is that of a simple span where the entire slab is poured at once, where dead load moment is maximized. Thus, this is the default slab dead load considered.

- A 15 PSF allowance is given for formwork and the work platform, per the MDOT Bridge Design Manual.

- The fascia jack (overhang support bracket) weight, as described in Chapter 7.

8.2.2.4 Live Loads

- Based on recommendations provided in the *AASHTO Design Guide Specifications for Bridge Temporary Works* (2008), CLL is described as that of the construction equipment, a 20 PSF allowance for miscellaneous items and workers, and 75 PLF applied to the outer edge of the overhang. Thus, the following three construction live loads are applied:

- 20 PSF on the girder tributary area and worker platform (workers, miscellaneous equipment).

- A 75 PLF line load on the outer edge of the work platform.

- Wheel loads from the finishing machine. Various options are available that affect machine weight. Based on literature from Terex (2010), combining the heavier options available and assuming a 48 ft wide Bid-Well 4800 machine results in a total weight of approximately 14,000 lbs, with each wheel (separated approximately 4 ft each) in a standard 4-wheel bogie having a maximum reaction of 2800 lbs when the screed roller is moved to the far side of the machine where the operator's carriage is placed. No information is available on the lateral force placed on the concrete surface due to the roller/screed head. Based on conversations with the MDOT Research Advisory Panel, the finishing machine wheel loads are placed on the centerline of the fascia girder rather than on the edge of the deck overhang.

- Wind load was calculated above for an active work zone (2.47 PSF). For an inactive work zone, at which time the slab may continue to cure, wind loads are specified to be substantially higher. However, in this case, no live loads would be present nor could the wind be applied to the concave side of the beam, as it would be shielded by the adjacent beam in the structural system. Initial calculations have indicated that applying the wind load on the convex side of the beam without live loads will not govern. Thus the inactive worksite wind loading was not further considered. Conservatively, the active worksite wind load was applied to the shielded (concave) side of the beam to account for possible suction forces, although this load is small and has little effect on the analysis.

Note that the geometry of the fascia jacks, formwork, and work platform were not directly included in the FEA models. Rather, the equivalent reactions of these items were applied to the beam in the analysis, as shown in Figure 8.4.
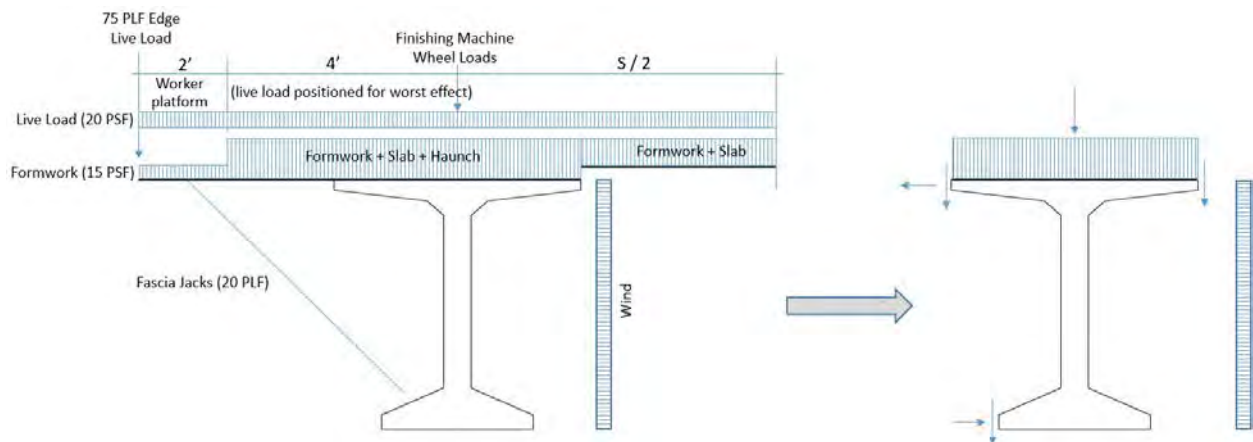
Figure 8.4. Loads and Idealization on Beam Model.

Given the relatively closely-spaced nature of the fascia jacks as well as the finishing machine wheels relative to the girder spans considered, to facilitate automation of load data input, all loads are modeled as equivalent pressure or traction loads along length of beam (for jack reactions) and along the distance between the first and last wheels of the finishing machine, which are taken symmetric to girder midspan.

8.3 LTB Evaluation Criteria

Once stable (braced), the girder within the bridge structural system falls under AASHTO LRFD provisions, Section 3.4.2.1, thus load and resistance factors are used to account for uncertainties rather than an acceptable factor of safety as for girder rollover.

Applicable load combinations are taken as: Service I (cracking; based on the AASHTO allowable tension stress of $0.24f'_c{}^{0.5}$); Strength I (normal use during construction), III (wind event during construction), and IV (high dead to live load ratio check). Strength V, which has a lower factor for construction live load but simultaneously includes wind, was not checked since live loads greatly outweighs the small wind load effect and will not govern. AASHTO LRFD states that the

minimum load factors for construction loads are to be 1.25, and to be taken as 1.5 if dynamic effects are to be included. With this guidance, the following load factor combinations are used for this study (PCI 2016):

Service I: 1.0DC + 1.0CDL + 1.0CLL+1.0W   (8.1)

Strength I: 1.25DC + 1.5CDL + 1.5CLL   (8.2)

Strength III: 1.25DC + 1.5CDL + 1.25W   (8.3)

Strength IV: 1.5DC + 1.5CDL   (8.4)

where:

DC = factory-cast dead load (self weight of the girder)
CDL = construction dead load (weight of the slab and formwork)
CLL = construction live load (workers, equipment, and finishing machine).

Note that these limit states are evaluated specifically for LTB only, the failure mode that lateral bracing or the presence of an ID can affect. That is, in the case of Service I, cracking stress is monitored only at the top flanges in the lateral direction, where stresses from lateral deflection and twisting from LTB is greatest. As the beams considered were not designed for construction loads, flexural (or shear) performance under these loads is beyond the scope of the evaluation. That is, as the presence of an ID would not change flexural performance, this type of failure is inapplicable to ID assessment and therefore not considered. Similarly, the strength limit states are regarded as satisfied if the beam does not experience LTB failure and remains stable under the loads imposed.

Resistance factors for PC girders in flexure are 1.0 and 0.75 for a tension-controlled and compression-controlled beam, respectively. However, a resistance factor for LTB is not specified in AASHTO LRFD. Based on FHWA suggestions (Garlich et al. 2015), a resistance factor of 0.90 is used to assess sufficiency of LTB strength.

8.4 Results

8.4.1 Exterior Girders

8.4.4.1 Lateral Bracing at Girder Supports

Following the modeling assumptions described above, beams are laterally constrained at the top and bottom flanges at either end to prevent twisting and allow evaluation of LTB resistance. Results are given in Tables 8.1 – 8.7, where three outcomes are possible for each of the limit states described above: "ok": the beam did not require IDs; "ID": the beam required one ID at midspan to prevent LTB (in no cases were more than 1 ID required); and "NA": the case was not applicable for diaphragm evaluation, because the beam (with uncured slab) could not support the construction loads imposed and failed in flexure with and without lateral bracing. When this occurred, the result was verified with a simple calculation of flexural capacity and imposed bending moment. In these cases, the beams were found to be compression-controlled, with the stress block usually

falling deep into the beam web. However, in a few cases at the longer (HS25) span lengths, an apparent flexural failure occurred when the stress block dropped only slightly below the top flange and into the web. This can be attributed to a combination of the beam asymmetry due to the twisting/sweep imperfection imposed, as well as the conservatism of the concrete material model, which ignores tension capacity; as discussed previously, the approach used was meant to model LTB behavior rather than ultimate flexural capacity. As shown in the tables, some cases were not run, in the situation where it was clear what the outcome would be based on prior case results. Such cases are noted in the tables, or designated "NR".

An example of typical load increment-displacement graphs is shown in Figure 8.5, where the horizontal axis, the incremented time in the analysis, approximately (not precisely) corresponds to the increment of load specified that was applied to the section.

Here the three-stage analysis loading can be seen, where first prestress is applied, increasing midspan deflection from zero to a maximum in load increment 1; next dead load was more gradually applied through increments 2 – 10; and finally the construction loads above were more gradually applied throughout the remaining increments 11-30. In this case, the beam failed in STR I but survived when loaded in STR III and IV. Although not apparent in the graph below, most results were accompanied by larger than expected deflections. This is because, as discussed in Chapter 5, the model essentially assumes that the beam is in a cracked state prior to any loads being imposed, as the tension strength of the concrete was practically neglected, as this was shown to best match experimental LTB strength results, although stiffness was significantly under-predicted.
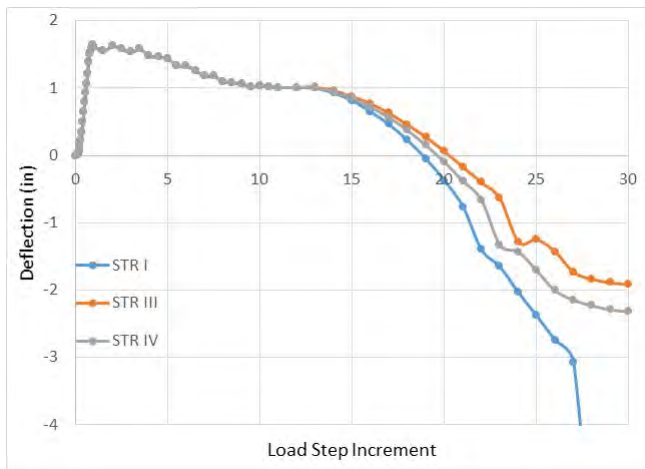
Figure 8.5. Example Load Increment-Displacement Result.

Results in all tables except Table 8.6 are based on beam lengths designed assuming an 8 ft girder spacing. To verify results for different girder spacing possibilities, a sample of beams were redesigned for 6, 10, and 12 ft spacing and analyzed for LTB. These results are given in Table 8.6. For beams in which no strength case allowed diaphragm evaluation (i.e. if all were labeled "NA"), because the beam was overloaded in flexure, construction loads were reduced on the beam until AASHTO LRFD criteria were met for construction loading as well and the beam had the fundamental (compressive) flexural strength to survive if instability was not an issue. These results are given in Table 8.7.

121

For AASHTO beams, as shown in Table 8.1, Types I-III required IDs to prevent LTB if sized for HL93-mod length, while Type IV could not carry the imposed construction loads. Reducing construction loads to meet beam design criteria resulted in the Type IV beam to survive without the diaphragm, as shown in Table 8.7. Increasing AASHTO beam length for HS25 criteria resulted in the Type I requiring an ID, while the other beams had insufficient strength to carry the construction loads.

No box beam required IDs for HL93-mod length, though these sections generally failed in flexure under the construction loads for HS25 length (Table 8.2). However, the were found to not need an ID when the construction loads were appropriately reduced, as shown in Table 8.7. This is not unexpected, given the large lateral flexural and torsional stiffness of these sections relative to the other beam types.

As shown in Table 8.3, none of the 61 in. flange bulb tees required IDs if sized to HL93-mod. When increased in length for HS25, however, two of the sections that could be evaluated for IDs required IDs (BT60 and BT48). When considering the 49 in. flange bulb tees (Table 8.4), only one required an ID at HL93-mod length, the BT60. The BT72 could not be evaluated for stability, as indicated in the table, unless construction loads were reduced. When increased to HS25 length, the 49 in. flange BTs could not be evaluated for stability. Using reduced construction loads resulted in no instability problems with the BTs, as shown in Table 8.7.

The MI-1800 girder could not be evaluated for stability (Table 8.5). However, reducing the construction loads resulted in a stable beam without IDs (Table 8.7).

As discussed above, because all beams were sized in length based on an assumed 8 ft girder spacing, additional cases where evaluated to verify results for other cases. Table 8.6 presents these results for a selection of bulb tees that indicated no IDs were needed. As shown, changing girder spacing from 6 ft to 12 ft did not alter results, indicating that these sections are stable without IDs across this wider range of girder spacing considered.

Table 8.1. LTB, AASHTO Beams.

Beam	HL93mod Length				HS25 Length			
	SERV I	STR I	STR III	STR IV	SERV I	STR I	STR III	STR IV
Type I	ok	NA	ID	ID	NA	NA	ID	NA
Type II	ok	NA	ID	ID	NA	NA	NA	NA
Type III	ok	NA	ID	ID	NA	NA	NA	NA
Type IV	ok	NA	NA	NA	NA	NA	NA	NA

Table 8.2. LTB, Box Beams.

Beam	HL93mod Length				HS25 Length			
	SERV I	STR I	STR III	STR IV	SERV I	STR I	STR III	STR IV
60x48	ok	ok	ok	ok	NA	NA	NA	NA
54x48	ok	ok	ok	ok	NA	ok	ok	ok
42x36	ok	ok	ok	ok	ok	NA	NA	NA
39x36	ok	ok	ok	ok	ok	NA	NA	NA

Table 8.3. LTB, 61" Flange Bulb Tees.

Beam	HL93mod Length				HS25 Length			
	SERV I	STR I	STR III	STR IV	SERV I	STR I	STR III	STR IV
BT72-61	ok	ok	ok	ok	NA	NA	NA	NA
BT66-61	ok	NA	ok	NA	NA	NA	NA	NA
BT60-61	ok	ok	ok	ok	ID	NA	NA	NA
BT54-61	ok	ok	ok	ok	ok	NA	NA	NA
BT48-61	ok	ok	ok	ok	ok	NA	NA	ID
BT42-61	ok	ok	ok	ok	ok	NA	ok	NA
BT36-61	ok	ok	ok	ok	ok	ok	ok	ok

Table 8.4. LTB, 49" Flange Bulb Tees.

Beam	HL93mod Length				HS25 Length			
	SERV I	STR I	STR III	STR IV	SERV I	STR I	STR III	STR IV
BT72-49	ok	NA	NR*	NR*	not run based on HL93mod results			
BT66-49	not run; BT66-61 failure				not run; BT66-61 failure			
BT60-49	ok	ID	NR*	NR*	not run; BT60-61" failure			
BT54-49	ok	ok	NR*	NR*	ok	NA	NR*	NR*
BT48-49	ok	ok	NR*	NR*	ok	NA	NR*	NR*
BT42-49	ok	ok	NR*	NR*	ok	NA	NR*	NR*
BT36-49	ok	ok	NR*	NR*	ok	NA	NR*	NR*

*Not run based on STR I result

Table 8.5. LTB, MI-1800.

Beam	HL93mod Length				HS25 Length			
	SERV I	STR I	STR III	STR IV	SERV I	STR I	STR III	STR IV
MI-1800	ok	NA	NA	NA	not run based on HL93mod results			

Table 8.6. LTB, Alternative Girder Spacing.

HL93mod Length - Alternative Girder Spacing				
Beam	SERV I	STR I	STR III	STR IV
BT72-61 (S = 6')	ok	NA	NR*	NR*
BT72-61 (S = 12')	ok	ok	NR*	NR*
BT36-61 (S = 6')	ok	ok	NR*	NR*
BT36-61 (S = 10')	ok	ok	NR*	NR*
BT48-49 (S=6')	ok	ok	NR*	NR*
BT48-49 (S=10')	ok	ok	NR*	NR*

Table 8.7. LTB, Reduced Construction Loads.

Beam	SERV I	STR I	STR III	STR IV
AASHTO Type IV*	ok	ok	NR	NR
60x48 Box	ok	ok	ok	ok
54x48 Box	ok	ok	NR	NR
42x36 Box	ok	ok	NR	NR
39x36 Box	ok	ok	NR	NR
BT54-61	ok	ok	ok	NR
BT72-49*	ok	ok	NR	NR
BT36-49	ok	ok	ok	NR
MI-1800*	ok	ok	NR	NR
*HL93-mod length; unmarked cases are sized for HS25.				

8.4.4.2 Lateral Bracing at Midspan

As it is common practice the the beam end walls are poured simultaneously with the deck, the end walls cannot be relied upon as lateral bracing elements prior to deck cure. Thus, the beams were also checked for stability during construction assuming no lateral bracing at the beam ends but with bracing placed at midspan only. These results are given in Tables 8.8 and 8.9. As shown in Table 8.8, all beams avoided LTB failure with the exception of three BTs; BT66-61, BT60-61, and BT36-61. The box beams and several BTs that could not be evaluated for LTB at the HS25 length were reanalyzed under reduced construction loads. As shown in Table 8.9, all of these cases survived except for the BT54-61.

8.4.2 Interior Girders

A selection of sections that failed in LTB when subjected to exterior girder loads were analyzed for interior girder loads. When considering LTB, this results in elimination of the worker platform and associated live loads on the platform, as well as the finishing machine load. As shown in Table 8.10, all of these girders survived LTB.

124

Table 8.8. LTB, Lateral Bracing at Midspan Only.

Beam	HL93mod	HS25
AASHTO Type I*	ok	ok
AASHTO Type II*	ok	NA
AASHTO Type III*	ok	NA
AASHTO Type IV*	NA	NA
Box 60x48	ok	NA
Box 54x48	ok	ok
Box 42x36	ok	NA
Box 39x36	ok	NA
BT72-61	ok	NA
BT66-61*	FAIL	NA
BT60-61	FAIL	NA
BT54-61	ok	NA
BT48-61	ok	NA
BT42-61	ok	NA
BT36-61	ok	FAIL
BT72-49	NA	NR
BT66-49	NR	NR
BT60-49	NR	NR
BT54-49	FAIL	NA
BT48-49	ok	NA
BT42-49	ok	NA
BT36-49	ok	NA
MI-1800	NA	NR
*Checked for STR III only; others checked at STR I		

Table 8.9. LTB, Lateral Bracing at Midspan Only, Reduced Loads, HS25 Length.

Beam	SERV I	STR I
60x48 Box	ok	ok
42x36 Box	ok	ok
39x36 Box	ok	ok
BT54-61	ok	FAIL
BT42-61	ok	ok
BT36-49	ok	ok

Table 8.10. LTB, Interior Girders.

Beam	Constraints	Result
AASHTO Type II*	Ends only	ok
BT60-61	Midspan only	ok
BT60-49	Ends only	ok
BT66-61*	Midspan only	ok
BT36-61**	Midspan only	ok
*STR III. All others STR I.		
**HS25 length. All others HL93-mod.		

8.4.3 Lateral Bracing Forces

The total torsional moments in kip-ft required for stability during the LTB analysis are given in Tables 8.11 and 8.12. The values presented assume that the girders first reach equilibrium under self-weight, with an angle of tilt of 1%, then the lateral bracing is applied, followed by the construction loads. Although a 2% tilt angle was taken for the rollover analysis, this angle was deemed unrealistically severe in this case, as here a system of girders is considered, linked together with lateral bracing elements, rather than individual girders with no bracing as in the rollover case. The 1% thus represents a system-average maximum girder tilt. The total torsion on the beam is caused by the imposed unbalancing construction loads, with eccentricity to the girder roll center, as affected by the tilt angle, girder sweep, additional lateral displacement due to the imposed loads, and bearing eccentricity, as determined from the rollover model. The maximum torsion generated from each of the LTB load cases (Eqs. 8.1 – 8.4) is provided. Typically, this was caused by the Strength I load combination. The values in the Tables apply to non-curved girders only. Even slightly intentionally curved girders will greatly increase torsion demand and a refined analysis is required for each particular case.

In this analysis, it is assumed that the lateral bracing is very stiff relative to the bearing roll stiffness, such that all rotational resistance is provided by the bracing. The values presented thus represent the torsional resistance needed to hold the beam in equilibrium under the construction loads without any additional rotation beyond the self-weight equilibrium position. Note that values are provided for all beams even if bracing is not required to prevent tipping. If lateral bracing is provided in any case, however, sizing the bracing members to carry less than the torsion values specified may cause bracing member failure even if the girder is stable once the bracing members fail, as these values represent the torsion generated by the tipping motion of the beam upon application of construction loads.

The values presented in Table 8.11 are based on a 8 ft girder spacing, while Table 8.12 considers the effect of 6 ft and 12 ft spacing. For all of the cases considered in Table 8.12, a highly linear relationship was found between girder spacing and torsional load. Therefore, the values in Table 8.11, based on 8 ft girder spacing (T_8) can be accurately adjusted to torsion T_s at an alternative girder spacing (S) (ft) by proportion:

$$T_s = T_8 * (S/8) \tag{8.5}$$

The torsion on the entire girder is provided. A detailed analysis of dividing this total torsional load into different lateral bracing components (for example, at the girder ends and midspan, if so provided) is beyond the scope of this study. However, it is suggested that a reasonable approach is to divide the total torsion given in Table 8.11 (or 8.12) equally into the different bracing components attached to the girder, with the assumption that each component imposes equal torsional stiffness onto the girder. For example, if an interior girder has lateral bracing on either side of the web on both ends of the beam, as the typical case, the torsional load to each bracing component (i.e. diaphragm or end wall cast between adjacent girder webs) would be the value given in the table divided by 4. Similarly, for an exterior girder braced at both ends and at midspan, the total torsion applied to each component could be taken as the tabular value divided by 3. Once the torsional load to each bracing component is determined, conversion into equivalent lateral

forces into the top and bottom connection points between the diaphragm and girder can be determined by dividing the torsion value by the vertical distance between connection points.

For example, say an interior AASHTO Type IV (54 in. depth) girder spaced 6.5 ft and does not exceed HL93-mod length requirements for strength, serviceability, and deflection, is braced at both ends and at midspan, where the midspan bracing component is an ID with web connection points separated by 1 ft 5-7/8 in. (1.49 ft), as specified by the Bridge Design Guide Sheet 6.60.12A (pg. 135). According to Table 8.11, the total torsion demand on the girder is 49.5 k-ft. Converting to 6.5 ft girder spacing using Eq. 8.5 results in: $T_{6.5} = (49.5) * (6.5/8) = 40.2$ k-ft. Distributing this torsion load equally to each bracing component results in $40.2 / 6 = 6.7$ k-ft. Thus the beam member acting as the ID (specified as an MC18 x 42.7 in the Bridge Design Guide) must resist 6.7 k-ft of moment, and each web connection bolt on the ID must then withstand: 6.7 k-ft / 1.49 ft = 4.5 kips. Note that this value includes load factors as well as a resistance factor of 0.9.

Table 8.11. Maximum Torsion Load (k-ft).

Beam	HL93-mod		HS25	
	Exterior	Interior	Exterior	Interior
AASHTO Type I	43.0	12.6	48.6	15.0
AASHTO Type II	63.3	20.3	74.0	25.4
AASHTO Type III	93.6	32.9	121	47.3
AASHTO Type IV	131	49.5	181	78.3
Box 60x48	175	65.8	232	94.3
Box 54x48	153	55.7	197	76.3
Box 42x36	98.2	33.3	113	39.9
Box 39x36	87.3	28.6	104	35.5
BT72-61	172	95.4	280	166
BT66-61	151	81.5	223	128
BT60-61	131	69.4	184	102
BT54-61	114	58.9	151	80.8
BT48-61	98.7	49.6	124	64.5
BT42-61	84.6	41.3	104	52.2
BT36-61	70.6	33.4	84.3	41.0
BT72-49	195	93.7	322	174
BT66-49	170	78.7	256	131
BT60-49	148	65.9	208	101
BT54-49	129	55.3	173	79.0
BT48-49	113	46.6	142	61.7
BT42-49	96.8	38.3	117	48.4
BT36-49	81.2	30.7	96.6	37.9
MI-1800	177	89.7	297	168

Table 8.12. Maximum Torsion Load, Alternative Girder Spacing (k-ft).

Beam	HL93-mod		HS25	
	Exterior	Interior	Exterior	Interior
	6' Girder Spacing			
AASHTO Type III	78.3	27.4	103	40.3
Box 60x48	144	54.4	197	80.6
Box 39x36	72.2	23.5	86.3	29.5
BT72-49	161	79.1	284	156
BT36-49	64.2	25.0	77.6	31.5
MI-1800	75.8	146	262	151
	12' Girder Spacing			
AASHTO Type III	127	42.4	156	57.1
Box 60x48	240	85.8	312	119
Box 39x36	120	38.1	139	45.8
BT72-49	261	119	399	204
BT36-49	114	40.9	133	49.1
MI-1800	234	112	356	191

CHAPTER 9: CONCLUSIONS AND RECOMMENDATIONS

9.1 Introduction

In this chapter, a few general conclusions are made, as well as suggestions for the use of IDs for in-service live load distribution as well as girder rollover and lateral torsional buckling during construction. The recommendations herein are based on the loads and modeling assumptions used during this study. Although some guidelines are available, a standard for the evaluation of beam instability during construction does not exist, and other reasonable approaches are possible. The analysis approaches used have shown that, in some cases, no lateral bracing is required. For additional conservatism and to guard against other unknown load scenarios, more stringent bracing rules might be considered, such as requiring some form of bracing in all cases, for example. Note that stability recommendations for construction refer to requirements for "lateral support". This refers to any kind of lateral bracing in temporary or permanent form (such as an ID), that satisfies the strength requirements given in Chapter 8 for such bracing.

9.2 IDs for In-Service Live Load Distribution

As the AASHTO LRFD live load distribution factor expressions were developed from FEA models without IDs, it is implicitly assumed by the Specifications that bridges will have no IDs when live load effects are calculated. As such, when using these expressions, the use of IDs increases conservatism on the structure, where the degree of conservatism desired, if any, is subjective.

It was found that IDs have a generally increasing effect on live load distribution as the ratio of girder flexural stiffness to transverse deck flexural stiffness increases, as well as ID stiffness increases. Thus, bridges with stiff, widely spaced girders using concrete diaphragms generally benefit most from IDs for live load distribution.

In Chapter 6, it was found that when using 1 ID at midspan, the average increase in interior girder DF across the cases considered is the same for each type of beam (bulb tee, AASHTO, box); approximately 3% considering all cases. That is, the average DFr, the ratio of DF without IDs to that with IDs, is approximately 1.03. No significant changes were found for the cases of skew, curvature, or continuity. The largest DFr values occurred for cases where the beams were reasonably sized but more stiff than needed for the span length.

For bulb tees and box beams, the maximum DFr for any case was 1.09 and 1.05, respectively. For AASHTO beams, using steel diaphragms as specified in the MDOT Bridge Design Guide and considering 2 lanes loaded, which is assumed to be the governing live load effect for design, the maximum DFr was 1.06.

Thus, although special cases (for example, overly-stiff beams with wider girder spacing paired with concrete diaphragms) can result in significantly greater changes in DF when IDs are used, the use of IDs for typical cases does not have a large impact on DF. It should be further noted that the DF values found from the FEA models without IDs were generally significantly lower than AASHTO LRFD DF values, and in no case was it found that interior DFs (without IDs) exceeded the AASHTO specified values (though for a few special cases of curved and skewed structures the 1-lane loaded case exceeded AASHTO DF values for exterior girders). It was also found that for

girders with wide top flanges such as bulb tees and box beams, including the thickness of the flange in the AASHTO LRFD DF expressions for deck thickness reduces conservatism and increases accuracy.

From the live load distribution results, the following suggestions are provided:

- To limit change in DF to within approximately 5% for typical cases, IDs are not needed for box and AASHTO beams, but 1 ID at midspan is needed for bulb tees for all spans.

- To limit the change in DF to within approximately 9% for typical cases, IDs are not needed for any beam type.

9.3 Lateral Support to Prevent Rollover During Construction

It was found that the most critical design parameter that affects rollover resistance is the lateral rotational stiffness of the bearing pad, which is greatly dependent on the bearing width. Beam length is also a factor, but not as significant as the bearing pad when reasonable beam lengths are considered. To minimize rollover potential, bearings should be designed as wide (as close as feasible to the lower flange width) and thin as possible to maximize lateral rotational stiffness, and beams with wide bottom flanges (such as bulb tees or box beams) used if feasible to allow wide bearings. Unlike the case of live load distribution, existing criteria exist to evaluate stability, where the beam either requires lateral support to prevent rollover or it does not. Although AASHTO does not provide design criteria for rollover, PCI suggests factors of safety for several rollover criteria, including prevention of cracking, the beam beginning to lift from the bearing, and actual rollover (PCI CB-2-16-E, 2016). Note that lateral support, or bracing, for rollover need not represent an ID nor necessarily remain permanently. Rather, the bracing must remain until the beam is permanently stabilized, such as by the curing of the end walls or the deck. For bulb tees, different results were obtained whether girder tipping, cracking, and liftoff (kern evaluation) criteria were considered. Because the kern criterion was found to be less reliable and typically more often violated than the tipping and cracking failure modes, including this evaluation is usually more conservative. Moreover, as noted in Chapter 7, the tipping criterion is more conservative for beams with smaller width bearings, and several beam cases were potentially affected and prematurely flagged for failure (when sized to HL93-mod: BT72-61; BT72-49; and MI-1800). Finally, when girders were evaluated for rollover under full construction loads, the 75 PSF edge live load was applied across the entire span length in one evaluation and only across the central 20 ft of span for an alternative less conservative case.

As such, two sets of recommendations are given; a minimal set and a conservative set, where the conservative set includes the potentially overly-conservative underestimations of rollover capacity as well as the kern limit evaluation, and applying the edge live load along the entire span when full construction loads are evaluated, while the minimal set does not. Based on the rollover evaluation results, the following recommendations can be made:

Nomenclature and Assumptions: b_{bf} = girder bottom flange width; b_w = bearing pad width. For rollover, "lateral support" refers to temporary or permanent lateral bracing applied at any point(s) along the beam length that meets the resistance requirements specified in Chapter 8. It is further assumed that the bearing pad height does not significantly exceed that required.

9.3.1 When Subjected to Seating Loads (girder self-weight and fascia jacks)

9.3.1.1 Exterior Girders

- All AASHTO beams require lateral support upon seating.

- No box beams require lateral support.

- For bulb tees, not considering the kern limit nor the overly-conservative FS_{tip} results:

    o When sized to HL93-mod criteria, no lateral support is required.
    o When sized to HS25 criteria, no lateral support is required when using bearings with $b_w \geq b_{ff} - 6$".
    o When sized to HS25 criteria and using bearings that satisfy $24" \leq b_w \leq b_{ff} - 6$", BT60 and larger sections require lateral support; for $b_w < 24$", all sections require lateral support.

- For bulb tees, considering the kern limit and unadjusted FS_{tip} results (more conservative):

    o When sized to HL93-mod and using bearings with $b_w \geq b_{ff} - 6$", no lateral support is required, except for a BT72 section.
    o When sized to HL93-mod and using bearings that satisfy $24" \leq b_w \leq b_{ff} - 6$", all BTs except the BT36 require lateral support.
    o When sized to HS25 and using bearings with $b_w \geq b_{ff} - 6$", no lateral support is required except for BT60 and larger.
    o When sized to HS25 with $b_w < b_{ff} - 6$", lateral support is required.

- For the MI-1800 girder:

    o Not considering the kern limit nor the overly-conservative FS_{tip} results, no lateral support is required.
    o Considering the kern limit and unadjusted FS_{tip} results (more conservative), lateral support is required.

9.3.1.2 Interior Girders

- For all beam types, not considering the kern limit:

    o When sized to HL93-mod or HS25 criteria, no lateral support is required when using bearings with $b_w \geq b_{ff} - 6$".

- For all beam types, considering the kern limit (more conservative):

    o Exterior vs interior loading has no significant effect on the kern limit. Thus, follow the (kern limit) recommendations specified for exterior girders.

9.3.2 When Subjected to Full Construction Loads (from girder seating to deck finishing)

9.3.2.1 Exterior Girders

- All AASHTO beams require some form of lateral support.

- For box beams:

  o Applying the edge live load only on the central 20' of span length, and when sized to HL93-mod, with an overhang no greater than 2.5' (from center of girder), and placed on bearings with $b_w \geq b_{ff} - 3$", the 48" wide sections do not require lateral support, while the 36" sections require lateral support.

  o Applying the edge live load along the entire span length (more conservative), all box beams require lateral support.

- For bulb tees:

  o Applying the edge live load only on the central 20' of span length, not considering the kern limit, and when sized to HL93-mod with an overhang no greater than 2.5' (from center of girder), and placed on bearings with $b_w \geq b_{ff} - 3$", no bulb tee beam requires lateral support.

  o Applying the edge live load along the entire span length and considering the kern limit (more conservative), all bulb tee beams require lateral support.

- The MI-1800 girder requires lateral support.

9.3.2.2 Interior Girders

- For all beam types except AASHTO beams, not considering the kern limit:

  o When sized to HL93-mod criteria, no lateral support is required when using bearings with $b_w \geq b_{ff} - 6$".

  o When sized to HS25 criteria, no lateral support is required when using bearings with $b_w \geq b_{ff} - 6$", except the MI-1800 girder.

- For AASHTO beams, not considering the kern limit, lateral support is required.

- For AASHTO beams, bulb tees, and the MI-1800 girder, considering the kern limit, lateral support is required.

- For box beams, considering the kern limit, no lateral support is required when using bearings with $b_w \geq b_{ff} - 3$",

9.4 Lateral Bracing to Prevent Lateral Torsional Buckling During Construction

Although the last edition of the AASHTO Standard Specifications (2002) specified ID requirements as a function of bridge length, no such relationship was found with regard to LTB (nor rollover) stability in this study. Rather, the governing factor is beam length relative to beam section rigidity, where beams conservatively sized for their span, as expected, have less potential for instability. For a PC girder carrying an uncured deck, based on the conservative material model used, many of the girders investigated at HS25 length did not have the compressive flexural capacity needed to carry the construction loads imposed, and some of the girders lacked this capacity even when evaluated with a less conservative, traditional model such as the Whitney stress block approach. Given these results, it may be worthwhile to investigate design requirements for construction in a future study. Recommendations to prevent LTB are as follows:

Nomenclature: For LTB, "lateral support" refers to temporary or permanent lateral bracing applied at the locations specified that meets the resistance requirements specified in Chapter 8.

9.4.1 When lateral supports are placed at both beam ends

9.4.1.1 Exterior Girders

- AASHTO beams require lateral support at midspan.

- Box beams do not require additional lateral support.

- For bulb tees:

    o When sized for HL93-mod, only the BT60 with 49" flange requires lateral support at midspan.
    o When sized for HS25, the BT60 and BT48 require lateral support at midspan.

- The MI-1800 could not be evaluated for stability unless designed for flexure under construction loads. If done so, it did not require additional lateral support. Thus;

    o It is reasonable to assume that the MI-1800 does not require additional lateral support if sized to HL93-mod.
    o It is conservative to assume that the MI-1800 requires lateral support at midspan.

9.4.1.2 Interior Girders

- No sections require lateral support at midspan.

9.4.2 When lateral support is placed at midspan only, without lateral support of beam ends

9.4.2.1 Exterior Girders

- All sections that could be evaluated for stability under construction loads did not require lateral support at the beam ends, with the following exceptions: BT66-61, BT60-61, and BT54-49; and sections BT36-61 and BT54-61 when sized to HS25 length. Thus:

  - Bulb tees require lateral support at beam ends for sections BT54 and larger at HL93-mod length, and all sections require lateral support at beam ends for HS25 length.

  - Box beams do not require lateral support at beam ends.

  - It is reasonable to assume that AASHTO beams and the MI-1800 girder do not require lateral support at beam ends.

  - It is conservative to assume that AASHTO beams and the MI-1800 girder require lateral support at beam ends.

9.4.2.2 Interior Girders

- No sections require lateral support at the beam ends.

9.5 Summary of Combined Recommendations

The suggestions above are combined into two sets of recommendations: a minimal set and a more conservative set. The minimal set considers the need for IDs in-service for when their presence on typical cases causes changes in DF greater than 9%; and lateral support to prevent rollover while eliminating the kern check, the potentially overly-conservative tipping results, and loading the central 20 ft beam length with the edge live load rather than the entire span length. The conservative set considers the need for IDs in-service for when their presence on typical cases causes changes in DF greater than 5%; and lateral support to prevent rollover while including the kern check, the unadjusted overly-conservative tipping results, and loading the entire length of the beam span with the edge live load. As noted earlier, "lateral support" refers to either permanent or temporary bracing, that could take on any form that meets the torsional resistance requirements given in Chapter 8, and that is needed during construction only. In nearly all cases this is the only requirement. "ID" refers to a permanent interior diaphragm for in-service use, and assumes that the ID design represents that currently specified by MDOT for the beam types and section sizes considered. The latter requirement only appears within the Conservative Recommendations for interior girders.

9.5.1 Minimal Recommendations

Nomenclature and Assumptions: b_{bf} = girder bottom flange width; b_w = bearing pad width. "Lateral support" refers to temporary or permanent lateral bracing that meets the resistance requirements specified in Chapter 8. It is further assumed that bearing height does not significantly exceed that required.

- All intentionally curved girders require lateral support at beam ends and at midspan.
- No girder can be left laterally unsupported on an inactive construction site prior to deck cure. The following recommendations apply to active construction sites prior to deck curing:

9.5.1.1 Exterior Girders

- All AASHTO beams require lateral support at the beam ends or near midspan during construction.

- 36" wide box beams require lateral support at the beam ends or near midspan during construction.

- 48" wide box beams that do not exceed HL93-mod length criteria, with an overhang no greater than 2.5' (from center of girder), and placed on bearings with $b_w \geq b_{ff} - 3$", do not require lateral support. 48" box beams that do not meet all of these criteria require lateral support at the beam ends or near midspan during construction.

- Bulb tees that do not exceed HL93-mod length criteria with an overhang no greater than 2.5' (from center of girder), and placed on bearings with $b_w \geq b_{ff} - 3$", do not require lateral support. Sections that do not meet all of these criteria require support as follows:

  o When sections do not exceed HL93-mod length criteria, BT54 and larger sections require lateral support at beam ends, and sections BT60 are larger with 49" flanges require lateral support at beam ends and near midspan. Otherwise, lateral support can be provided at either the beam ends or near midspan.

  o For sections that do not exceed HS25 length criteria, lateral support at beam ends is required, and BT48 and larger sections require additional lateral support at midspan.

- The MI-1800 girder requires lateral support at the beam ends or near midspan during construction.

9.5.1.2 Interior Girders

- AASHTO girders require lateral support at beam ends or near midspan.

- Box beams and bulb tees that do not exceed HS25 length criteria require no lateral support if placed on bearings with $b_w \geq b_{ff} - 6$". Otherwise, lateral support must be provided at beam ends or near midspan.

- The MI-1800 girder does not require lateral support if it does not exceed HL93-mod length criteria and if seated on bearings with $b_w \geq b_{ff} - 6$". Otherwise, lateral support must be provided at beam ends or near midspan.

9.5.2 Conservative Recommendations

Nomenclature: b_{bf} = girder bottom flange width; b_w = bearing width. "Lateral support" refers to temporary or permanent lateral bracing that meets the resistance requirements specified in Chapter 8.

- All intentionally curved girders require lateral support at beam ends and midspan.

- No girder can be left laterally unsupported on an inactive construction site prior to deck cure. The following recommendations apply to active construction sites prior to deck curing, where "ID" refers to a permanent addition to the structure:

9.5.2.1 Exterior Girders

- AASHTO beams and the MI-1800 girder require lateral support at the beam ends and near midspan.
- Box beams require lateral support either at the beam ends or near midspan.
- Bulb tees that do not exceed HL93-mod criteria require lateral support at beam ends or near midspan, while bulb tees BT60 and larger require additional lateral support near midspan.
- Bulb tees that do not exceed HS25 criteria require lateral support at beam ends or near midspan, while bulb tees BT48 and larger require additional lateral support near midspan.

9.5.2.2 Interior Girders

- All girder types except for box beams require lateral support at beam ends or near midspan.
- Bulb tees additionally require one ID at midspan (for live load distribution).
- For box beams seated on bearings with $b_w \geq b_{ff} - 3$", no lateral support is required. Otherwise, lateral support must be provided at beam ends or near midspan.

9.6 Recommendations for Further Research

As a result of this study, several additional research needs have been identified as:

1. Consideration of the development of a closed-form expression to modify AASHTO DF values to account for the presence of IDs. This would allow a more realistic assessment, perhaps most useful for load rating, of girder load effect.

2. Further development of the analytical rollover model, to more specifically define tipping point location as a function of bearing characteristics and other factors. The model presented is applicable to a reasonable but relatively narrow range of design parameters that were used in this study. A more universal expression that can account for variations in these parameters would be useful to more accurately estimate the tipping factor of safety for individual cases.

3. Development of MDOT construction load design provisions. As discussed in Chapter 8, in their non-composite state, some beams did not have the compressive flexural capacity to carry the construction loads imposed. The provisions used for rollover and LTB acceptability (PCI CB-02-16-E and the AASHTO *Guide Design Specifications for Bridge Temporary Works*) were not developed from a reliability-based assessment of safety and thus the appropriateness of the loads, load factors, and factors of safety within these guidelines is uncertain. Moreover, the beam flexural failures raise concerns about the current practice of neglecting design for construction loads. Therefore, it is recommended that construction design provisions specifically for MDOT needs are developed.

REFERENCES

AASHTO *Guide Design Specifications for Bridge Temporary Works*, 2nd ed., Washington, D.C., 2017.

AASHTO *Guide Specifications for Wind Loads on Bridges During Construction*, 1st ed., Washington, D.C., 2017.

AASHTO *LRFD Bridge Design Specifications*, 8th ed., Washington, D.C., 2020.

AASHTO *Standard Specifications for Highway Bridges*, 17th ed., Washington, D.C., 2002.

Abdel-samad, S., Wright, R., and Robinson, A. "Analysis Of Box Girders With Diaphragms." ASCE Journal of the Structural Division, 1968.

Abendroth, R., Fanous, F., and Andrawes, B. *Steel Diaphragms in Prestressed Concrete Girder Bridges*. Report No. TR-424, Iowa Department of Transportation, 2004.

Abendroth, R., Klaiber, F, and Shafer, M. *Lateral load resistance of diaphragms in prestressed concrete girder bridges*. Iowa DOT Project HR-319, 1991.

Abendroth, R., Klaiber, F., and Shafer, M. "Diaphragm Effectiveness In Prestressed-Concrete Girder Bridges." ASCE Journal of Structural Engineering, Vol. 121, No. 9, 1995.

Alfarah, B., Lopez-Almansa, F., and Oller, S. "New Methodology for Calculating Damage Variables Evolution in Plastic Damage Model for RC Structures." Engineering Structures, No. 132, 2017.

Ashebo, D., Chan, T., and Yu, L. "Evaluation of Dynamic Loads on a Skew Box Girder Continuous Bridge Part I: Field Test and Modal Analysis." Engineering Structures, Vol. 29, No. 6, 2007.

Beal, David B. "Load Capacity of Concrete Bridge Decks." ASCE Journal of Structural Engineering, Vol 108, No. ST4, 1982.

Cai, C. and Avent, R. *Assessing the Needs for Intermediate Diaphragms in Prestressed Concrete Bridges*. LADOT Report No. FHWA/LA.06/420, 2008.

Cai, C., Shahawy, M., and Peterman, R. "Effect of diaphragms on load distribution in prestressed concrete bridges." Transportation Research Record, 1814. Transportation Research Board, Washington, D.C., pp. 47–54, 2002.

Cai, C., Araujo, M., Chandolu, A., Avent, R., and Alaywan, W. "Diaphragm Effects of Prestressed Concrete Girder Bridges: Review and Discussion." ASCE Practice Periodical on Structural Design and Construction, Vol. 12 No. 3, 2007.

Cai, C., Chandolu, A, and Araujo, M. "Quantification of intermediate diaphragm effects on load distributions of prestressed concrete girder bridges." PCI Journal, Vol. 54, No. 2, 2009.

Campbell-Allen, D., and Wedgwood, R. "Need For Diaphragms In Concrete Box Girders." ASCE Journal of the Structural Division, 1971.

Cojoaru, R. and Moen, C. VT Lifting Stability Analysis, https://vtechworks. lib.vt.edu/handle/ 10919/23723, 2013.

Dilger, W., and Ghoneim, G., "Diaphragms In Skew Box Girder Bridges." Canadian Journal of Civil Engineering, National Research Council of Canada, Vol. 15, No. 5, 1988.

Dupaquier, S., Marshall, J., and Stallings, J. "Intermediate Diaphragm and Temporary Bracing Practice for Precast Concrete Girder Bridges." ASCE Practice Periodical on Structural Design and Construction. Vol. 21, No. 2, 2016.

Eamon, C., Darwish, I., and Alsendi, A. "Development of Secondary Route Bridge Design Plan Guides." MDOT Research Report SPR-1669, 2018.

Eamon, C., Kamjoo, V., and Shinki, K. "Design Live Load Factor Calibration for Michigan Highway Bridges." ASCE Journal of Bridge Engineering, Vol. 21, No. 6, 2016.

Eamon, C., and Nowak, A.S., "Effect of Edge-Stiffening and Diaphragms on the Reliability of Bridge Girders," ASCE Journal of Bridge Engineering, Vol. 10, No. 2, 2005.

Eamon, C., and Nowak, A.S., "Effect of Secondary Elements on Bridge Structural System Reliability Considering Moment Capacity," Structural Safety, Vol. 26, No. 1, 2004.

Eamon, C., and Nowak, A.S., "Effects of Edge-Stiffening Elements and Diaphragms on Bridge Resistance and Load Distribution," ASCE Journal of Bridge Engineering, Vol. 7, No. 5, 2002.

Eamon, C., Parra-Montesinos, G;, and Chehab, A. "Evaluation of Prestressed Concrete Beams in Shear." MDOT Research Report RC-1615, 2014.

Eamon, C., Chehab, A., and Parra-Montesinos, G. "Field Tests of Two Prestressed Concrete Girder Bridges for Live Load Distribution and Moment Continuity." ASCE Journal of Bridge Engineering, Vol. 21, No. 5, 2016.

El-Mezaini, N., Citipitioglu, E., "Finite Element Analysis of Prestresses and Reinforced Concrete Structures." ASCE Journal of Structural Engineering, Vol. 117, No. 10, 1991.

Egilmez, O., Helwig, T., and Herman, R. "Buckling Behavior of Steel Bridge I-girders Braced by Permanent Metal Deck Forms." ASCE Journal of Bridge Engineering, Vol. 17, No. 4, 2012.

Fang, I.K., et al. "Behavior of Isotropic RC Bridge Decks on Steel Girders" ASCE Journal of Structural Engineering, Vol. 116, No. 3, 1990.

Gamco. *Bridge Deck Forming Manual.* Cincinnati, OH., n.d; accessed 2020.

Garcia, T.M. "IDs for Precast Prestressed Concrete Bridges." Proceedings, Western Bridge Engineer's Seminar, Seattle, WA, 1999.

Garlich, M. et al. *Engineering for Structural Stability in Bridge Construction.* Report No. NHI-15-044. US Dept. of Transportation, FHWA, 2015.

Ghosn, M., Yang, J., Beal, D., and Sivakumar, B. NCHRP Report 776. B*ridge System Safety and Redundancy.* National Academies of Sciences, Engineering, and Medicine, Washington, D.C., 2014.

Green, T., Yazdani, N., and Spainhour, L. "Contribution Of Intermediate Diaphragms In Enhancing Precast Bridge Girder Performance." ASCE Journal of Performance of Constructed Facilities, Vol. 18, No. 3, 2004.

Green, T., Yazdani, N., Cai, C.S., and Spainhour, L. "Intermediate Diaphragms and Temperature Effects on Concrete Bridge Performance." Transportation Research Record, Vol. 1814, No. 1, 2002.

Griffin, J., Harik, I., and Allen, D. *Experimental Analysis and Analytical Modeling of Bridges with and without Diaphragms.* Kentucky Transportation Center, Report KTC-98-12, 1998.

Gull, J. and Azizinamini, A. *Steel Plate Girder Diaphragm and Cross Bracing Loads.* Florida Department of Transportation, 2014.

Helwig, T., and Yura, J. "Shear Diaphragm Bracing of Beams. II: Design Requirements." ASCE Journal of Structural Engineering, Vol 134, No. 3, 2008.

Helwig, T., and Yura, J. "Shear Diaphragm Bracing of Beams. I: Stiffness and Strength Behavior." ASCE Journal of Structural Engineering, Vol 134, No. 3, 2008.

Hurff, J. "Stability of Precast Prestressed Concrete Bridge Girders Considering Imperfections and Thermal Effects." Ph.D. Dissertation, School of Civil and Environmental Engineering, Georgia Institute of Technology, 2010.

Hurff, J. and Kahn, L. "Lateral-torsional Buckling of Structural Concrete Beams: Experimental and Analytical Study." ASCE Journal of Structural Engineering, Vol. 138, No. 9, 2012.

Hurff, J. and Kahn, L. "Rollover Stability of Precast, Prestressed Concrete Bridge Girders with Flexible Bearings." PCI Journal, Fall 2012.

Ibrahim, A., and Salim, H., "*Finite- Element Analysis of Reinforced-Concrete Box Girder Bridges under Close-In Detonations*." American Society of Civil Engineers, CF1943-5509.0000360.

Kalkan, I. "Lateral Torsional Buckling of Rectangular Reinforced Concrete Beams," Ph.D. Dissertation, School of Civil and Environmental Engineering, Georgia Institute of Technology, 2009.

König, G. and Pauli, W. "Ergebnisse von Kippversuchen an Schlanken Fertigteilträgern aus Stahlbeton und Spannbeton", *Beton- und Stahlbetonbau*, Vol. 85, No. 10, 1990.

Krahl, P., Carrazedo, R., and El Debs, M. "Rollover Stability of Precast Concrete Beams Supported by Elastomeric Bearing Pads." Ibracon Structures and Materials Journal, Vol. 10, No. 6, 2017.

Krahl, P., Oliveria, M., Siqueira, G., and Vidigal de Lima, M. "Analytical Nonlinear Rollover Behavior of Cambered Precase Concrete Beams on Flexible Supports." ASCE Journal of Structural Engineering, Vol. 146, No. 2, 2020.

Li, L. and Ma, Z. "Effect of Intermediate Diaphragms on Decked Bulb-Tee Bridge System for Accelerated Construction." Journal of Bridge Engineering, Vol. 15, No. 6, 2010.

Lin, C. and VanHorn, D. *The Effect Of Midspan Diaphragms On Load Distribution In A Prestressed Concrete Box-Beam Bridge, Philadelphia Bridge*. Lehigh University; Pennsylvania Department of Highways; Bureau of Public Roads /US, 1968.

Massey, C. and Walter, K. "The Lateral Stability of a Reinforced Concrete Beam Supporting a Concentrated Load", Building Science, Vol. 3, No. 1, 1969.

Mast, R. "Lateral stability of long prestressed concrete beams," PCI Journal, February, 1989.

Mast, R. "Lateral Stability of Long Prestressed Concrete Beams, Part 2," PCI Journal, Vol. 38, No. 1, Jan-Feb, 1993.

Memberg, M. A., Yura, J.A., Williamson, E. B. and Frank, K.H., "*A Design Procedure for Intermediate External Diaphragms on Curved Steel Trapezoidal Box Girder Bridges*." Report FHWA/TW-03/1898-1, 2002.

MDOT Bridge Design Guides. Michigan Department of Transportation, n.d., accessed 2020.

MDOT Bridge Design Manual. Department of Transportation, n.d., accessed 2020.

Miller, R., Castrodale, R., Mirmiran, A., and Hastak, M. NCHRP Report 519. *Connection of Simple-Span Precast Concrete Girders for Continuity.* National Academies of Sciences, Engineering, and Medicine, Washington, D.C., 2004.

Mohseni, Iman, et al. "Effect of Intermediate Diaphragm on Lateral Load Distribution Factor of Multicell Box-Girder Bridges." KSCE Journal of Civil Engineering 18.7, 2014.

Murray, C.D., Diaz Arancibia, M., Okumus, P., Floyd, R.W., "Destructive Testing and Computer Modeling of a Scale Prestressed Concrete I-girder Bridge." Engineering Structures Vol. 183, No. 15, 2019.

Newmark, M., Siess, C., and Renman, R. "Studies of Slab and Beam Highway Bridges Part I: Tests of Simple-Span Right I-Beam Bridges." University of Illinois Bulletin, Vol. 43, No. 42 (Engineering Experiment Station Bulletin Series No. 363), 1946.

Nguyen, Q. and Livaoglu, R. "The Effect of the Ratio of Λ-Shaped Shear Connectors on the Flexural Behavior of a Reinforced Concrete Frame." Advances in Structural Engineering, Vol. 23, No. 12, 2020.

Nowak, A.S., and Eamon, C. "Reliability Analysis of Plank Decks", ASCE Journal of Bridge Engineering, Vol 13, No. 5, 2008.

Nutt, Redfield and Valentine. NCHRP Report 620. *Development of Design Specifications and Commentary for Horizontally Curved Concrete Box-Girder Bridges*. Transportation Research Board, Washington, D.C., 2008.

Oesterle, R. NCHRP Report 322. *Design of Simple-Span Precast Prestressed Bridge Girders Made Continuous*. Transportation Research Board, Washington, D.C., 1988.

Oesterle, R., Sheehan, M., Lotfi, H., Corley, W., and Roller, J. *Investigation of Red Mountain Freeway Bridge Girder Collapse.* Final report, Arizona Department of Transportation, CTL Group, Skokie, IL, 2007.

Okeil, A., Cai, C, Chebole, V., and Hossain, T. *Evaluation of Continuity Detail for Precast Prestressed Girders.* Report FHWA/LA.11/477. Louisiana Department of Transportation, 2011.

Plaut, R., and Moen, C. "Stability of Unbraced Concrete Beams on Bearing Pads Including Wind Loading." Engineering Structures, No. 69, 2014.

Precast/Prestressed Concrete Institute. MNL-116-99. *Manual for Quality Control for Plants and Production of Structural Precast Concrete Products*. PCI, 1999.

Precast/Prestressed Concrete Institute. CB-02-16-E. *Recommended Practice for Lateral Stability of Precast, Prestressed Concrete Bridge Girders*. PCI, 2016.

Precast/Prestressed Concrete Institute. MNL-135-00. *Tolerance Manual for Precast and Prestressed Concrete Construction.* PCI, 2000.

Revathi, P. and Menon, D. "Estimation of Critical Buckling Moments in Slender Reinforced Concrete Beams", ACI Structural Journal, Vol. 103, No. 2, 2006.

Roddis, W., Kulseth, P., and Liu, Z. *Torsional Analysis for Exterior Girders Version 2.0.* KDOT Report KTRAN: KU-00-3, 2002.

Roddis, W., Winters, E., and Soudeh, B. *Cross-Frame Diaphragm Bracing of Steel Bridge Girders.* KDOT Report K-TRAN: KU-01-2, 2008.

Roeder, C., Stanton, J., and Taylor, A. NCHRP Report 298. *Performance of Elastomeric Bearings.* Transportation Research Board, Washington, D.C., 1987.

Reichenbach et al. NCHRP Report 962. *Proposed Modification to AASHTO Cross-Frame Analysis and Design.* Transportation Research Board, Washington, D.C., 2021.

Saber, A, Toups, J, Guice, L., and Tayebi, A. *Continuity Diaphragm for Skewed Continuous Span Precast Prestressed Concrete Girder Bridges.* Report FHWA/LA04/383. Louisiana Transportation Research Center, 2004.

Saber, A. *Field Verification for the Effectiveness of Continuity Diaphragms for Skewed Continuous P/C P/S Concrete Girder Bridges.* Report FHWA/LA.09/440. Louisiana Department of Transportation, 2009.

Sakai, F., and Okumura, T. *Influence Of Diaphragms On Behaviour Of Box Girders With Deformable Cross Section.* International Association of Bridge & Structural Engineers, Switzerland, 1972.

Sant, J., and Bletzacker R. "Experimental Study of Lateral Stability of Reinforced Concrete Beams," ACI Journal, Proceedings V. 58, No. 12, 1961.

Siev, A. "The Lateral Buckling of Slender Reinforced Concrete Beams", Magazine of Concrete Research, Vol. 12, No. 36, 1960.

Seniwongse, M. "Concrete Beam and Slab Deck Without Diaphragms. HPC: Build Fast, Build to Last." Concrete Bridge Conference, National Concrete Bridge Council, 2006.

Sithichaikasem, S., and Gramble, W.L., "Effects of Diaphragms in Bridges with Prestressed Concrete I-section Bridges." Illinois Cooperative Highway Research Series #128, University of Illinois at Urbana-Champaign, Urbana, IL, 1972.

Sisodiya, R., Ghali, A., and Cheung, Y. "Diaphragms In Single-And Double-Cell Box Girder Bridges With Varying Angle Of Skew." American Concrete Institute Journal & Proceedings, Vol. 69, No. 7, 1972.

Stanton, J. et al. NCHRP Report 596. *Rotation Limits for Elastomeric Bearings.* Transportation Research Board, Washington, DC, 2008.

Stith, J. et al. *Guidance for Erection and Construction of Curved I-80 Girder Bridges*, TxDOT Report 0-5574-1, Center for Transportation Research, The University of Texas at Austin, 2010.

Sumer, Y., and Aktas, M. "Defining Parameters for Concrete Damage Plasticity Model." Challenge Journal of Structural Mechanics, No. 3, 2015.

Terex. *Bid-Well Wheel Load Calculator* (excel spreadsheet), 2010.

Tomasz, J. and Tomasz, L. "Identification of Parameters of Concrete Damage Plasticity Constitutive Model." Foundations of Civil and Environmental Engineering, No. 6, 2005.

Vu, Q.V., Thai, D. K. and Kim, S.E., "Effect of Intermediate Diaphragms on the load-carrying capacity of steel-concrete composite box girder bridges." Thin-walled Structure 122, 2018.

Wahalathantri, B., Thambiratnam, D., Chan, T., and Fawzia, S. "A Material Model for Flexural Crack Simulation in Reinforced Concrete Elements Using ABAQUS." Proceedings, eddBE2011, Infrastructure, Transportation, and Urban Development, 2011.

Wipf, Terry J., Klaiber, Wayne F., Funke, Robert W., "Longitudinal Glued Laminated Timber Bridge Modeling," ASCE Journal of Structural Engineering, Vol. 116, No. 4, 1990.

WiDOT. *Bridge Manual*. Wisconsin Department of Transportation, 2019.

Wei, X. and Bruneau, M. IDEA 172. *Bidirectional-Ductile End Diaphragms for Seismic Performance and Substructure Protection.* Transportation Research Board, Washington, D.C., 2015.

White et al. NCHRP Report 725. *Guidelines for Analysis Methods and Construction Engineering of Curved and Skewed Steel Girder Bridges.* Transportation Research Board, Washington, DC, 2012.

Yang, M., Qiao, P., McLean, D., and Khaleghi, B. "Effects of Overheight Truck Impacts on Intermediate Diaphragms in Prestressed Concrete Bridge Girders." PCI Journal, Vol. 55, No. 1, 2010.

Zhou, J., Bennett, C., Matamoros, A. Li, J, and Rolfe, S. *Skewed Steel Bridges: Effect of Cross-Frame Layout on Lateral Flange Bending Stresses.* KDOT Report K-TRAN: KU-13-3, 2016.

Zokaie, T., Imbsen, R., and Osterkamp, T. "*Distribution of Wheel Loads on Highway Bridges.*" Transportation Research Record No. 1290, 1991.

Zureick, A-H., Kahn, L., Will, K., Kalkan, I., Hurff, J., and Lee, J.H. *Stability of Precast Prestressed Concrete Bridge Girders Considering Sweep and Thermal Effects.* Final Report, Georgia Department of Transportation Project 05-15, 2009.

APPENDIX A. SUMMARY OF BRIDGE CHARACTERISTICS

Bridge Location	ID	Span (ft)	Girder	Spacing (ft)
I-75 over Goddard Rd	S27-1 & 2 of 82191	2 x 116	42" BT	5.5
I-75 over Otter Creek	B04-1 & 2 of 58151	3 x 80	39" Box	7.5
I-75 under Laplaisance Rd	S10 of 58151	2 x 96	42" BT	8.1
I-94 under Concord Ave	S11 of 82024	117 & 93	48" BT	6.5
I-94 under French Rd	S03 of 82025	2 x 99	42" BT	7.0
M-57 over Shiawassee R	B02 of 73021	1 x 142.5	MI-1800	7.1
M-89 over Kalamazoo R	B01 of 03021	1 x 31	17" Box	8.0
M-311 over Kalamazoo R	B02 of 13016	1 x 150	60" BT	7.5
I-75 over Barnard Drain	B05-1 of 63174	1 x 41	36" Type 2	8.8
I-75 over 14 Mile Rd	S05-1 of 63174	1 x 156	60" BT	6.8
I-75 over Big Beaver	S09-1 of 63174	2 x 107	48" BT	7.8
Wattles Rd over I-75	S10 of 63174	83 & 99.5	42" BT	8.9
I-75 Over Long Lake	S11-1 of 63174	1 x 139	54" BT	8.5
Corporate Dr over I-75	S12 of 63174	66 & 108	42" BT	8.1

APPENDIX B. DOT SURVEY RESULTS

Survey Document

The Michigan Department of Transportation (MDOT) and Wayne State University (WSU) are working on a research project to evaluate the current practice of intermediate diaphragm (ID) use on prestressed concrete (PC) girder bridges with low skew (< 30˚) and low curvature (radius > 800 ft). The goal of the project is to develop guidelines for ID placement on such structures.

To help our team narrow the research focus, we would like to understand the current state of practice for ID use on low skew, low curvature PC bridges. As such, we would appreciate it if you could take a few minutes to answer questions about your State's practice for ID use for PC bridges. We would find it beneficial if you would answer as many of the questions that you can.

Please respond by Friday, January 31, 2020.

Thank you for your participation. If you have any questions please feel free to contact Christopher Eamon (eamon@eng.wayne.edu or (313) 577-3766).

1. Does your State require intermediate diaphragms (IDs) for low skew, low curvature PC bridges?
2. If required, where and under what conditions must they be placed (e.g. based on bridge geometry, beam size, end bearing details, deck overhang, sequence of deck placement, etc.?) If a reference exists that summarizes these requirements, can you please provide a link to, or name of, the reference?
3. If required, what is the purpose(s) of IDs on these structures?
4. If you do not use IDs to mitigate the effects of over-height vehicle impacts, is there another mechanism that you use for this purpose?
5. What type of IDs (cast-in place concrete, steel cross-bracing, or another configuration) are allowed on these structures? Does the allowed type change in different scenarios?
6. In cases when there is an end diaphragm/dependent backwall, do you require the installation of the end diaphragm prior to the placement of the deck?
7. Does the placement of end diaphragms prior to the placement of the deck affect the policy for requiring IDs?
8. Does your State have a clear policy that distinguishes between the responsibilities of the contractor and the engineer of record to provide stability during construction? If so, can you please briefly describe?
9. Has your State recently changed its policy on ID placement for low skew, low curvature PC bridges? If so, why?
10. Has your State recently sponsored any research on this topic? If so, can you please provide a link to, or name of, the reference?

All Survey Responses

Question 1

yes

Yes, current practice is to always require a mid-span ID, even for straight, square bridges.

No, CDOT require the designer to check the stability of the girders during construction at the Strength I limit state, including wind load, to determine if ID's are needed. In older bulb tee/I girder work sheets, CDOT recommended at least one ID in the middle of the span, but this is not the current practice. In general, CDOT require the Contractor to maintain and take responsibility of the structure stability during construction.

Yes

Florida Does not require ID's on straight and skewed Prestressed Concrete Girder (PCG) bridges.

Yes

IDOT requires IDs for all Precast Prestressed I beams, regardless of skew or curvature.

Yes

Yes

We require temporary intermediate diaphragms for our prestressed concrete girder bridges. For such a tight radius KDOT would most likely use a different option for bridge type.

No, unless the bridges are crossing over navigable roadways, railroads, or waterways, or subject to large lateral external forces such as waves or wind.

We occasionally require galvanized intermediate diaphragms

Yes

Yes

No

Yes, NCDOT requires intermediate diaphragms on all PC girder spans > 40 ft. regardless of skew and curvature.

Yes.

- There are no skew or curvature limit thresholds for the use of intermediate diaphragm. However, NYS requires intermediate diaphragms on all PS beams over 65' long.

Yes

Yes.

Yes

Yes.

Question 2.

All precast, prestressed girder bridges are to have a mid-span diaphragm. Infrequently, more than one intermediate diaphragm will be used. The Alaska DOT&PF Bridges and Structures Manual includes some information but use is based primarily on past practice and performance.
http://www.dot.state.ak.us/stwddes/desbridge/bridgemanual.shtml

IDs are always required. IDs are always placed midspan. We require temporary IDs near integral end diaphragms—see response to (6). We also always require end diaphragms (ED), even for non-continuous girders supporting continuous decks (i.e. "link slab" configuration).

See the answer to question 1 above. These requirements are incorporated in CDOT Bridge Design Manual and other publications. These documents are available under the following link: https://www.codot.gov/library/bridge/bridge-manuals

Section 106.9.3 of our Bridge Design Manual (https://deldot.gov/Publications/manuals/bridge_design/pdfs/2019/bridge_design_manual_2019.pdf?cache=1578342486739) states as follows:
Diaphragms for prestressed beams shall be cast-in-place or precast concrete for spread box beam and NEXT beam bridges. Diaphragms for PCEF bulb-tee beams may be either cast-in-place concrete, precast concrete, or steel diaphragms. Steel diaphragms for PCEF bulb-tee bridges are permitted with approval of the Bridge Design Engineer. Concrete end diaphragms shall be provided at all bearing lines. Interior diaphragms shall be provided for all prestressed beam bridges with recommended diaphragm spacing, as shown below:
- 1/4 points of span for 120 feet < span length ≤ 160 feet
- 1/3 points of span for 80 feet < span length ≤ 120 feet
- Mid-point of span for 40 feet < span length ≤ 80 feet
- No diaphragms required for span lengths ≤ 40 feet

NA

Staggered perpendicular to girder for skews greater than 20 degrees.
Number per span dependent on span length

146

See online Bridge Design LRFD Manual Article 5.12.4 – Diaphragms
Not required on Deck Tee Girders with spans less than 120'
Not required between two different stages of construction.

Intermediate diaphragms are required on all Precast Prestressed Concrete I-Beams. For span lengths up to 90 feet, permanent bracing is placed at .33L and .67L. For span lengths greater than 90 feet, bracing is placed at .25L, .5L and .75L. For more details, see link below to IDOT's Bridge Manual. See section 3.4.9, pages 3-213 to 3-216.
http://www.idot.illinois.gov/Assets/uploads/files/Doing-Business/Manuals-Guides-&-Handbooks/Highways/Bridges/Bridge%20Manual%202012.pdf

Intermediate diaphragms are required for prestressed beams as follows:
For I-beams and Bulb-tee beams.
- For a span greater than 80 ft and less than 120 ft, one diaphragm placed at midspan.
- For a span greater than 120 ft, two diaphragms at third points.
For Spread-Box beam superstructure having an inside radius of less than 800 ft, intermediate diaphragms shall be place between individual boxes. The spacing depends upon the radius of the curvature and the proportions of the webs and flanges. They are placed on the radial lines.
Other box-beam superstructure do not require intermediate diaphragms.
Reference:
https://www.in.gov/indot/design_manual/files/Ch406_2013.pdf

Bridge Design Manual 5.4.1.4.2 as quoted below.
https://iowadot.gov/bridge/policy/05-04-00PpcbLRFD.pdf
For A-D standard beams in superstructures above vehicular roadways, cast-in-place intermediate diaphragms are required [OBS SS 1036A]. For superstructures above railways or waterways the designer may select intermediate diaphragms of steel or cast-in-place concrete [OBS SS 1036]. For either choice one diaphragm at midspan is required. Coil ties are required at the locations of concrete diaphragms, and cast bolt holes are required at locations of steel diaphragms. At any location below a longitudinal bridge deck construction joint, a cast-in-place concrete intermediate diaphragm shall be omitted [OBS SS 1036A] and the bolts for a steel intermediate diaphragm shall not be tightened until stage two of the bridge deck has been placed [OBS SS 1036].

For BTB-BTE standard beams, only steel diaphragms are permitted, and the office standard diaphragm configuration varies depending on whether the bridge crosses a roadway or a waterway [OBS SS 1036- BTBR, 1036-BTBW, 1036CR, 1036CW, 1036DR, 1036 DW, 1036-BTER, 1036-BTEW]. For all spans up to and including 120 feet one diaphragm at midspan is required. For BTD and BTE beams with spans greater than 120 feet two diaphragms are required at 20 feet on each side of the center of the beam. For skews of 7.5 degrees or less the diaphragms are to be skewed; for larger skews diaphragms are to be perpendicular to the beams and staggered as shown on the standard sheets.

A-D and BTB-BTE standard beam and diaphragm details can be found at this link:

The use and where placed of temporary intermediate diaphragms is determined by span length. See attached Temporary Diaphragms Details sheet.

Our ID policy is summarized below. The attributes listed in the question were looked at as potential controlling variables in study looking at the effectiveness of IDs, however it was determined they didn't have a tangible effect on the flexural capacity of the girders. (See the study linked in following questions)

This policy can be found in Part II, Volume 1, Chapter 5.13.2 of our Design manual at the following link:
http://wwwsp.dotd.la.gov/Inside_LaDOTD/Divisions/Engineering/Bridge_Design/Pages/BDEM.aspx

Policy for Intermediate Diaphragms
Situations Requirement for Intermediate Diaphragms (ID)

All spans unless otherwise specified as follows: ID is not required.

Case 1: Spans over roadways, railroads, navigational channels, and water body with anticipated marine traffic under normal loading condition except for Cases 2 and 3

(One ID shall be provided at center of span.)

Case 2: Spans on curve (Requirement of ID shall be determined for the design condition. Minimum one ID shall be provided.)

Case 3: Spans subject to wave force, extreme high wind conditions, other anticipated lateral forces, or other unusual loading conditions (Requirement of ID shall be determined for the design condition. Minimum one ID shall be provided)

They are required when it required for stability prior to and during the deck placement and if there are under bridge utilities

For PC beam 35 inches and greater in depth:

Intermediate diaphragms are not required for single spans of 45'-0" or less. Provide one diaphragm per every 45 feet of span length, spaced evenly along the span as stated in Table 5.4.1.1.

Table 5.4.1.1

h (ft)	Intermediate diaphragms
Less than 45'-0"	0
45'-0" to 90'-0"	1 located at midspan
90'-0" to 135'-0"	2 located at the third points
135'-0" to 180'-0"	3 located at the quarter points
Greater than 180'	4 plus an additional diaphragm for each additional 45 ft of span length greater than 180'-0"

- Use for all spans over 50 feet except for NU 35 and NU 43 girders.
- Use straight diaphragm normal to girders for skews thru 20°.
- Use stepped diaphragm for skews over 20°.
- Spans of 90 feet or less require one intermediate diaphragm per span.
- Spans over 90 feet require two intermediate diaphragms per span.
- Spans over 140 feet require three intermediate diaphragms per span.
- Space diaphragms equally as allowed by clearance to harped strands.
- Maximum spacing is 50 feet (from support and between diaphragms).
  Engineering Policy Guide 751.22.3.13 Intermediate Diaphragms

Only on spans of 150' or greater.

Please refer to SMU Design Manual Section 6.3.3.2 for guidance.
https://connect.ncdot.gov/resources/Structures/Pages/Design-Manual.aspx
Excerpt from Section 6.3.3.2:
The number of intermediate diaphragms required per span shall be as follows:
- None for spans less than 40 feet,
- One at mid-span for spans between 40 and 100 feet, inclusive,
- Two at third points for spans over 100 feet.

For skews between 70° and 110°, the diaphragm(s) shall be placed along the skew with bent connector plates. For all other skew angles, detail the diaphragms normal to the girder web and stagger the connector plates. For prestressed concrete girder superstructures with a closure pour, do not detail intermediate diaphragms in the staging bay.

When we used NEBTs an intermediate diaphragm was required halfway along the beam when the beam was longer than 80 feet. When we use voided slabs and box beams an internal intermediate diaphragm is typically located halfway along the beam. We now will use NEXT beams for our low skew and approximately up to 70 feet long bridges and we don't require an intermediate diaphragm for them.

- No intermediate diaphragms are required for spans up to 65'-0" Midspan diaphragms are required for spans greater than 65'-0", and up to 100'-0". Spans greater than 100'-0" require diaphragms at the 1/3 points.

Intermediate diaphragms are required at midspan for spans < 80-ft and at quarter points for spans ≥ 80-ft. Reference: ODOT Standard Bridge Drawing PSID-1-13, sheet 5 of 10.

Details have been standardized for worst-case scenarios

For all bridge spans greater than 40 ft

https://www.scdot.org/business/pdf/structural-design/SCDOT_Bridge_Design_Manual.pdf
https://www.scdot.org/business/pdf/structural-design/bridge-memos/DM201103.pdf

Structures Design and Detailing Manual (SDDM), SD-08 drawing:
General requirement (regardless of geometry, beam size, end bearing details, etc.) –
        Provide intermediate diaphragms at: ½ points for spans less than 80 ft
                                              1/3 points for spans from 80 ft to 120 ft
                                              ¼ points for spans from 120 ft to 160 ft
                                              1/5 points for spans greater than 160 ft

Question 3.

Lateral support to address wind and vehicle collision loads, improved stiffness and load distribution.

Traditional practice at ARDOT has always been to brace girder systems with IDs and EDs. While not explicitly stated, the primary purpose of IDs and EDs is to brace the girder system during the deck pour. EDs also function to maintain the position of the girder ends prior to the deck pour and affixing the girders to the bearings. They are also necessary to help brace the system for the seismic event. Approximately two-thirds of Arkansas would be characterized as either Seismic Zone 2, 3, or 4. Also see response to (6).

To provide stability during construction.

Construction stability and load distribution.

NA

To provide stability during erection/deck placing.
To provide impact resistance resulting from over-height loads

Primary purpose of providing bracing is to ensure beam stability during erection and deck construction.

To Resist Lateral forces and transmit loads to points of supports.
To provide stability for the beams during construction.
See Section 406-11.01 of the reference provided above.

The main purpose is to provide some degree of stability during erection and the deck pour. However, a plan note is added which places the burden for beam stability on the contractor until the deck reaches its full 28day compressive strength (see answer to Question 8). For bridges over roadways, stiffer diaphragms (concrete diaphragms for A-D beams and steel diaphragms with extra strengthening between the bottom exterior flanges and first interior girder flanges for BTB-BTE beams) are used with the idea of mitigating over-height vehicle impacts.

The Iowa DOT is likely to discontinue use of concrete intermediate diaphragms and the extra strengthening for the steel diaphragms. However, we intend to keep using steel diaphragms.

To stabilize the beams during construction of the deck

LADOTD policy only requires IDs for bridges over navigable crossings (including vehicular, rail, and marine) as well as bridges located in areas subject to wave force, high wind conditions, or other conditions that are subject to large lateral loads.

Essentially the purpose is to mitigate the effects of overheight vehicles and marine vessels, as well as large lateral loads.

A study was performed providing results that show IDs minimally affect the live load distribution. Inclusion of IDs increase the live load demand for exterior girders, while decreasing the live load demand for interior girders.

Construction Stability and utilities

The ID are provided to ensure bracing/stability of girders during erection and for stability if a redecking of the bridge occurs in the future. We are not sure whether the presence or absence of these diaphragms is a benefit during an OH impact event.

Stability during construction.

Construction stability

IDs provide PC girder stability during construction and if a girder is impacted the ID should provide some resistance to the impact and distribute load to adjacent girders.

For the NEBT beams, it is for stability. The NEXT beams, which in essence is a double tee, are stable due to their shape.

- Stability during construction and long-term redundancy.
Primary purpose is for bracing of the beams for lateral stability prior to and during deck placement.

The purpose is to resist lateral forces during service life.

Stability during construction.

Primarily for constructability

Question 4

NA

While we see the benefit of IDs for vehicle impacts, it has not been a reason for requiring IDs, as IDs are required for all PC girder systems.   Note that, due to the complexity involved with repairing PC girders, ARDOT requires an extra 1' of vertical clearance when PC girders are used to overpass a roadway.

No.

No.

None.

N/A

NA

Yes, Vertical Clearance deficiency warning sign.

No

KDOT currently does not have any mechanisms for this purpose.

LADOTD policy calls for IDs for spans over roadways for this reason. There is no other standard mechanism the department uses to mitigate over-height vehicle impacts currently.

clearance

NA

No other than good permitting process.

MS raises problem bridges that are regularly struck. MS does not use any other mechanism to mitigate strikes. In our experience, bridges without diaphragms have performed as well if not better than those with diaphragms.

N/A

No but we do specify clearance envelopes underneath the bridge depending what type of road is below and above the bridge (i.e. local road over Interstate)

- No.

No

No. However, where possible and where new PCPS beam are used, we require a minimum vertical clearance of 16'-3", not including 3" in future asphalt overlays.

None

No.

Question 5.

In the past, we used steel cross-frames on a spacing of 25-ft or less but for the last 15 years we have used only cast-in-place diaphragms.

Cast-in-place diaphragms are the default, but a detail is always provided allowing an alternate steel diaphragm. Typically, the Contractor will choose the alternate steel diaphragm.

So far, CDOT specify galvanized steel cross-bracing in the bridge work sheets.

We allow all 3 for bulb-tee girders and CIP & PC diaphragms for spread box beams and NeXT Beam bridges.

NA

CIP concrete diaphragms are required. Steel cross frames are generally not allowed due to fit up issues resulting from camber growth and limited impact resistance. Steel cross frames can be used for temporary additional bracing on deep girders.

For 36" and 42" PPC-I beams, bracing consist of Steel Channels (C12x25). For deeper PPC-I beam shapes, angles are used for bracing (3.5" x 3.5"). See link below to IDOT's Bridge Manual for details of internal diaphragms, section 3.4.9.

Structural Steel diaphragms are required to be specified. If the designer determines to provide concrete diaphragms, Director of Bridges shall be provided with a written justification for the use of concrete diaphragms.

See previous comments.

Temporary intermediate diaphragms are bent plates. No changes to the type of diaphragm for different scenarios.

LADOTD utilizes cast-in-place concrete IDs on concrete I-girder bridges. Steel cross-bracing is very rarely used on concrete girder bridges.

Galvanized cross bracing.

MnDOT used steel cross bracing only.

- C15 x 33.9 channel for smaller beams.
- 5/16" x 44" bent plate for larger beams.
                    Diaphragm Standard Drawings

MS will allow cast in place or steel cross bracing at the contractor's request. Steel cross bracing is required to be removed after construction. On bridges that cross open public roads or pedestrian facilities, MS requires the use of temporary steel diaphragms (designed and stamped by the contractor's engineer) to prevent beam tipping.

Steel diaphragms are used on PC girder structures. ID configuration is based on girder depth. See Standard Drawings PCG10 & PCG11.

We have allowed both cast-in-place concrete and steel bracing for IDs. The type allowed for different scenarios can be either but in the field it is easier to use the steel bracing instead of trying to form a cast-in-place diaphragm.

- Single member steel "W" or "MC" shape. Size of diaphragm member changes based on beam type/height.

ODOT Standard Bridge Drawing PSID-1-13 provides details for cast-in-place concrete and steel x-frame type diaphragms.   Steel x-frame diaphragms are not permitted for beam depths less than 60-in because of geometry. Bolted steel channel type diaphragms do not provide sufficient slip

resistance at the ID spacings referenced in #2 above and are therefore not permitted. Due to the presence of draped strands, additional steel channel ID locations within a span are not practical.

We only use cast-in-place concrete.

Both cast-in place concrete, steel cross-bracing allowed if lowest elevation of span is 20 MSL or above.

If the lowest elevation of the span is below 20 MSL, the intermediate diaphragms must be constructed of cast-in-place concrete.

1. Steel bent plate diaphragm (UDOT SDDM, WS-11) are typically used for reasons of cost, simplicity, and schedule.
2. Cast-in-place concrete diaphragms are allowed.

Question 6.

Yes.

We recently began using fully-integral abutments on PC girder bridges meeting our integral bridge criteria. When integral abutments are used, the integral end diaphragm is poured monolithically with the deck to minimize locked-in stresses. For PC girders, a temporary steel diaphragm is required immediately adjacent to the abutment to brace the girder ends prior to, and during, the pouring of the deck and integral end diaphragm.

No, but CDOT Bridge Design manual alerts the designer to allow the girder to rotate at the ends during the deck pour, and require the contractor to pour the deck within two hours from pouring the diaphragms.

Typically yes.

No end diaphragm is required. Florida uses thickened slab end.

Yes

No

No, it is optional.

End diaphragms are concrete and are poured with the deck. Decks are typically poured from end to end.

Yes, the concrete for the end diaphragm is poured just before paving train operations begin for the deck. This is done in a manner to avoid a cold joint in the diaphragm.

We are not sure exactly what is meant by "end diaphragm/dependent backwall", but LADOTD requires end diaphragms on all bridges regardless of whether an intermediate diaphragm is present. The existence of the end diaphragm has no effect on our intermediate diaphragm policy.

All bracing is install during beam erecting

We allow the casting of the end diaphragm either before or with the deck placement.

End diaphragms are concrete and are cast integral with placement of deck.
Engineering Policy Guide 751.22.3.11 Non-Integral End Bent Diaphragms
Engineering Policy Guide 751.22.3.12 Non-Integral Intermediate Bent Diaphragms

They are not required to be poured prior to the deck and are setup to be poured monolithic with the deck in the plans. However, most contractors do elect to pour them prior to the deck for construction stability.

No, the contractor has the option to either pour the end diaphragm prior to deck placement or to pour the diaphragm monolithically with the deck.

For NEXT beams the deck and the end diaphragm are poured together. It is similar for voided slabs and box beams. NEBT did require the end diaphragm to be in place before the deck was poured.

ODOT will permit the installation of end diaphragms for superstructure skews less than 10 degrees. For larger skew angles, the diaphragms are placed at the end of the deck placement or upon approval of a contractor request to delay the initial set of the diaphragm concrete until the adjacent span is complete.
- No.

Yes.

No

The end walls shall be cast concurrently with the deck slab

No. Deck is placed before CIP end diaphragms to reduce deck cracking.

Question 7.

No

No, IDs are still required midspan.

No.

No.

NA

Most of our bridges have integral abutments that don't require end diaphragms

NA

No.

No

No.

No, LADOTD plans typically provide permissible construction joints between the top of end diaphragm and bottom of deck, however, the presence of the end diaphragms has no bearing on the intermediate diaphragm policy.

MaineDOT places the end diaphragms with the deck to eliminate the construction joint

No

Not applicable.

No

No.

No

-No.

No

No.

No

N/A

Question 8.

See construction specifications at this site:
http://www.dot.state.ak.us/stwddes/dcsspecs/assets/pdf/hwyspecs/sshc2020.pdf

We do not have a clear policy. Our Standard Specifications provide a two-paragraph Subsection 802.22(f)(3) on handling, but we do not mention construction stability. It is generally assumed that the IDs and EDs are sufficient to provide stability of our AASHTO shape PC girders during deck construction.

Yes, this is clearly stated in the first sheet of the plans with the following note: "The Contractor shall be responsible for the stability of the structure during construction".
Also, the following notes are included in CDOT girder worksheets:
"4. The Contractor is responsible for determining necessary bracing requirements and for providing adequate bracing for the specific wind and weather conditions to be encountered for each specific project.

We do not have a policy defining responsibility for determining stability during construction. For structures requiring refined analysis (high skew and/or curvature), the designer is required to check construction stability.

Yes, the contractor is required to brace the beams and to design the bracing members for the for the bracing forces shown in the plans.

We review the Contractor's erection and bracing plan during construction. However, the Contractor is ultimately responsible for the stability.

The EOR is required to show in the plans the number of brace required during construction and the forces the bracing is required to resist.

Responsibility is with the Contractor. See IDOT's Standard Specifications for Road and Bridge Construction, section 105.04, 504.06 (See 1st Link below).
Also Guide Bridge Special Provision (GBSP) 96, see second link below.

Yes,
EOR shall provide construction loading check. If the EOR determines that lateral stability should be provided, a note to the contractor should be placed on plans to provide lateral stability during construction.
https://iowadot.gov/bridge/policy/13-00-00CaddNoteLRFD.pdf

E202: Prestressed concrete beam bridge, temporary bracing

THE CONTRACTOR SHALL BE RESPONSIBLE FOR ENSURING STABILITY OF PRESTRESSED CONCRETE BEAMS DURING ERECTION AND CONSTRUCTION UP THROUGH THE CONCRETE BRIDGE DECK REACHING ITS FULL 28-DAY STRENGTH. THE CONTRACTOR SHALL PROVIDE SUFFICIENT TEMPORARY ANCHOR BRACING AT BEAM ENDS AND TEMPORARY INTERMEDIATE BRACING AS NEEDED TO ENSURE PRESTRESSED BEAM STABILITY. PARTIALLY OR FULLY INSTALLED PERMANENT BRACING AS SHOWN IN THESE DESIGN PLANS SHALL NOT BE ASSUMED SUFFICIENT TO BRACE PRESTRESSED BEAMS DURING ERECTION AND CONSTRUCTION. TEMPORARY BRACING SHALL NOT BE WELDED TO PRESTRESSED BEAM STIRRUPS.
Include this plan note in the General Notes for all new PPCB bridges and projects involving deck replacements.

See attached KDOT's Field Erection specification
Outside of the EOR ensuring that the fabricated girder doesn't exceed stress limits on dunnage in the fabrication yard and stress limits (vertical and lateral) from lifting (both usually 3 feet from girder end), the Contractor is responsible for the stability of the girder from creation to final acceptance of the construction project.
LADOTD policy is stated on our design manual and on our standard PPC girder details included in every PPC girder bridge. It states: "The contractor is responsible for stability of precast prestressed concrete girders during fabrication, storage, transportation, erection, and deck placement." Furthermore, the same note continues with: "Any inherent stability provided by cast-in-place diaphragms shall not be considered by the contractor in designing the required construction bracing. The diaphragms are provided to restrain lateral movement of girders when the bridge is in service and are not intended or allowed for use as construction stability bracing."

The use of diaphragms is determined during design

On bridges without diaphragms the contractor is responsible for stability. On PC beam bridges the contractor must ensure stability of the fascia beam with overhang bracket loads accounting for bidwell/loading during deck placement. Interior beams are assumed stable.

Other than the following note used on the plans for beams that are too shallow to allow for intermediate diaphragms, there is no specific policy concerning stability.

> The contractor shall provide bracing necessary for lateral and torsional stability of the girders during construction of the concrete slab and remove the bracing after the slab has attained 75% design strength. Contractor shall not drill holes in the girders. The cost for furnishing, installing, and removing bracing will be considered completely covered by the contract unit price for Prestressed Concrete NU-Girder.

MS places all of the liability for designing and maintaining stability during construction on the contractor. The contractor is required to provide a stability submittal that is designed and stamped by the contractor's engineer. On hydraulic bridges and bridges not over open public facilities, contractors will weld bars to the shear steel and/or add timber spreaders, etc.

The Contractor is responsible for girder stability during construction. Section 420-3 of the Standard Specifications and Structure Management Unit's Falsework and Formwork Special Provision provide a guide to the contractor for designing and constructing falsework and formwork. The engineer reviews the contractor's falsework and formwork drawing submittals.

Our specifications has a section titled "Contractor's Responsibility for Work" which does not specifically talk about stability but puts the onus on the Contractor to protect the Work against all injury or damage from all causes. The Contractor does submit an erection plan which we receive for documentation.

ODOT requires the erection plan to be sealed by an Ohio licensed engineer, ODOT C&MS 501.05.B. Doing so defines responsibility for erection stability until the framing shown in the Plans is in complete. Once the framing is in place, the responsibility would switch to the Ohio licensed engineer responsible for the design of the framing.

- The NYS Prestressed Concrete Construction Manual, requires PE stamped erection drawings that demonstrate stability of the PS units during erection. A note on the contract plans states that the contractor is responsible for beam stability during all phases of construction.

We do not have a written authorized policy. We generally place a note on the Plans stating that it is the Contractor's responsibility to provide stability during construction. We ask that the Contractor submit erection procedures, including computations, as a shop drawing for review. This item would appear in a list of Shop Drawings (required) either on the Plans, in the Contract documents, or both.

No.

Constructability requirements (UDOT SDDM 12.8) emphasizes and clarifies requirements in AASHTO LRFD Bridge Design Specifications, 2.5.3.

12.8 CONSTRUCTABILITY

Reference: LRFD Article 2.5.3

The EOR is responsible for designing a constructable bridge. Constructability includes consideration of deflection, strength of steel and concrete, and stability during critical stages of construction. The following applies:

- Designs that are self supporting or that use standardized falsework systems are normally preferred to designs requiring unique and complex falsework.
- Ensure that at least one feasible method to construct the bridge exists. Show the assumed construction method (e.g., bracing, sequence) in the plans for unusual or complex bridges. Bracing of deck overhangs that exceed the AASHTO limitations (which can occur when replacing the deck on an existing bridge) are considered unusual or complex for this requirement.
- State the need in the contract documents for strengthening and/or temporary bracing or support during erection if required by the selected construction method.
- Emphasize constraints to the construction method or sequence if required by the design.

Girder plans require Contractor to "Brace girders to prevent tipping and to control lateral bending during shipping. Brace girders laterally to prevent tipping until the diaphragms are installed."

Question 9.

No

No, our policy to require IDs and EDs, regardless of girder configuration, has not changed.

No.

No.

No. The current policy was implemented several years back.

No

No, we have used internal diaphragms since 2012.

No.

See answer to Question 4.

161

No.

LADOTDs most recent change in its ID policy consisted of removing the requirement of IDs for BT-78 and Quad Beam girders as our study (referenced below) showed that IDs have insignificant added value to the flexural capacity of the interior girders of the bridges. Attributes such as skew, girder spacing, span length, and connection detail of diaphragm to girder web were all considered in the study. Additionally, the study concluded that curve radii and cross slope (up to 10%) had the same insignificant value added. It was concluded to be more efficient to add any required additional capacity to the girder design if needed.

NO

No recent changes but our R&D committee is considering a reevaluation of our guidance.

No.

MS discontinued the use of IDs in 2014

No.

No

-No.

No

No.

No

No, however the requirements will be revised soon to the following:
        Provide intermediate diaphragms at: Not required for spans less than 90 ft.
                                            ½ points for spans from 90 ft to 135 ft
                                            1/3 points for spans from 135 ft to 180 ft
                                            ¼ points for spans greater than 180 ft.

Why the change? Intermediate diaphragms are for constructability, however contractors often place them after placing the deck, which defeats the purpose. Contractor will be responsible for bracing the girders during construction.

Question 10.

No

Not this topic.

No.

No.

Florida conduct research on this topic.
https://www.fdot.gov/structures/structuresresearchcenter/CompletedResearch.shtm

No

No

No.

Certainly not recent, but here are a couple of reports…
Steel Diaphragms in Prestressed Concrete Girder Bridges; TR-424, September 2004
http://publications.iowa.gov/2487/
Lateral Load Resistance of Diaphragms in Prestressed Concrete Girder Bridges, HR-319, 1991
http://publications.iowa.gov/16262/

No.

Our state performed a study on this topic which can be found in Part IV Chapter 3 of our Bridge Design Manual at the following link: (Part of the study included surveying what the other DOTs had in place as policy for IDs.)
http://wwwsp.dotd.la.gov/Inside_LaDOTD/Divisions/Engineering/Bridge_Design/Pages/BDEM.aspx

NO, Maine has had no reason per code or inservice needs to evaluate this.

None

Unaware of any research on this topic.

No, at the time MS decided to remove IDs, there was sufficient documentation they do not add a substantial benefit for the cost. This has been our experience. We save approximately $30,000

per bridge and provide a safer working environment for the contractor's employees and our inspector.

No.

No.

-No.

No

No.

No

No.

APPENDIX C. BEARING ROTATIONAL STIFFNESS VERIFICATION

Experimental values are taken from NCHRP 596 (Stanton et al. 2008), while theoretical values were calculated using Eq. 7.23, with mean and coefficient of variation (COV) of the experimental / theoretical ratio given.

#	Bearing Pad Specimen (from NCHRP 596)	Experimental Rotational Stiffness (kip-in/rad)	Theoretical Rotational Stiffness (kip-in/rad)	Experimental / Theoretical
1	CYC5-A1	2930	3867	0.76
2	CYC5-A2	2820	3535	0.80
3	CYC5-B1	2700	4711	0.57
4	CYC5-C1	3650	4530	0.81
5	CYC5-D1	3520	3808	0.92
6	CYC7-A1	3730	3867	0.96
7	CYC7-A2	3740	3535	1.06
8	CYC7-B1	3270	4711	0.69
9	CYC7-C1	4190	4530	0.92
10	CYC7-D1	4050	3808	1.06
11	CYC8-A1	4760	3867	1.23
12	CYC9-A1	7170	3867	1.85
13	CYC9-A2	6740	3535	1.91
14	CYC9-B1	5840	4711	1.24
15	CYC9-C1	6800	4530	1.50
16	CYC9-D1	8270	3808	2.17
17	CYC11-A1	4580	3867	1.18
18	CYC11-A2	4450	3535	1.26
19	CYC11-B1	4200	4711	0.89
20	CYC11-C1	5220	4530	1.15
21	CYC11-D1	4910	3808	1.29
22	CYC12-A1	3060	3867	0.79
23	CYC12-A2	2830	3535	0.80
24	CYC12-B1	2840	4711	0.60
25	CYC12-C1	4010	4530	0.89
26	CYC12-D1	4250	3808	1.12
27	CYC13-A1	5920	3867	1.53
28	CYC14-A1	3550	3867	0.92
29	CYC15-C1	5990	4530	1.32
			mean:	1.11
			COV:	0.35